Soft-lithographic Patterning of Functional Oxide and Composite Materials

by

Sajid Ullah Khan

Committee members:

Chairman:	
Prof. dr. G. van der Steenhoven	(University of Twente)
Promotor:	
Prof. D. H. A. Blank	(University of Twente)
Assistant Promotor:	
Dr. J. E. ten Elshof	(University of Twente)
Members:	
Prof. R. Lammertink	(University of Twente)
Prof. H. Gardeniers	(University of Twente)
Dr. H.T.J.M. Hintzen	(Technical University Eindhoven)
Prof. B.J. Kooi	(University of Groningen)

The research work presented in this thesis was carried out at the Inorganic Materials Science group, MESA$^+$ Institute of Nanotechnology, University of Twente, The Netherlands, and was financially supported by the Netherlands Organization for Scientific Research (NWO) in the framework of the Innovational Research Incentives (VIDI Scheme).

ISBN: 978-90-365-3054-5

Printed by Ipskamp Drukkers B.V., Enschede, The Netherlands

SOFT-LITHOGRAPHIC PATTERNING OF FUNCTIONAL OXIDE AND COMPOSITE MATERIALS

DISSERTATION

to obtain
the degree of doctor at the University of Twente,
on the authority of the rector magnificus,
Prof. dr. H. Brinksma,
on the account of the decision of the graduation committee,
to be publicly defended
on Wednesday, June 30th 2010, at 13.15 hrs

by

Sajid Ullah Khan
Born on 15th of August 1977
in Thana, Pakistan

This dissertation is approved by the promotor Prof. dr. ing. D.H.A. Blank
and the assistant promotor Dr. ir. J.E. ten Elshof

to my Parents

Contents

Summary

The research work was mainly focused on the molding based patterning techniques. It describes the patterning of TiO_2, $Pb(Zr,Ti)O_3$, and $LaPO_4$:Eu and $CePO_4$:Tb nano-particles embedded in hybrid organosilica. These materials were derived from their respective sol-gels and/or dispersion solutions. These were successfully patterned with a resolution from tens of micrometers down to 100 nm. The various shapes obtained were lines, pillars, and pit patterned films.

Titania derived from both sol-gel and dispersion solution was patterned by the micromolding in capillaries (MIMIC) technique. The sol-gel based patterns showed good adhesion to the substrates, however suffered from a high degree of volumetric shrinkage. The final patterned features after annealing at 550 °C had only 2-5% of the volume of the corresponding cavities in the mold. On the other hand the dispersion based patterns showed lower shrinkage; however, they were more porous and needed higher temperatures for densification. The sol-gel derived patterns were more regular in shapes and have smooth surfaces and edges. Both precursor types were also used to produce layer-by-layer type 3D patterns. This was accomplished by introducing an extra step and material to the process. The formation of an undesirable thin film in-between patterned features, the so called "residue layer", was also investigated. In order to prevent its occurrence, the surface properties of the mold were altered. That was achieved by tailoring the surface energy of the protruding parts of the molds. The results indicated that the residue layer formation can be totally avoided.

Two types of photoluminescence nanoparticles (NPs), i.e. $LaPO_4$:Eu and $CePO_4$:Tb embedded in hybrid organosilica, were patterned. Besides MIMIC, a new technique known as microtransfer molding (μTM) was also applied for the patterning. The two techniques and their advantages were compared with each other in terms of pattern shape formation, their adhesion to the substrate, and residue layer formation. Both techniques were applied as well for 3D patterning in the same manner as used for making TiO_2 patterns. Interestingly, it was found that the shapes of the features derived by the two techniques were different while using the same material. This suggests that both the filling and drying behavior have profound effects on the shape formation.

The compositional analyses of the surface region of the patterned features were performed with low energy ion scattering (LEIS), secondary ion mass spectroscopy (SIMS) and x-ray photoelectron spectroscopy (XPS), which revealed the absence of nanoparticles. This was further assisted by the photoluminescence microscopy which showed reduced intensities of the patterned films. This suggests that either the NPs are

buried under the surface or some quenching effects might have reduced the total yields. Nevertheless, it was shown that both techniques have their own advantages and limitations and can be adopted depending on the applications of the patterned features.

I applied soft-lithographic techniques to pattern PZT at various lengths scales and with various geometries. Cracking was totally avoided by patterning in combination with proper thermal processing protocols. Unlike the oxide materials mentioned above, the shape formation of the PZT line patterns was found unusual. The patterned lines showed the so-called "double peak profile" which might limit their use for certain applications. It is always desirable to be able to replicate the exact shape of the master in the patterned features. This aspect, i.e. the *shape evolution,* was investigated in great detail in order to be able to have good control over the shape replication. This was achieved by saturating the mold with the solvent(s) of the precursor material in order to avoid the preferential drying at the corners of the capillaries. However, it could not avoid the double peak formation and instead resulted in the formation of more porous patterned lines due to a reduced evaporation rate of the solvents. Other factors, such as drying of the patterns at different hot plate temperatures (80-400 ^{o}C), and their effects on the pattern formation and shrinkage, were investigated as well. The role of heating rates during annealing was investigated by applying the very rapid thermal annealing in a microwave furnace and in a conventional furnace. The results showed only a difference in degree of the total volumetric shrinkage of the patterned lines, but no significant effect on the double peak profile formation.

When patterning sub-100 nm sized features was targeted, the role of particle sizes became imperative. In other words, the particle size in the solution should be smaller than the feature size of the mold for its reproduction with high fidelity. Therefore, a comprehensive small angle x-ray scattering (SAXS) analysis of PZT sol-gel was performed to study the size and shape of the structural entities. Their in-situ and ex-situ growth at ambient and elevated temperatures as a function of time was examined. The various stages starting from their liquid phase sols to thermally annealed films were studied this way. The SAXS study revealed that the structural entities in the solution have an effective particle size of ca. 1 nm, which is small enough for patterning at small scales.

Two other soft-lithographic techniques, namely soft confocal imprint lithography (SCIL) and nanotransfer molding (NTM), were applied to produce PZT nanopatterns with 100 nm resolution, using the same flexible PDMS molds. The patterns obtained with SCIL technique have a comparatively thicker residue layer than those derived with NTM. Nonetheless, the thick residue layer has the advantage that it improves the

adhesion of the patterned features to the substrate. Additionally, SCIL is relatively straightforward in terms of surface energies adjustments of the mold.

Samenvatting

Het merendeel van het onderzoek is gebaseerd op patroneertechnieken. Het beschrijft het patroneren van TiO_2, $Pb(Zr,Ti)O_3$, $LaPO_4$:Eu en $CePO_4$:Tb nanodeeltjes omringd door hybride organosilica's. Deze materialen zijn verkregen uit de respectievelijke sol-gels en/of dispersies en zijn succesvol gepatroneerd met een resolutie van tientallen micrometers tot 100 nanometer. De gemaakte structuren zijn lijnen, pilaren en putjes in een dichte laag.

Titanium oxide verkregen uit een sol-gel en een dispersie werd gepatroneerd met de 'micromolding in capillaries (MIMIC)' techniek. De patronen gebaseerd op sol-gel bleken een goede hechting met het substraat te hebben; hoewel de patronen leden onder een hoge mate van volumeverlies. Na annealen op 550 °C hadden de uiteindelijke patronen slechts 2-5% van het volume van de mal. De patronen verkregen uit een dispersie bleken minder volumeverlies te hebben. Echter, deze vertoonden meer porositeit en hadden een hogere temperatuur nodig om de dichtheid te verhogen. De sol-gel gebaseerde patronen waren regelmatiger in vorm met gladde oppervlakken en eenduidige hoeken.

Beide types precursor werden ook gebruikt om driedimensionale laag-op-laag patronen te produceren. Dit werd mogelijk gemaakt door een extra stap en een extra materiaal aan het proces toe te voegen.

De vorming van een niet gewilde dunne film tussen de patronen, de zogenaamde 'residue layer' is ook onderzocht. Om dit tegen te gaan zijn de oppervlakte-eigenschappen van de mal aangepast door de oppervlakte-energie van de uitstekende delen van de mal aan te passen. Uit de resultaten bleek dat de 'residue layer' in zijn geheel kan worden voorkomen.

Twee types fluorescerende nanodeeltjes, $LaPO_4$:Eu en $CePO_4$:Tb omringd door hybride organosilica, zijn gepatroneerd. Naast MIMIC is een nieuwe techniek genaamd 'microtransfer molding (μTM)' toegepast. De twee technieken en de voordelen daarvan werden vergeleken op basis van de uiteindelijke vorm van de patronen, de hechting aan het substraat en de vorming van de 'residue layer'. Beide technieken zijn ook gebruikt voor het maken van driedimensionale patronen zoals genoemd bij titanium oxide. Belangwekkend is dat de verkregen vormen verkregen met beide technieken verschillen, hoewel hetzelfde materiaal is gebruikt. Dit suggereert dat het vulgedrag van de mal en het drooggedrag een grote invloed hebben op de totstandkoming van de uiteindelijke vorm van het patroon.

De analyse van de samenstelling van de oppervlaktes van de patronen werden uitgevoerd door middel van 'low energy ion scattering (LEIS)', 'secondary ion mass spectroscopy (SIMS)' en 'X-ray photoelectron spectroscopy (XPS)'. Deze technieken toonden de afwezigheid van de nanodeeltjes aan. Dit werd ondersteund door 'photoluminescence microscopy' doordat een lagere intensiteit van de patronen werd aangetoond. De resultaten suggereren dat de nanodeeltjes zich onder het oppervlak bevinden of een 'quench-effect' de totale hoeveelheid heeft verminderd. Hoe dan ook, er is aangetoond dat beide technieken voordelen en beperkingen hebben en dat ze kunnen worden gebruikt naargelang de applicatie van de patronen.

Ik heb 'soft-lithography' technieken toegepast om PZT op verschillende lengteschalen en met verschillende geometrieën te patroneren. Het barsten van de patronen is voorkomen door het patroneerproces te combineren met geschikte thermische behandelingsproto-collen. In tegenstelling tot boven genoemde oxide materialen is de vorm van de PZT patronen ongebruikelijk. De patronen vertoonden een 'dubbele-piek-profiel' die de toepassingen van het materiaal kunnen limiteren. Het is altijd gewenst om de exacte vorm van de mal te reproduceren. Dit aspect, met andere woorden *de vormevolutie*, is in groot detail onderzocht om een goede controle over de reproduceerbaarheid van de vorm te krijgen. Dit werd bereikt door de mal met een gepast oplosmiddel c.q. oplosmiddelen te verzadigen van de precursor ten einde de preferentiële droging in de hoeken van de capillairen te voorkomen. Echter, het 'dubbele-piek-profiel' kon niet worden voorkomen. In plaats daarvan waren de gepratoneerde lijnen poreuzer als gevolg van een verminderde verdampingssnelheid van de oplosmiddelen. Andere factoren, zoals het drogen van de patronen bij verschillende temperaturen van de verwarmplaat (80-400°C) en het effect daarvan op het volumeverlies, zijn ook onderzocht. De rol die de verwarmingssnelheden spelen tijdens annealen is onderzocht door het toepassen van een zeer snelle thermische annealing in een magnetron oven en een conventionele oven. De resultaten lieten alleen een verschil in volumeverlies van de gepatroneerde lijnen zien, maar geen noemenswaardig effect op het 'dubbele-piek-profiel'.

Als patronen onder het 100 nanometer regime een doel zijn, wordt de grootte van de deeltjes belangrijk. Met andere woorden, de deeltjesgrootte in de oplossing moet kleiner zijn dan de opening van de mal waardoor een goede reproduceerbaarheid mogelijk is. Daarvoor is een 'small angle X-ray scattering (SAXS)' analyse van de PZT sol-gel uitgevoerd om de grootte en vorm van de aanwezige structuren te onderzoeken. In-situ en ex-situ groei bij kamertemperatuur en hogere temperaturen als functie van tijd werden onderzocht. De verschillende stadia tussen de vloeibare fase van de sol en ge-annealde dunne films werden op deze manier onderzocht. De SAXS-analyse liet zien

dat er zich structuren in de oplossing begaven met een effectieve deeltjesgroote van circa één nanometer. Dit is klein genoeg voor patroneren op kleine schaal.

Twee andere 'soft-lithography' technieken, namelijk 'soft confocal imprint lithography (SCIL)' en 'nanotransfer molding (NTM)' zijn toegepast om PZT nanopatronen te produceren met een 100 nanometer resolutie met behulp van dezelfde flexibele poly-dimethylsiloxaan (PDMS) mal. De patronen gemaakt met SCIL hebben een dikkere 'residue layer' dan die gemaakt met NTM. Niettemin, de dikke 'residue layer' verbetert de hechting tussen patroon en substraat. Daarbij is SCIL relatief simpel met betrekking tot het aanpassen van de oppervlakte energieën van de mal.

1

Introduction

1.1. Soft-lithography

The miniaturization of objects and device components down to the micron- and nanometer scale, and the development of methods to fabricate and register these, presents one of the main technological trends of the last decade, and has been reported in a large number of reviews, *e.g.* refs.[1-6]

Among these methods, a number of alternative techniques to traditional photolithography for patterning a variety of materials have been developed. Photolithography is commonly used in the electronics industry and has been under development for many decades. At present, feature sizes <<100 nm can be patterned in silicon on large scale. However, the drawbacks of the techniques are that high-end equipment and clean room conditions are required, and the methodology is applicable only to a narrow set of materials.

In an attempt to overcome these restrictions, a family of related patterning techniques was developed by the Whitesides group at Harvard University in the 1990s.[7-9] These so-called soft-lithography techniques are mainly parallel patterning methods, so large areas can be patterned in a relatively short period of time. They may provide cheap alternatives for the much more costly photolithographic processes, and are able to process a wider range of materials, including polymers, biomaterials, ceramics, hybrids, and composites. At least with some of these techniques, parallel patterning on sub-100 nm scale is possible. Since their development, soft-lithographic techniques have achieved widespread use in academic and industrial laboratories for applications in diverse fields, *e.g.*, photonics, biotechnology, microfluidics, and electronics. While most of these research efforts were focused on the patterning of polymers, biomaterials and self-assembled monolayers, it has also found application in the micrometer and sub-micrometer patterning of ceramics and organic-inorganic hybrid materials,[10] and that is the main topic of the present work.

All soft-lithographic techniques require an elastomeric mold or stamp that is patterned with a relief structure on its surface. One of the steps in the patterning process involves bringing the elastomer into conformal contact with a substrate, and be used as stamp or mold.[9] The patterned elastomer is made by casting a liquid pre-polymer onto a 3D patterned master structure,[11] followed by polymerization of the pre-polymer. In most cases the master structure is made from silicon or photoresist and obtained by

conventional photolithography. The most popular and widely used elastomeric material is polydimethylsiloxane (PDMS), a rubber-like material with a low surface energy that can be easily peeled off the master after cross-linking. To aid in the debonding process, the silicon master is usually silanized in order to make it hydrophobic prior to use. The final result is an elastomeric negative replica of the master structure with three dimensional patterns. Essentially, the patterned elastomer can be utilized for patterning in two different ways: (1) the protruding patches of the patterned elastomer can be employed to carry a precursor ink to the substrate (printing approach), or (2) precursor material is contained in the recessed regions between the protruding patches (molding approach). These two strategies will be discussed in more detail in the next chapter, with emphasis on the latter. In either case, the precursor is transferred to the substrate, and the stamp or mold aids in defining the locations where precursor material is deposited. For proper transfer of material, it is necessary that the stamp or mold makes good conformal contact with the substrate.

A general review on sub-micrometer scale parallel patterning of ceramic materials was published in 2004 by the Aksay group at Princeton.[10] More focused reviews on site-selective liquid-phase deposition of ceramics via photolithography-aided patterning techniques were published by Masuda, Koumoto and co-workers.[12, 13]

1.2. Scope

The thesis work addresses low-cost micron and submicron-scale parallel patterning methods, with emphasis on the formation of patterned thin films of solid state materials, more specifically metal oxides and organic-inorganic hybrid materials. It is motivated by the ongoing activity on the subject over the last years. The main focus of the current research will be on materials that can be deposited and patterned from liquid precursors, such as sol-gel solutions and colloidal suspensions.

Chapter 2 is an overview of the principles of the most commonly used parallel patterning methods and addresses the conflicting properties required for soft-lithographic stamps and molds. The inks, molecular precursor solutions and particle suspensions used in patterning, and their underlying chemistries are described in terms of viscosity, surface tension, solids content, and type of solvents. It also gives an overview of the progress made in recent years on submicrometer-scale patterning of functional ceramics and hybrid materials by molding-based approaches.

Chapter 3 describes the major materials used in this work and the characterization techniques applied to study the derived films and patterns. A brief introduction to small angle x-ray scattering technique is given which is an important technique in studying the structure and size of solutions.

Chapters 4 to 6 are about the syntheses and patterning of the various functional oxides and multi-component hybrid materials. Chapter 4 addresses the patterning of sol-gel

and dispersion based TiO_2 by micromolding in capillaries (MIMIC) technique. The various aspects such as shape formation, shrinkage, adhesion of the patterned materials are discussed. The residue layer formation and stable modification of the mold, and the 3D type patterning are presented as well. The patterning of two types of photoluminescence nanoparticles (NPs) embedded in hybrid organosilica is presented in chapter 5. Here an alternative molding technique called microtransfer molding (μTM) is applied and the shape formation is compared with those derived with MIMIC. The various aspects and advantages of the two techniques are compared. The distribution of nanoparticles is studied by compositional analyses with some spectroscopic techniques. Similarly, chapter 6 is about the synthesis and patterning of one of the most important functional oxide materials called lead zirconate titanate (PZT). The shape evolution of the derived lines patterns and the electrical properties are studied.

Chapter 7 is an intensive small angle x-ray scattering (SAXS) study of the sol-gel PZT solutions at various stages between sol synthesis and final sintered thin films. The various stock solutions are studied independently and in combination, the role of water addition and temperature effects on structure, size and composition are studied as well.

Chapter 8 focuses on nanometer scale patterning of PZT by two new techniques called Soft Confocal imprint lithography (SCIL) and Nanotransfer molding (NTM). With these techniques it has been shown possible to pattern PZT down to 100 nm lateral resolutions. The thesis closes with a short conclusions and outlook chapter.

References

[1] Xia, Y. N., Rogers, J. A., Paul, K. E. & Whitesides, G. M. *Chem. Rev.* 99, 1823-1848, **1999**

[2] Geissler, M. & Xia, Y. N. *Adv. Mater.* 16, 1249-1269, **2004**

[3] Gates, B. D., Xu, Q. B., Stewart, M., Ryan, D., Willson, C. G. & Whitesides, G. M. *Chem. Rev.* 105, 1171-1196, **2005**

[4] Henzie, J., Barton, J. E., Stender, C. L. & Odom, T. W. *Accounts Chem. Res.*, 2006, 39, 249-257, **2006**

[5] del Campo, A. & Arzt, E. *Chem. Rev*.108, 911-945, **2008**

[6] Heule, M., Vuillemin, S. & Gauckler, L. J. *Adv. Mater.* 15, 1237-1245, **2003**

[7] Kumar, A. & Whitesides, G. M. *Appl. Phys. Lett*. 63, 2002-2004, **1993**

[8] Zhao, X. M., Xia, Y. N. & Whitesides, G. M., *Adv. Mater.* 8, 837-840, **1996**

[9] Xia, Y. N. & Whitesides, G. M. *Annu. Rev. Mater. Sci.* 28, 153-184, **1998**

[10] Martin, C. R. & Aksay, I. A. *J. Electroceram*. 12, 53-68, **2004**

[11] Rogers, J. A. & Nuzzo, R. G. *Materials Today* 50-56, **2005**

[12] Masuda, Y. *J. Ceram. Soc. Jpn.*115, 101-109, **2007**

[13] Koumoto, K., Saito, N., Gao, Y. F., Masuda, Y. & Zhu, P. X. *Bull. Chem. Soc. Jpn.* 81, 1337-1376, **2008**

2

Literatue Survey

Micrometer and Nanometer-scale Parallel Patterning of Ceramic and Organic-inorganic Hybrid Materials[†]

Abstract

This chapter gives an overview of the progress made in recent years in the development of low-cost parallel patterning techniques for ceramic materials, silica, and organic-inorganic silsesquioxane-based hybrids from wet-chemical solutions and suspensions on the micrometer and nanometer scale. The emphasis of the discussion is placed on the application of soft-lithographic methods. In general, molding-based patterning approaches and surface modification-based patterning approaches can be distinguished. Lateral resolutions well below 100 nm have been accomplished with some of these methods, but the fabrication of high-aspect ratio patterns remains a challenge.

2.1. Principles of soft-lithographic patterning

2.1.1. Soft lithographic and lithographic techniques

The ability to generate and integrate small objects and device components, and to develope novel methods is one of the main technological trends.[1-6] Most of the patterning techniques that will be discussed here, belongs to the family of soft-lithographic processes.[7-11] The main focus will be on materials that can be deposited and patterned from liquid precursors, such as sol-gel solutions and colloidal suspensions. Polymers, metals[11] and colloidal assemblies[16-18] are outside the scope of this survey. Neither does it address serial patterning methods, such as ink jet printing,[18] dip-pen nanolithography,[20-22] direct ink writing,[23] nor ion-beam and e-beam methods.[2]

Soft-lithographic methods can be divided into two main categories, namely molding-based approaches and surface modification-based approaches.[10] Molding-based patterning approaches and their application to forming ceramic and hybrid micro- and nanopatterns are discussed in section 2.2. They include conventional micromolding, microtransfer molding, and micromolding in capillaries. They all

[†] This chapter was part of review published in Journal of European Ceramic Society

employ physical confinement of a liquid precursor solution or suspension to define the shape of the final pattern. They produce a negative replica of the pattern in the mold, and a positive replica of the original lithographic master. At least in principle high aspect ratio structures can be made by these approaches.

PDMS is permeable to many solvents but not to polymers or nanoparticles, so physical drying of a molded solution or suspension is possible by diffusion of the solvent into the PDMS mold. The precursor dries slowly and solidifies while it is still confined by the mold.[23] The resolution of the patterned material is determined by the surface energies of the components, and the ability of the mold to detach from the patterned material after drying. High resolution requires the selection of a mold material that has significantly lower adhesion energy with the pattern material than the substrate has with the material. After removal of the mold, the patterned material can be heat-treated, e.g. pyrolized, in order to obtain the final phase.

In microtransfer molding (μTM),[9] shown in **Figure 2.1a**, the precursor solution is deposited in the recessed regions of a patterned mold. Excess material on the protruding parts is removed and the mold is brought into conformal contact with a substrate. After a certain period of time, during which the precursor dries by solvent removal (physical drying) and/or condensation of precursors into –inorganic– polymeric networks (chemical drying), the mold is removed. If the adhesion to the (PDMS) mold is smaller than that to the substrate, the patterned material remains attached to the substrate, and can be given a final heat treatment.

The micromolding (embossing) process shown in **Figure 2.1b** involves imprinting a patterned mold into a continuous wet film by application of some pressure. Both soft (PDMS) and rigid (glass, poly(methyl methacrylate)) materials have been employed for the molds. The technique can pattern well in the sub-50 nm scale,[24, 25] a resolution that has not been met by any of the other techniques discussed in this chapter. The formation of a residual layer between the desired features of the patterns is inherent to the technique. This is why it is especially interesting for applications in which the presence of residual layers presents no problem. In other cases, a post-etching step after pattern formation is required.

An often used alternative term for micromolding is nanoimprint lithography (NIL).[26] Although NIL traditionally focuses on nanopatterning of polymers and is often done at elevated temperatures to reduce viscosity, and optionally involves a final UV curing step, the process is essentially similar to micromolding. Micromolding and microtransfer molding are both fast parallel patterning processes with which large areas can be patterned.

The idea behind micromolding in capillaries (MIMIC),[27] is that the formation of residue layers is avoided. The process is schematically shown in **Figure 2.1c**. A clean patterned mold is brought into conformal contact with the substrate before the liquid

precursor is supplied. A network of empty microcapillary channels forms in the mold. A precursor solution is then supplied to the entrances of the capillaries at the side of the mold. The precursor solution is drawn into the microchannels by capillary force. In principle, no residue layer can form in areas where adhesive conformal contact between mold and substrate is already established. MIMIC is a semi-parallel patterning process. It takes time for the precursor fluid to fill the entire pattern under the mold. For example, the Washburn equation predicts that the penetration rate of water in a straight 1 μm diameter channel at 298 K is such that its penetration length is 1.5 mm after 1 s, but only 10 mm after 50 s. In narrower channels the penetration rate is even lower and becomes impractical for most purposes. It is clear that such kinetic factors will play a role in determining the quality of the final pattern.

In the surface modification-based patterning approaches first a chemically contrasted substrate is generated. After that a layer is grown or material deposited selectively on those patches of the substrate which have proper surface chemistry. Examples of chemical contrasts are hydrophobic-hydrophilic contrast, (electrical) charge contrast, and chemically specific contrasts such as catalytic activity for transformation of one or more of the components in the precursor solution into solids.

Since the surface modification based methods do not rely on physical confinement, the ultimate lateral resolution of the method is lower than what can be accomplished by molding-based methods. The height of the formed oxide patterns is usually in the range of 20-80 nm, so the aspect ratios are quite low.

A general soft-lithographic surface modification approach is micro-contact printing (μCP),[7] shown in **Figure 2.1d**, with which the chemistry of a surface can be locally modified. Chemically contrasted substrates are made by printing self-assembled monolayers or very thin multilayers of an ink that was carried to the substrate by the stamp and is transferred by conformal contact. Well-known examples are octadecyl trichlorosilane (OTS; $Cl_3Si\text{-}C_{18}H_{37}$) on silicon oxide and octadecanethiol ($C_{18}H_{37}\text{-}SH$) on gold. They yield a thin multilayer and self-assembled monolayer after drying, respectively, and both are very hydrophobic.[2] When the substrate is exposed to a particle suspension or chemical solution, heterogeneous nucleation and growth of oxide precursors occurs more readily on polar (hydrophilic) surface patches. The adhesion of oxide nanoparticles or inorganic polymers to a surface is also favoured by the presence of polar groups at the surface. Hence, hydrophobic patches on a substrate inhibit the local formation of a ceramic phase, which can be exploited to generate local patterns of ceramics on the other, *i.e.* the more hydrophilic patches.

The confocal contact printing method in **Figure 2.1e** is technically simple. The precursor is directly printed onto a substrate in a single patterning step. However, the disadvantage is that the resolution and quality of replication of the pattern are controlled entirely by the rheological properties of the precursor ink and the drying rate,

which requires careful engineering of the precursor solution. In micro-contact printing-based approaches the functions of pattern definition and film formation are carried out by different components. This makes optimization of the patterning process easier, since they involve two independent steps. In practice, the resolution of confocal printing is much higher than 50 μm.[28] However, much smaller pattern features could be possible once a better control of the solution chemistry and the printing conditions is established.

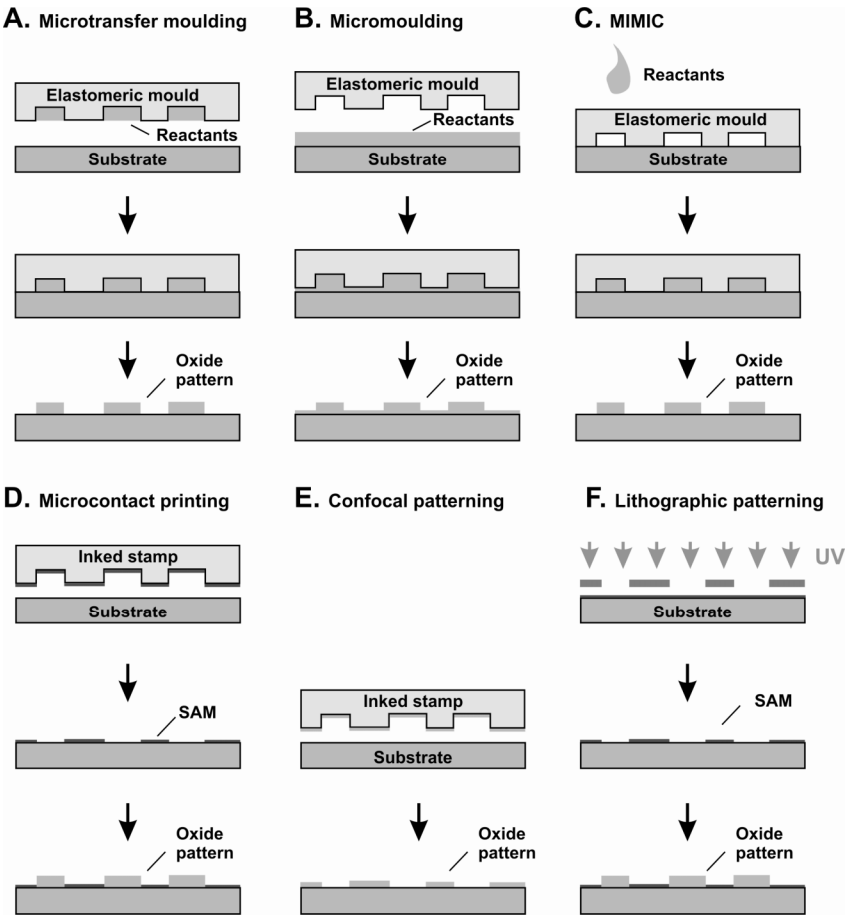

Figure 2.1: Soft-lithographic (a-e) and hard-lithographic (f) patterning processes. (a) Microtransfer molding; (b) Micromolding/nano imprint lithography; (c) Micromolding in capillaries; (d) Microcontact printing of self-assembled monolayer or multiple layer (SAM); (e) Confocal patterning; (f) Lithographic patterning of SAM.

One of the limitations of soft-lithographic patterning techniques in general concerns the registry of the formed patterns.[10] Therefore, it remains problematic to fabricate hierarchical structures with a more complex function by combining several patterning steps in sequence. This is one of the reasons why several investigators have explored possibilities to micropattern ceramic materials by a conventional hard-lithography-supported approach. Photolithography-aided patterning, illustrated in **Figure 2.1f**, uses the tools of photolithography, a well-known technology that has been developed over the last decades for silicon technology and microelectronics. It involves exposing a substrate to UV light via a shadow mask, so that only certain parts of the substrate are actually exposed. The UV energy can be employed either to generate chemically contrasted substrates (prior to film deposition or growth) by selectively decomposing a preformed SAM, or locally transform UV sensitive ceramic precursors into a condensed phase. The resolution of the whole process is in principle limited only by that of the photolithographic process. An advantage of this approach is that the presently available technology developed for conventional photolithography can be used to transfer patterns. All required equipment and UV photomasks are readily available.

2.1.2. Properties of elastomer materials

All soft-lithographic techniques depend on surface topographical relief patterns of elastomeric stamps and molds. Of these, PDMS made from Sylgard 184 (Dow Corning Inc.) is the most popular type of polydimethylsiloxane for making soft-lithographic stamps. It combines flexibility and conformal contact to an extent that is sufficient for many processes. Sylgard 184 consists of a silicone resin cross-linked by a mixture of vinyl-terminated PDMS and trimethylsiloxy-terminated poly(methylhydro-siloxane) polymers. The resulting material has a highly cross-linked three-dimensional structure. It offers a high elongation at break (>100%).

When used for confocal patterning, intimate contact with the substrate is achieved locally at the protruding areas, while a gap remains between the substrate and the recessed areas. Essentially, this requires the stamp (or mold) to have two conflicting properties with respect to its Young's modulus. On the one hand, the stamp should be soft enough to enable good conformal contact with the substrate. It should adapt elastically to small substrate surface variations (roughness) and not leave any voids between stamp and substrate. This requires a low Young's modulus and high work of adhesion. On the other hand, a precise definition of micro-patterns requires a rigid material. This implies a high Young's modulus.[29] The conflict between these two properties sets a limit on the resolution that can be achieved with soft elastomeric stamps with good conformal contact.

Various authors have pointed out that deformation of soft stamps may lead to various kinds of collapse of the pattern, *e.g.*, ref. [30] For example, in rubber stamps with

low aspect ratio patterns, where the protruding features are widely interspaced, so-called roof collapse may occur, in which the recessed areas deform to such an extent that they touch the substrate. Quantitative criteria against roof collapse have been proposed.[31] On the other hand, soft stamps with high-aspect ratio structures suffer from buckling, pairing and collapse to the ground. It has been proposed that decreasing the work of adhesion between stamp and substrate helps to prevent ground collapse, [32] and increasing the pattern density was found to be beneficial for pattern transfer fidelity.[33]

The use of composite stamps with a stiff backbone and a soft patterned layer may improve pattern quality,[34] but increasing the stiffness of the stamp will remain crucial for the definition and stability of patterns at ultimate resolution in many processes.[29] Also, when pre-ceramic suspensions are used, harder masks that are less prone to deformation are preferred as they will withstand increased pressures with less deformation.

Another problem with PDMS is its interaction with certain organic solvents. Lee, Park, and Whitesides investigated the compatibility of PDMS with a wide range of solvents, and considered three aspects of compatibility, namely (i) the swelling of PDMS in a solvent, (ii) the partitioning of solvent between PDMS and solvent phase, and (iii) the dissolution of small oligomeric fragments of PDMS in the solvent.[23] Of these three, swelling was found to exert the largest influence. Among the solvents that swelled PDMS the least were water, glycerol and ethylene glycol. Highly swelling solvents were very polar solvents such as pentane and xylene.

The resolution achievable with standard PDMS, made from Sylgard 184, has often been limited to >100 nm because of the low compression modulus of 2 MPa.[35] The use of a harder version of PDMS, called hard-PDMS or h-PDMS, with a compression modulus of 9 MPa has increased the resolution to 50 nm, but not for densely spaced features, or high aspect ratio patterns.

H-PDMS is prepared from trimethylsiloxy-terminated vinylmethylsiloxane-dimethylsiloxane (VDT-731; Gelest) and methylhydrosiloxane-dimethylsiloxane (HMS-301; Gelest) copolymers. The h-PDMS system has cross-linkers that have relatively short lengths as compared to those in Sylgard 184 PDMS. Composite bi-layer patterning elements that use a thin patterned layer of h-PDMS with a thick back layer of Sylgard 184-PDMS effectively combine some of the attractive features of these two materials for certain applications.[36]

Rigid molds made of quartz may stick to the imprinted materials unless they have been treated with an anti-sticking release layer. Polymers such as poly(methyl methacrylate) (PMMA) can also be used as a mold material, however an anti-sticking treatment using low-surface-energy materials such as fluorosilane self-assembled monolayer is still needed for easy release. Several alternative polymeric materials have

been proposed for use in stamps, *e.g.*, refs.[35-37] Some examples are listed in **Table 1**. In recent years a number of fluorinated polymers have been developed for use in stamps.[38-42] They exhibit good mechanical properties, while having a lower surface energy (γ<20 mJ/m^2) than PDMS (γ=21.6 mJ/m^2), and being less prone to swelling by solvents. Other essential properties of the stamp or mold are its surface energy and the nature of any present surface functional groups, because these determine the wetting and dewetting behaviour of precursor solutions in the mold, as will be elaborated in more detail below for the respective techniques.

Table 1: Comparison of Young's modulus, elongation at break, toughness and shrinkange upon polymerization in a nanoimprint lithography mold. (Data taken from refs. [36] and [38]).

Mold material	Tensile modulus (MPa)	Elongation at break (%)	Toughness (MPa)	Shrinkage (%)
PDMS (Sylgard 184)	1.6-1.8	146-160	4.77	1.1
Hard-PDMS	8.2	6.5-7.0	0.02	1.6
Soft-PDMS	0.6	70	0.13	3.1
hv-PDMS [36]	3.4	54	0.41	0.6
Fluorinated hybrimer [38]	33.5 – 40	5.3	1.12	2 – 2.5
Flexible fluorinated hybrimer [38]	32.5	30	4.5	2 – 2.5

Sylgard 184 PDMS is hydrophobic, *i.e.*, water has a contact angle >90° and does not spread on the surface of PDMS. While this may be advantageous for the debonding step in micromolding and microtransfer molding, as will be discussed in section 2.1.4, it is disadvantageous when a MIMIC process for aqueous solutions is targeted, because water will probably not like to enter a predominantly hydrophobic micron-sized capillary. A variety of methods have been proposed to alter the chemical properties of PDMS. The simplest and most commonly used method to make the surface of PDMS hydrophilic is by an oxygen plasma treatment for periods of a few tens of seconds.[43] The resulting surface modification is consistent and reproducible, yielding contact angles <5°, and requires no special chemicals. The oxygen plasma oxidizes the surface of PDMS, so that a thin hydrophilic SiO_x layer with surface silanol groups Si-OH form. Unfortunately, it is well-known that the hydrophilic modification is not permanent. In the course of time, typically hours, low molecular weight siloxane residuals migrate to the surface and cover the SiO_x layer with a low surface energy film, so that the surface becomes hydrophobic again. The same residuals are responsible for the reported

contamination of substrate surfaces during conformal contact. Detailed studies have shown that silicone-related material is transferred from flat stamps, and even more material is transferred from patterned stamps.[44] Silicone transfer can be minimized by curing the PDMS stamps at elevated temperatures, but also depends on the pretreatment of the stamp and the type of ink used.[45, 46] Furthermore, it has been suggested that the transferred material also contains traces of platinum, which are present in Sylgard 184 as cross-linking catalyst.[46] No fast and easy method is known that can completely and permanently remove these residuals from the stamp. An exhaustive week-long cleaning procedure has been proposed that yields PDMS stamps containing no or very little oligomer material.[47] However, the hydrophobic recovery after oxygen plasma treatment of cleaned PDMS stamps is only slightly affected when stored in air. This suggests that the stamps probably regain their ability to contaminate and transfer PDMS residues.[46]

Alternative ways to modify the stamp's surface energy more permanently are through chemical modifications, for which several routes have been proposed. Sol-gel coatings based on titanium alkoxide, zirconium alkoxide and vanadium alkoxide have been reported.[48] Also thiol, amine, sulfonic-acid and cyano-functional coatings have been applied on PDMS.[49-51] In these cases the PDMS surface was first plasma-treated to form silanol groups to which the sol-gel precursors could attach. Modification with plasma-polymerized acrylic acid yielded hydrophilic PDMS surfaces for several days,[52] and a poly(urethaneacrylate) coating was shown to lead to a significantly reduced rate of swelling by solvent absorption.[53]

2.1.3. Precursor formulations

Any physically drying sol-gel system, dispersion, polymeric, colloidal, or ionic solution can in principle be used as a precursor for patterning. Essentially, homogeneous solutions and particle suspensions can be distinguished. The components in the precursor "*ink*" should be at least approximately one order of magnitude smaller than the feature sizes of the pattern. Other requirements for the precursor depend on the actual patterning process.

Different chemistries have been utilized to make precursor formulations for pattering. They are essentially similar to the chemistries that are employed for wet-chemical processing of ceramic thin films.[54-56] Especially sol-gel chemistry, metal-organic decomposition (MOD), and chemical bath decomposition (CBD) are popular. Apart from achieving a high solids content in solution, which is not possible in combination with low viscosity, these chemistries can easily meet most of the other requirements mentioned above. Only in cases where patterns with a high aspect ratio are required, or

the chemical transformation from liquid precursor to final ceramic phase has to be avoided, suspension-based precursors are preferentially utilized.

***Sol-gel processing**:* This is the most commonly used chemistry for precursor solutions. Sol-gel alkoxide chemistries can be divided into two classes, depending on whether or not the element silicon is involved.[57] In silicon alkoxide chemistry, hydrolysis and condensation of molecular precursors $Si(OR)_4$ or R'-$Si(OR)_3$ into condensed pre-polymers proceeds via the following two fundamental reactions:

$$\text{Hydrolysis} \quad = Si{-}OR + H_2O \xrightarrow{H^+} = Si{-}OH + ROH$$

$$\text{Condensation} \quad = Si{-}OH + HO{-}Si = \xrightarrow{H^+} = Si{-}O{-}Si = + H_2O$$

Here R represents an alkyl group, and R' an arbitrary side group that can carry virtually any functionality. The reactions are catalyzed by protons and hydroxyl groups. This chemistry has been employed for making low-*k* dielectrics, such as porous silicas and organosilicas. The reactions are usually carried out in alcoholic solution with some water added, see *e.g.* refs.[58-61] Furthermore, lower alcohols are compatible with PDMS.[23] By controlling the reflux, catalysis and hydrolysis conditions, the nature of the resulting solution precursors and gels can be controlled. An advantage of $Si(OR)_4$ and silsesquioxane R'$Si(OR)_3$-based sols is that they can be made in a relatively stable form even at high solids concentrations. This minimizes shrinkage upon gelation. And since no crystallization or precipitation occurs, the replicated pattern shapes can be retained more easily.

Similar formulations can also be made using non-silicon alkoxides, *e.g.* $Ta(OC_2H_5)_5$,[62] $SnCl_2$,[63] and $Ti(OC_2H_5)_4$[64] in ethanol or 1-propanol. However, the details of the chemistry of hydrolysis and condensation are different since the reactions are thermodynamically rather than kinetically controlled,[57] and precipitation will eventually occur upon drying.

Many synthetic approaches start from short-chain carboxylate precursors dissolved in carboxylic acid, *e.g.*, $M(CH_3COO)_n$ in acetic acid, and metal alkoxides.[55] The carboxylic acid serves both as solvent and as chelating stabilizer for the very reactive metal alkoxides, and some exchange of ligands takes place after mixing. In this way precursor formulations for $Pb(Zr,Ti)O_3$ (PZT)[65] and $BaTiO_3$ (BTO)[63] have been prepared. During drying, they react with water to form condensed structures. Also the formation of ZnO from $Zn(CH_3COO)_2$ and water is an example of such a process.[63]

***Metal-organic decomposition (MOD)*:** In this approach metal carboxylates and acetates with long-chain ligands are dissolved in a common unreactive solvent, usually

xylene.[55] Since the starting compounds are insensitive to water, the metal organic solutions are essentially simple mixtures of the starting compounds. The inorganic phase is only accomplished in the final thermal treatment step after patterning and drying. The precursor formulation has a low surface energy, but a serious disadvantage of xylene as a solvent is the high degree of swelling that PDMS undergoes when it is exposed to non-polar solvents.[23] MOD synthesis has been employed to pattern several complex oxides, *e.g.*, epitaxial $SrBi_2Ta_2O_9$ (SBT)[66] and PZT.[67]

Chemical bath decomposition (CBD): This synthesis route is used to grow solid films from solution by single or repeated immersions of a substrate in a bath. Usually pH, temperature and/or composition of the source solution are adjusted.[56] When pre-patterned substrates are employed, site-selective nucleation and growth may occur. This approach has been explored in particular by the group of Koumoto at Nagoya University.[14] A typical example is the formation of titania from $(NH_4)_2TiF_6$ and H_3BO_3:[68]

$$TiF_6^{2-} + 2\ H_2O \rightarrow TiO_2 + 4\ H^+ + 6\ F^-$$
$$BO_3^{3-} + 4\ F^- + 6\ H^+ \rightarrow BF_4^- + 3\ H_2O$$

The second reaction scavenges the produced fluoride and is used to control the rate of titania formation.[69] The bath solutions are usually very dilute, so they are not commonly used in molding-based processes.

Nitrate route: This route has been used in soft-lithography by few researchers.[70, 71] Essentially, the precursor solution is made by simply dissolving metal nitrates. To avoid substrate dewetting and recrystallisation phenomena during drying of the precursor, metal-coordinating polymers such as poly(acrylic acid) can be added to the solution.[70]

Suspensions: Suspensions are employed in particular in those cases in which relatively large dimensions, and/or patterns with high aspect ratios are targeted.[72, 73] The volume fraction of solids in suspensions can be raised to higher values than is possible with the solution based approaches described above. Moreover, although the relative degree of shrinkage of a precursor solution upon drying and consolidation may be independent of the actual size of the feature that is formed, absolute shrinkage scales with object size. This is why high aspect-ratio objects with dimensions above 10-20 μm are best made from suspension-based precursors. The successful use of suspensions with solids volume concentrations up to 40 vol% and reasonable viscosities has been reported.[73]

The four key physical properties of precursor solutions and suspensions are:

1. **Solids content (or equivalent)**: High solids contents are favourable since the metal concentration is related to the solids volume in the final oxide. Shrinkage upon drying and thermal after-treatment is suppressed when the solids content is increased. For instance, the quality of shape replication in molding-based processes is improved when the metal concentration in the precursor is increased.[73]
2. **Viscosity and rheology**: In MIMIC, low viscosities are needed in order to enable fast penetration of the precursor into the micropatterned channels.[73] This implies a high solvent concentration and low solids content. If necessary, raising the temperature during patterning may help to decrease the viscosity of the precursor further.[74] The shear rate dependence of viscosity is particularly important when non-Newtonian fluids are applied in MIMIC, since the rate of penetration is not constant during the patterning process.[73]
3. **Surface energy**: The surface tension of precursor solutions determines the wetting interaction of the ink in the mold, as will be discussed in more detail in sections 2.1.4 and 2.2. Low surface tension promotes wetting of a relief-patterned stamp and is required when water-based solutions are employed, but good wetting may hamper the debonding step in which stamp and ink are separated.[75]
4. **Types of solvents**: The concentration and volatility of solvents determines the drying rate and drying time. Faster evaporation will lead to faster solidification of a precursor, and increase the through-put that can be accomplished in industrial processes. On the other hand, it has also been shown that the packing efficiency of particle-based suspensions is improved when the drying process inside the channels proceeds slower.[76] Alternative ways to slow down the drying rate are soaking of the mold in the solvent prior to use, and/or drying in atmospheres in which solvent vapour is already present. Solvent types also determine the degree of swelling of the elastomeric mold.[23]

2.1.4. Wetting, demolding, and thermal after-treatment

Optimal wetting of microchannels by fluids is an important factor in molding-based approaches. A rich variety of mechanically stable, metastable, and unstable liquid morphologies can be found, [77, 78] depending on (i) the contact angle between fluid and surface, and (ii) the geometric details (aspect ratio) of the grooves.

Obviously, a very large contact angle (>90°) indicates that the interfacial energy between ink and mold is rather unfavourable. This promotes the dewetting (debonding) of the grooves of a mold, in particular when the height-to-width aspect ratio of the structure is smaller than 0.5. When the aspect ratio is higher, even fluids with a very

large contact angle can fill microchannels in a thermodynamically stable way. Small contact angle fluids fill the channels spontaneously,[78] but release from the mold after patterning may be problematic.[75] When the contact angle is smaller than 45°, wedge wetting may occur, a thermodynamically stable mode of filling in which only the corner edges of a channel are filled with fluid.[78] The special feature of wedge wetting is that feature sizes can be printed that are much smaller than the resolution of the mold. In order to print (polymeric) patterns that resemble the shape of the stamp, one should work in a wetting regime where the liquid forms elongated channels with negligible Laplace pressure.[77]

It has been shown theoretically that relatively large contact angles between mold and precursor solution are required to facilitate debonding after molding-based patterning, ideally >90°,[75] **see Figure 2.2**. Under such conditions the energy released per unit area of crack (debonding) extension, is very large for small cracks. This promotes the release of dried precursor from the mold. For contact angles smaller than 90°, the driving energy for crack propagation is rather small and concave surfaces effectively inhibit debonding.

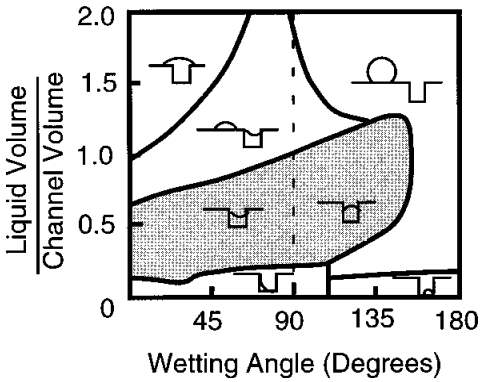

Figure 2.2: Equilibrium configurations of a liquid on a channelled stamp. The ratio of liquid volume over channel volume is plotted versus contact angle of the liquid. The grey area represents the conditions in which channel filling is stable. Reprinted with permission from ref.[75] (Copyright 1999, American Institute of Physics)

Most of the formed patterns require a post-patterning heat treatment step to convert the dried precursor into the desired crystalline phase, remove residual organics and densify the thin film. Due to the small sizes of the features to be sintered, relatively low sintering temperatures and short sintering times are sufficient. Shrinkage presents a serious technical problem in ceramics processing in general and in the micro- and nanopatterning of ceramics in particular, since it limits the quality of pattern

replication. An overall shrinkage of 80-95% is common for many of the reported chemistries.[65, 70] For many applications this may not present a problem. However, when more complex, hierarchical patterns are to be realized, factors like 3D topography, shape replication fidelity, and edge sharpness become crucial factors to consider.[38, 79]

Cracking may present a problem, but micropatterned ceramics are able to release mechanical stresses in both the vertical direction and lateral direction, and this helps to form higher structures than would be possible in the case of continuous thin films. It has been shown that there are limits to sub-micrometer resolution patterning of macromolecular fluids and low molecular weight polymer because of the Rayleigh instability.[46] The Rayleigh instability is primarily a geometrical effect, and becomes relevant for pattern transfer in the 100-1000 nm range. Where precursor solutions and suspensions are concerned, the extent to which this effect can play a role depends on the rate at which the precursor solution dries physically via evaporation of solvents, and/or condenses chemically into a higher molecular weight network.

2.2. Molding-based patterning techniques

2.2.1. Microtransfer molding (μTM)

Micro-transfer molding has not been explored widely for the formation of metal oxide patterns, which is somewhat surprising considering its speed, ease of patterning isolated features, and ability to pattern on non-planar substrates. The concept of microtransfer molding was introduced by Zhao, Xia, and Whitesides in 1996 and demonstrated for several polymers and spin-on glasses.[8] From a simple model it can be concluded that the following general condition should be fulfilled in order to both pattern and demold line features:[80]

$$\gamma_{sol} < \gamma_{mold} < (2a+1)^{-1}\gamma_{substrate} \qquad (1)$$

Where "a" is the aspect ratio of the line structure, and γ_{sol}, γ_{mold} and $\gamma_{substrate}$ are the surface energies of liquid precursor solution, mold, and substrate on which the pattern is formed, respectively.

Lange and co-workers described the epitaxial patterning of 500 nm wide lines of ZrO_2 on single crystal cubic zirconia, and the epitaxial patterning of 50 μm wide lines of $SrBi_2Ta_2O_9$ (SBT).[66, 75] Metal-organic decomposition (MOD) solutions of metal (Sr,Bi,Zr) 2-ethylhexanoates and tantalum ethoxide in xylene were spin-cast onto a patterned PDMS mold, and transferred to the substrate. In the case of SBT, it was shown that the oxide had a (00*l*) out-of-plane orientation after thermal processing, and a single in-plane orientation on (001) $SrTiO_3$. Microtransfer molded patterns have also

been reported in a few other cases, *i.e.*, mesostructured mesoporous silica lines of 1-3 μm width and 1-2 μm height with a low refractive index (1.15) for waveguide arrays.[81] Nanotransfer molding with elastomeric PDMS molds has been demonstrated for PZT line and pit patterns with lateral resolutions down to 100 nm, and a feature height of ~25 nm after thermal treatment.[80]

Patterns with much higher aspect ratios can also be made by microtransfer molding, *i.e.*, for the fabrication of ceramic microcomponents for microelectro-mechanical systems (MEMS).[72, 82-84] Such components are typically in the millimetre size range, they contain features of 30-100 μm, and have high aspect ratios of up to 10. Because of their large sizes it is of the utmost importance to minimize shrinkage upon drying and thermal post-treatment. Concentrated ceramic suspensions of α-alumina with up to 80-84 wt% solids were therefore used with added dispersants. Smaller features in the micron range would be possible if finer particles with 0.1-0.2 μm would be used, but these also suffer more from shrinkage.[85] It is important to form the feature directly in its final form, since post-processing such as grinding and polishing are difficult, especially on the scale of the feature sizes. Due to the high viscosity of the used suspensions, centrifugal casting has been introduced to improve the filling of the PDMS mold, and thereby the densification of the green bodies within the molds. This process has been termed centrifugally aided soft molding (CASM).[84]

2.2.2. Micromolding (Embossing)

Micromolding is much more commonly used for patterning oxides than transfer molding. All-printed all-inorganic transistors, photodetectors, resistors, and multilayer structures with sacrificial layers and vias have been made.[86] An advantage of micromolding is that less stringent conditions apply to the wetting properties of the precursor solution or dispersion with respect to the mold than in microtransfer molding. Nonetheless, Marzolin *et al.* pointed out that the liquid should spontaneously dewet the elastomer surface so that the protruding parts of the mold make conformal contact with the substrate, and thus avoid a residual layer.[60] The dewetting process is driven by both the applied pressure and the differences in interfacial tensions, *i.e.* substrate-elastomer γ_{SE}, substrate-liquid γ_{SL}, and liquid-elastomer γ_{LE}. The dewetting speed is proportional to S, where

$$S = \gamma_{SL} + \gamma_{LE} - \gamma_{SE} \qquad (2)$$

Since γ_{LE} is more or less fixed, the solution can be optimized by adding low viscosity solvents with a high surface tension which do not swell the mold.[60] Residual layers are very hard to be avoided.[87] For applications in which merely a patterned surface is

needed, this may not present an important issue. However, when isolated features are required, an etching step or another equivalent method to remove residual material between the patterned features will be necessary. The reported studies fall roughly in two categories, a) namely silica glasses and silicate-organic hybrid materials for optical and dielectric applications, and b) non-silicon based functional metal oxide materials, *e.g.*, ferroelectrics and electrically insulating materials. These will be discussed separately below.

1. Glasses and hybrids for optics and dielectrics

The first papers date back to 1988[58] and precede the soft-lithography era which started in 1993.[7] Tohge *et al.*[58] reported the fine-patterning of sol-gel derived boron-doped silica on glass substrates. Features with a width of 1.2 μm and thicknesses of 100-300 nm after thermal treatment were made. The nature of the rigid mold was not mentioned.

Optical waveguiding applications typically require thicker patterns, in the order of one micrometer. Alternative materials were proposed to meet this criterion, such as organically modified ceramic (ORMOCER) from a precursor mixture of methacryloxypropyl trimethoxy silane, methacrylic acid, and zirconium alkoxide.[59] ORMOCERs have a lower elastic modulus and are more ductile than inorganics, so shaping the precursor into the mold is easier, while cracking occurs less easily during the embossing step. Square array and line patterns after UV curing had lateral dimensions of 10 μm and a thickness of no less than ~3 μm. The aspect ratio of about 0.3 is still quite modest.

Soft-lithographic patterning of sol-gel solutions using PDMS was first demonstrated by Marzolin *et al.*[60] They employed a tetramethylorthosilicate-based solution, an elastomeric mold with micrometer-sized features, and applied a pressure onto the mold of about 0.7 bar during the process. Glassy titanosilicate (Ti/Si=0.07) membranes, and aluminosilicate (Al/Si=0.09) and borosilicate (B/Si=0.1) line patterns with waveguiding capacity were formed following the same approach. When sol-gel derived organic-inorganic hybrid materials such as silsesquioxanes and organosilanes are applied to the micromolding technique instead of glass precursors, the hardness and shrinkage can be optimised by adjusting the type and amount of organic groups. Mixed sol-gel solutions of $(MeSiO_{3/2})$-(SiO_2)[88] and $(MeSiO_{3/2})$-$(C_6H_5\text{-}Si\text{-}O_{3/2})$[79] on glass can replicate the features of a mold nearly perfectly with minimal shrinkage (~4%), provided that a hard mold is used. Moreover, optical properties like transmittance and refractive index can be controlled through proper selection of the organic groups, which is why these materials are so popular for these applications.[89] A comparison between soft-lithographically produced photonic crystal laser resonators from epoxide- and methyl-functional organosilanes, and photolithographically fabricated resonators in

silicon showed that the laser emission spectra were of equal quality.[90] Patterned features were ~500 nm in width and ~50 nm in depth, and could be solidified at 60 °C.

Closely related sol-gel processed organosilicas have been studied for use in interlayer dielectric (ILD) insulator films. The low dielectric constant $k < 2.3$ that is required in next generation ILDs to suppress cross-talk between neighbouring interconnect lines and minimize power dissipation can only be realized by introducing large-scale nano-porosity. Other requirements are an elastic modulus $E>6$ GPa, and a low thermal expansion coefficient TEC<30x10^{-6} °C^{-1}. Ro *et al.* demonstrated nanoporous poly(methylsilsesquioxane)-based patterns that meet all these requirements.[91] Nanoporosity was introduced into the patterned material by incorporating a poly(ethylene oxide)-*b*-poly(propylene oxide) copolymer amphiphile in the liquid precursor, a concept that was originally introduced by Yang *et al.*[92] The surfactant was burnt out in the final thermal treatment step. The porosity was ~20%.[91] The mold was a rigid silicon oxide line gratings structure with 100 nm width and 170 nm height, with a pitch of 200 nm. During imprinting, pressures up to 34 bar, and temperatures up to 200 °C were applied, and the features of the mold could be replicated with high fidelity. Only modest shrinkage occurred, mainly in the vertical direction. In a later study,[93] the same group showed that decreasing the block copolymer porogen concentration in the solution led to lower levels of mesoporosity (pore size > 2 nm), but a substantial degree of microporosity (pore size << 2 nm) remained. The net effect was a decreased interconnectivity in the pore network, which is beneficial for electrical insulation. Moreover, it was shown that a dense skin formed over the patterns during the process. The skin can protect the porous ILD structure from reactive sources of contamination in subsequent processing steps.

Researchers from Philips Research demonstrated a soft imprinting technique with which they fabricated a 3D photonic woodpile structure made of sol-gel silica.[94] They employed a PDMS mold and used a combination of gravity and capillary force to imprint the mold into the wet layer. No external pressure was applied. In this way the distortion of the mold could be kept smaller than 0.03 % over an area of 15x15 mm^2. They imprinted a pre-dried 88 wt% methylsilsesquioxane-silica (1:1 molar ratio) thin film. The high solids content ensured minimal shrinkage (~7 %) during drying, and good shape replication of the square woodpile structures of 70x65 nm^2, which is crucial for making photonic crystals. After deposition of each line pattern, the empty volume between the lines was filled with polystyrene to planarize the layer for deposition of the next line grating. As polystyrene dewets the upper surface of the hydrophobic silica grating at elevated temperatures, a completely planar layer could be accomplished by exactly dosing of the amount of polystyrene to fill all voids between the woodpiles, and raising the temperature to 150 °C. Four layers were realized. Residual layers (~15 nm thick) after imprinting were removed with a short acid etch.

Solvent-free thermally curable epoxy-terminated siloxane prepolymers for low pressure NIL have also been developed.[37] A suitable prepolymer for this process should have a low viscosity at room temperature, while curing time and temperature should be minimal. As the process is solvent-free, shrinkage is minimal, and the time of solidification is short. The final polymer should be rigid to avoid deformation and exhibit good adhesion to different substrates (silicon, silica, GaAs, organic films), and the chemical structure of the polymer should allow for wet etching in organic solvents or aqueous solutions. The viscosity of the reported prepolymer was <10 mPa s at room temperature, and by stoichiometric reaction with diamines it was transformed into an epoxy-amine network. Line patterns of 60 nm width, 80 nm height, with a residual layer less than 20 nm thick were demonstrated. Imprinting even smaller features resulted in line deformation and collapse. An alternative solvent-free route to UV curable high refractive index organic-inorganic hybrids with both hydroxyl and vinyl functional groups has also been reported. [95] These materials were applied as imprint resist in NIL on 100-300 nm length scale. Polysiloxane prepolymers were made by non-hydrolytic alkoxylation of 3-(trimethoxysilyl)propyl methacrylate, diphenylsilanediol,[95] and titanium ethoxide precursors,[61] using $Ba(OH)_2 \cdot xH_2O$ as basic catalyst. The viscosity of the prepolymer was controlled between 20 and 220 mPa s,[96] so that little pressure was required to imprint a pattern. Imprinted layers were made using patterned PDMS, followed by low energy UV cross-linking of the reactive vinyl groups.[61, 97] Since PDMS is transparent, the pattern can be UV cured through the PDMS mold. Typical curing times were 30 s, using 365 nm UV light.[61, 98] It was shown that the refractive index of the hybrid material could be tuned between 1.47 and 1.53 to meet the requirements for waveguiding and photonic crystal applications.

A fluorinated version of the material with a relatively high E-modulus of 40 MPa, low surface tension, low shrinkage, and high etching resistance was also developed.[38, 96] It has been tried out as imprint resist,[99] but since the viscosity of the fluorinated prepolymer was rather high, it left a rather thick residual layer. The material is more interesting to be applied in nanopatterned molds for imprinting other materials.[96] The adhesive strength is low, substantially lower than non-fluorinated hybrids and even lower than perfluorocyclobutane, see **Table 2**.[98]

Table 2: Surface tension of imprinting materials and the adhesive force of the PDMS mold to each material. (Table adopted from ref. [98])

Imprinting materials	Surface tension (mN/m)	Adhesive force (mN)	Adhesive force/unit area (nN/nm^2)
Fluorinated methacryl hybrimer [98]	15.9 – 22.3	0.78-0.88	0.138 – 0.156
Methacryl hybrimer [95]	28	2.45	0.435

Perfluorocyclobutane	22.6	1.15	0.204
Tri(propylene glycol) diacrylate	30.3	2.5	0.43
PMMA	41.1	6.5	1.16

The flexibility of this so-called fluorinated hybrimer is lower than that of PDMS, which complicates achieving good conformal contact between mold and substrate. The prepolymer was therefore mixed with acrylate monomers to increase the flexibility of the resulting mold material. Alternatively, to make the material suitable for application as imprint resist, *tert*-butyl acrylate was added to the prepolymer to lower its viscosity.[38] Feature sizes as small as 40 nm with perfect replication of the shape of the mold were fabricated, as illustrated in **Figure 2.3**.

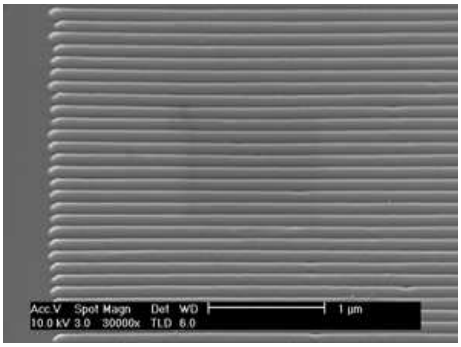

Figure 2.3: Imprinted line pattern on fluorinated resist with a line width of 40 nm using a modified flexible fluorinated hybrimer mold. Reprinted with permission from ref.[38] (Copyright 2006 Institute of Physics)

Titania films with a high density of high aspect ratio pores or pits perpendicular to the surface, and a diameter of 35-65 nm were made by imprinting a sol-gel titania with a hard PMMA mold and a soft PDMS mold that consisted of irregular arrays of rods.[64] The aspect ratios were 2 to 3. PDMS did not work well due to its low Young's modulus.

2. Functional metal oxides

The fabrication of complex three-dimensional lead zirconate titanate ($PbZr_xTi_{1-x}O_3$; PZT) micropatterns with 10–150 µm features and aspect ratios of 3-10 for microelectromechanical systems (MEMS) has been demonstrated using a lost mold method.[72, 82] PZT powder and an organic binder were calendered into a viscous polymer processed ceramic tape, which was subsequently embossed by a mold at 10 MPa. After drying the tape the PMMA mold was dissolved in acetone or chloroform.

The remaining left-over composite patterns were then calcined and sintered into solid PZT. Removal of the mold without damaging the green structure was found to be difficult when feature sizes were below 100 μm and aspect ratios >3 were targeted.

Nanopatterned arrays of PZT with 200-350 nm resolution have been made by imprinting sol-gel and MOD based precursor films with a hard silicon mold[67, 80, 100] and soft PDMS.[80] To maintain the shape of the imprinted pattern it is necessary that the grain size after annealing is at least an order of magnitude smaller than the feature size of the pattern. In practice the MOD-based imprinted patterns were found to have grains of 250 nm, close to the feature size, while the sol-gel based pattern has grains of 35 nm at a pattern height of ~50 nm. Loss of lead during annealing is an increasingly important issue in PZT nanostructure fabrication as the surface-to-volume ratio increases. In this study lead loss seemed to depend on the chemistry of the system, being more serious for MOD patterns than for sol-gel based patterns.

It has also been shown possible to pattern ferroelectric $PbTiO_3$ phase in lines and dots of 700-1000 nm width on $SrTiO_3$(001), with the $PbTiO_3$ grown epitaxially.[70] However, the shrinkage during drying and thermal after-treatment is in all cases very high. For example, ZnO and Al_2O_3 patterns that were embossed from poly(acrylic acid) (PAA)-based polymeric metal nitrate solutions typically exhibited a shrinkage of 80 % or more.[70, 87] Non-patterned continuous films shrunk only in the vertical direction, because of the constraint imposed by the substrate. Patterned films also showed lateral shrinkage by 40-90 %, depending on the nature of the substrate and/or the patterned material. Imprinting a PZT/Au bi-layer film in a single imprinting step is nonetheless feasible, as illustrated in **Figure 2.4.**[101, 102] In comparison with a single-layer PZT film, the profile in the bi-layer PZT/Au was much deeper and clearer. Apparently the soft gold cover layer helps to shape the PZT film.

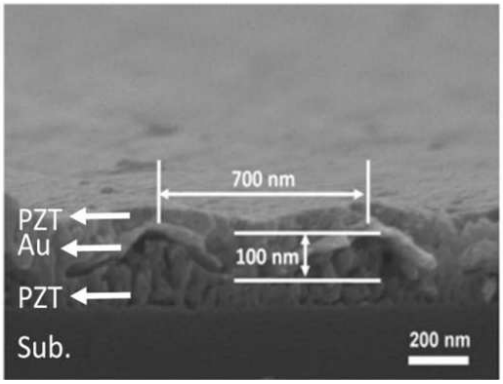

Figure 2.4: Electron microscope image of a PZT/Au/PZT nano-imprinted structure after sintering. Reprinted with permission from ref.[102] (Copyright 2008 Institute of Physics)

Sub-500 nm structures of various sol-gel derived functional oxides (TiO_2, SnO_2, ZnO, $In_xSn_{1-x}O_2$ (ITO) and $BaTiO_3$) with high aspect ratios were recently demonstrated by using a perfluoropolyether (PFPE) elastomer as mold material.[63] PFPE has a very low surface energy (γ<<20 mJ/m^2), is permeable to gas, and chemically inert to most solvents. The gas permeability of the molds allowed complete filling by the precursor, and drying of the embossed film. Nanoscale arrays with features of ~200 nm width, and aspect ratios up to 2.5 over mm-scale areas were realized.

Nanometer-scale titania features have also been made with conventional micrometer-scale patterned elastomers by exploiting the edge topography of the elastomer-substrate corner.[103] Essentially, a conventional PDMS mold was imprinted (p~0.08 bar) into a wet film of dilute sol, after which the film is dried while the mold was held in place. The capillary force drove the solution to form menisci between the stamp protrusions. At the same time, the solution moved to the edges of the stamp protrusions due to capillary flow, which resulted in isolated structures smaller than the lateral spacing of the stamp's protrusions. The dimensions could be controlled by setting the concentration of the solution, the duration of solvent evaporation, and the temperature. It may provide a facile route for fabricating large area patterns of metal oxide. The same strategy, i.e., exploiting the thermodynamically favourable confinement of the corner region to fabricate inorganic or hybrid structures with features smaller than the protrusions of the stamp, has also been demonstrated in a somewhat related gas phase process,[104] as discussed in the next section.

A variation to conventional micromolding was proposed and elaborated by the Gauckler group from ETH Zurich. Instead of molding a ceramic relief pattern on a flat substrate Schönholzer *et al.*, [85, 105] cast colloidal alumina suspensions onto pre-patterned substrates. Photoresist patterned silicon substrates were employed.[85] Defect-free ceramic replicas of alumina, zirconia, Gd-doped CeO_2, and tin oxide with a pattern resolution of ~1 μm and aspect ratio below 1 after sintering were accomplished in hydrophobic molds.[105] Hydrophilic molds suffered from too much adhesion between mold and ceramic, resulting in defect formation during the demolding step. The same approach has been employed later by others with different types of precursor solutions and patterned substrates, in a number of cases aimed at the fabrication of stand-alone ceramic micropatterns and nanopatterns.[106, 107] Examples are the fabrication of sol-gel titania nanowires on a groove patterned polymer,[106] AlN by reactive sputtering on micropatterned noble metal substrates,[108] PZT micro-cantilevers in silicon,[107] titania and graded titania-iron oxide nanorod arrays with 120 nm features by CBD on pre-patterned silicon and bioden acetate substrates,[109, 110] and titania gratings and arrays on indium tin oxide.[111]

A relatively recent nanoscale molding-like technique was proposed by Dravid and co-workers.[112] After creating a 3D patterned polymer-based resist film on a hard substrate using soft e-beam lithography, all formed voids in the resist film were filled with a spin-on sol-gel precursor, followed by removal of the resist and consolidation of the sol-gel. In this manner functional patterns of ZnO,[113] $BiFeO_3$,[114, 115] $BaTiO_3$,[116, 117] and $CoFe_2O_4$,[117] with resolutions down to 40 nm were made. The method illustrates how small the features are that can be realised with sol-gel chemistry. Although e-beam lithography is strictly speaking a serial patterning approach, similar objects and patterns would also have formed when a parallel pre-patterning technique had been used to make the bas-relief pattern.

2.2.3. Micromolding in capillaries (MIMIC)

The concept of Micromolding in Capillaries (MIMIC) was proposed by the Whitesides group in 1996.[27] Along with a number of polymers, they demonstrated it for a low viscosity spin-on glass, poly(ethoxymethylsiloxane), which was converted into silica by pyrolysis at 400 °C in air. The obvious advantage of MIMIC in comparison with micromolding and microtransfer molding is that the mold is dry when it is placed on and makes conformal contact with the substrate. Residual layers are therefore avoided. Hence, MIMIC could contribute to an all-additive fabrication scheme, excluding subtractive etching steps to remove undesired material. The applicability of the method has been illustrated by the fabrication of a tin oxide based microsensor,[118] and patterned etch resists in the fabrication of silicon MOSFETs (Metal Oxide Semiconductor Field Effect Transistors).[119] The latter study demonstrated the compatibility of MIMIC with Si fabrication processes.

Possible disadvantages of MIMIC are that (i) it is a quasi-parallel patterning technique with an inherently lower rate than true parallel patterning processes, (ii) the formation of isolated features is impossible, and (iii) the precursor viscosity should be low in order to ensure acceptable filling rates. The rate of infiltration of the precursor into the channel decreases as the length of the capillary increases. For a tubular channel with a hydraulic radius R, the rate of penetration dz/dt is expressed by the Washburn equation:[120]

$$\frac{dz}{dt} = \frac{R\,\gamma_{LV}\cos\theta}{4\eta z} = \frac{R\left(\gamma_{SV} - \gamma_{SL}\right)}{4\eta z} \qquad (3)$$

Here z is the length of the liquid capillary inside the channel, η is the viscosity of the penetrating liquid, R is the ratio between capillary volume and the surface area of the channel, and θ the contact angle of the fluid meniscus inside the capillary. The surface

tensions γ_{LV}, γ_{SV} and γ_{SL} are the surface tensions between liquid and air, channel wall and air, and channel wall and liquid, respectively. It follows after integration that

$$z(t) = \sqrt{\frac{R(\gamma_{SV} - \gamma_{SL})t}{2\eta}} \quad (4)$$

The equation shows that although the capillary force of a channel increases with decreasing hydraulic radius R, this effect is more than counterbalanced by the increased friction exerted by the channel walls, so filling rates are lower in smaller channels. A generally applicable method to increase the filling rate is to reduce the viscosity of the precursor solution by increasing the temperature during the MIMIC process,[74] but it has not been exploited for patterning ceramics to date.

The main driving force for MIMIC is the free energy change ΔG upon filling the channel with a fluid. For a square channel with width and height a, the free energy gain can be approximated by:[120]

$$\Delta G(t) = -a\, z(t)\, \gamma_{LV} (3 \cos \theta_{mold} + \cos\theta_{substrate}) \quad (5)$$

where θ_{mold} and $\theta_{substrate}$ are the contact angles of the liquid with the surfaces of the mold and the substrate, respectively. Detailed modelling and experimental studies have been reported by Huang, Liu, and Li.[121] For a hypothetical square channel with different contact angles θ_1, θ_2, θ_3, θ_4 for each of the surface walls, the equivalent contact angle θ can be expressed as:

$$\cos \theta = ¼ (\cos \theta_1 + \cos \theta_2 + \cos \theta_3 + \cos \theta_4) \quad (6)$$

The pressure drop Δp_{LV} over the meniscus of the capillary front for a square channel with sides a is given by:[121]

$$\Delta p_{LV} = \frac{4\gamma_{LV} \cos\theta}{a} \quad (7)$$

Hence, when the equivalent contact angle in Eq. (7) is smaller than 90°, spontaneous penetration into the channel occurs because of the positive pressure drop. Although penetration should be theoretically possible even in very narrow channels, numerical analyses and experimental evidence showed that surface tension can affect the filling

rate in a negative manner to such an extent that even pore blockage can occur near the exits of very small channels.[122] Optionally, the driving force for liquid penetration could be increased by 1 bar by generating a low vacuum in front of the penetrating liquid.[123]

The shape of the imbibition front of liquid precursors has been studied in detail.[120, 121] Depending on the surface energy of the channel wall γ_{SV}, different spreading regimes can be observed, as illustrated in **Figure 2.5**. Liquids penetrating a channel with walls of low surface energy show capillary fronts that advance as a whole. But as the surface energy of the channel increases, precursor structures advancing in front of the macroscopic body of liquid are observed, especially in the corners between mold and substrate. Some of these structures include slipping films and shoulders. Similar regimes have been observed with differences in the velocity of imbibition on surfaces of constant γ_{SV}.[120] The thermodynamics of wetting on patterned surfaces has been studied in detail by Seemann *et al.*[77, 78] as discussed in section 2.1.4. Modelling of the dynamics for penetrating liquids that have varying advancing contact angles with different walls of the channel indicate that a rich variety of capillary front shapes are possible.[121]

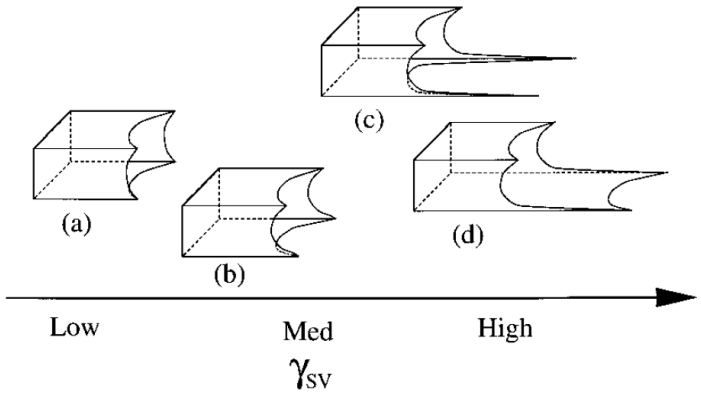

Figure 2.5: Schematic summary of different spreading regimes observed in MIMIC. Shapes of the penetrating liquids in PDMS capillaries are formed on (a) SAMs with low γ_{SV}, (b and c) SAMs with medium γ_{SV}, and (d) SAMs with high γ_{SV}. Reprinted with permission from ref.[120] (Copyright 1997 American Chemical Society)

The typical non-uniform cross-sectional topography, illustrated in **Figure 2.6** for patterned sol-gel PZT lines after drying and consolidation, was observed in several other studies.[65, 124, 125] The film thickness is greater near the lateral edges than in the middle. The phenomenon can be explained by preferential wetting of the gel to the corners of the PDMS mold, and subsequent locking-in of the structure by accelerated

drying rates at the corners. The double peak profiles were less prominent and had a higher density when the patterns dried more slowly.[65]

Quite a number of functional materials have been patterned using MIMIC, in most cases by employing low viscosity sol-gel precursor solutions. In the 1-10 μm lateral resolution scale, functional oxide micropatterns of SnO_2 and ZrO_2,[124] PZT and $Sr_2Nb_2O_7$,[125, 126] and $La_{0.7}Sr_{0.3}MnO_3$,[71] have been reported. Several luminescent materials have been patterned, *i.e.*, the green luminescent layered perovskite-type hybrid $PbI_4(C_6H_5C_2H_4NH_3)_2$ (resolution 0.8-50 μm),[127] YVO_4:A (A=Eu^{3+}, Dy^{3+}, Sm^{3+}, Er^{3+}),[128] $La_{9.33}(SiO_6)_4O_2$:A (A=Eu^{3+}, Tb^{3+}, Ce^{3+}),[129] Y_2O_3:Eu^{3+}[130] A_2SiO_5 (A=Eu^{3+}, Tb^{3+}, Ce^{3+}),[131] and Rhodamine B doped epoxy-functional organosilica[132] have been made. Also non-oxide ceramics SiC[133] and SiCN[134] have been patterned using MIMIC.

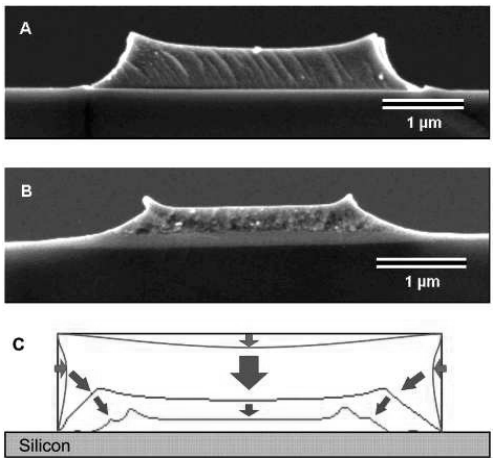

Figure 2.6: SEM images of a cross-sectioned 5 μm wide sintered PZT line on Si patterned from a 1.85 μm depth PDMS mold (a) after drying and (b) after heat treatment and (c) a schematic diagram of the drying process leading to peak formation. Reprinted with permission from ref.[65] (Copyright 2003 American Chemical Society)

Trau *et al.* applied a strong electrical field tangentially to the surface within the capillaries, so that an additional electroosmotic flow force was induced to increase and maintain the flow rate of the precursor.[135] Under these conditions, the viscous forces within the flowing solution were able to align tubular cetyl-trimethyl ammonium chloride surfactant micelles present in the solution parallel to the channel wall. In combination with the ongoing gelation of a silica sol, this resulted in silica

micropatterns with an internally oriented mesostructure.[135] In subsequent work, block copolymer templating of silica to fabricate patterned mesoporous optical waveguides,[81, 136] and the incorporation of close-packed 200-2000 nm polystyrene spheres into silica to make patterned photonic crystals[137] have been reported. Recently, Kim *et al.* developed photocurable 20 μm thick organosilica micropatterns for the immobilization of proteins.[138] The sol-gel hybrid had amine and methacryl functionalities for covalent linking with proteins and photocuring, respectively. Because the amine functionality is incorporated in all siloxane oligomers, immobilizing sites for proteins such as streptavidin are widely distributed over the surface of the material.

Organosilane patterns with nanometer lateral resolution have been made using a MIMIC-like gas phase deposition process using PDMS stamps with micrometer-scale features.[104] The stamps were placed in contact with a silicon substrate, after which the system was exposed to low pressure 3-aminopropyl triethoxysilane (APTES) vapour (p~10^{-5} bar). The precursor condensed selectively along the PDMS-substrate corner lines in the early stages of the process, to form 200 nm wide line patterns with a height of ~7 nm after 3 h of exposure. Long-term exposure led to condensation of APTES on the entire surface, and reduced the lateral resolution of the formed patterns to that of the stamp. The organosilane precursors used for forming such structures can also be supplied by spontaneous release from a preloaded PDMS stamp.[139]

An application for suspension based MIMIC has been demonstrated by the fabrication of a tin oxide gas sensor covering an area of only 10x40 μm^2, about 2 orders of magnitude smaller than commonly used today.[118] The sensor device shown in **Figure 2.7** included a heating element to increase sensitivity and response times, and Pt electrodes to measure resistance (changes) in the MIMIC-patterned SnO_2 lines when exposed to different gas mixtures. The tin oxide colloidal suspension containing 33 vol% solids was optimized for a low viscosity of 25 mPa s at a shear rate of 100 s^{-1}. Nanoparticle solutions and colloidal suspensions with a d_{50} of 280 nm were employed.[140, 141] Although the penetration rates are higher when low viscosity solutions (< 200 mPa s) and low solids loading (<5 vol%) are employed,[142] more concentrated suspensions can also be used, albeit that the penetration length of the suspensions becomes shorter as the viscosity increases.[73] However, the main advantage of higher concentrated suspensions was that higher aspect ratios, up to ~1 for 33-40 vol% SnO_2, could be accomplished.[73] The pattern after sintering consisted of 10 μm wide and 5 μm high lines of 1.0 mm length. The final lines were bell-shaped. No double peak profile[65] occurs here, since no gelation but only physical drying occurred. A practical limitation of MIMIC when applied to suspensions or sol-gels is the considerable degree of volumetric shrinkage that results from drying and thermal after-treatment.

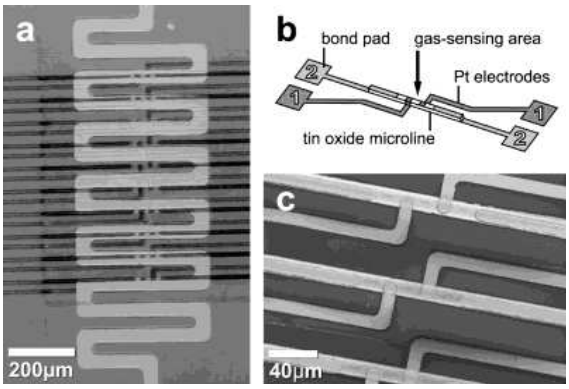

Figure 2.7: (a) Top view of gas sensor set-up seen through the photoresist mask before deposition of the Pt-thin film wires for resistance measurement. Connected ceramic microlines (dark horizontal lines) and heating element were present on each substrate; (b) Schematic drawing of the contact layout for a tin oxide line; (c) SEM of micrometer thick film gas sensors. Reproduced with permission from ref.[118] (Copyright Wiley-VCH Verlag GmbH & Co. KGaA)

In an attempt to overcome this problem for suspensions, Imasu and Sakka recently demonstrated the possibility to form very densely packed beds of powder using low solids suspensions (~5 vol%) and MIMIC. A requirement is that the nanoparticle suspension should be well dispersed into primary particles.[143]

To increase the penetration length, Ahn *et al.* proposed vacuum-assisted filling of channels. Moreover, slowing down the drying process inside the channels improves the packing efficiency of suspension particles.[76, 142] Some examples are shown in **Figure 2.8**. Although lower solids contents were used than employed by Heule and Gauckler, features of the channel were replicated better because of the slower drying process. Optical waveguides[89] and micro solid oxide fuel cells[144] have bee made via this approach.

An alternative solution to the problem of limited infiltration of viscous suspensions is to use a second liquid with large infiltrating capacity to help push the ceramic suspension forward and infiltrate further into the channel.[145] The second infiltrating liquid should be immiscible with the suspension, and be highly volatile, so that it can be easily removed afterwards.

Under the assumption that the ceramic suspension (fluid 1 with viscosity η_1 and surface tension γ_1) has reached position z_1 inside the capillary channel at the moment (t=0) that fluid 2 (with viscosity η_2 and surface tension γ_2) begins to infiltrate, the infiltration depth z_2 of fluid 2 after time t becomes[145]

$$z_2(t) = \sqrt{\frac{R(\gamma_1 - \gamma_2)t}{2\eta_2} + A^2} - A \qquad (8)$$

where $A=\eta_1 z_1/z_2$. In their experimental work, aqueous tin oxide suspensions (37 nm particles, 2 vol% solids) with a viscosity of 9 mPa s, and silicone oil were employed. An improvement of the process was reported, although the reproducibility was not optimal.

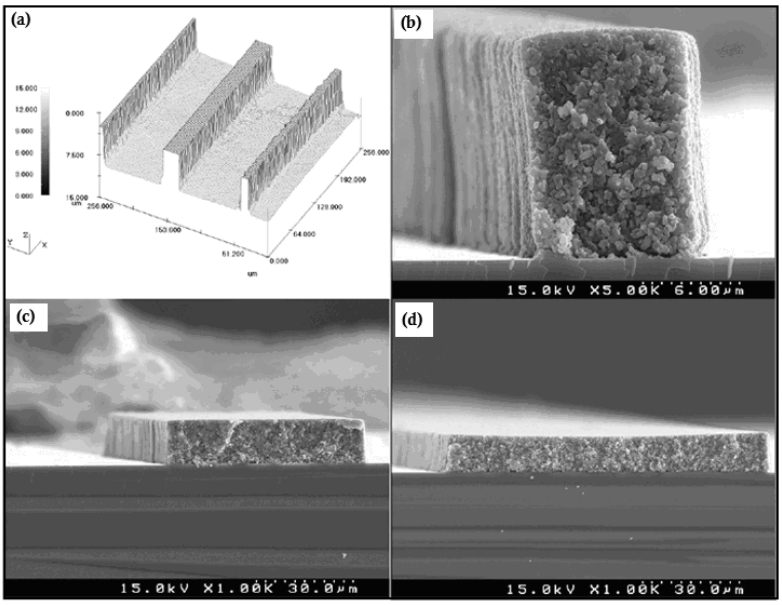

Figure 2.8: (a) Three-dimensional image of thin microlines of 10–20 µm widths; (b) cross-sectional scanning electron microscopy image of a 10 µm pattern made from a dilute suspension of 5 vol% aluminum oxide; (c) Line pattern with a line width of 50 µm; (d) Line with a width of 100 µm from a 20 vol% suspension. Reproduced with permission from ref.[76] (Copyright 2008 Wiley-Blackwell)

A simpler alternative to increase the rate of infiltration was proposed by Jeong, Ahn, and Moon,[89] who filled macroscopic reservoirs in direct contact with the microchannel system with a sol-gel silsesquioxane-based precursor solution. After evacuating the entire chamber to 10 Torr and then returning to atmospheric pressure, the microchannels filled within seconds. Surface modification-based techniques are not in the scope of this thesis and are explained in great detail in the review.[146]

2.3. Conclusions

Many kinds of ceramic materials and hybrids have been patterned in recent years on micrometer and sub-micrometer scale, and nanoscale objects with feature sizes smaller than 100 nm have been reported in literature. Especially with micromolding, a technique very similar to nano-imprint lithography, very small features can be made with high fidelity. Nonetheless, the fabrication of truly high aspect ratio structures still remains a challenge. Well-defined sub-micrometer scale objects with aspect ratios >1 are rarely reported. Furthermore, a fundamental problem concerns the low solids content in precursor solutions and ceramic suspensions. While solids content up to ~40 vol% may be possible in suspensions, much lower solids concentrations (typically <10 vol%) are present in solution-based precursors such as sol-gels. The shrinkage after a pattern has been defined and a wet film has been deposited is therefore considerable. This makes precise shape replication of a mold very difficult, if not impossible.

Besides improvement of lateral resolution and the possibility to register patterns in order to allow multiple layer fabrication,[12] a very important development concerns the ability to pattern ceramics on polymeric substrates. The ability to do so will open up many new possibilities to incorporate functional ceramic materials into low-cost polymer-based devices. A few studies with promising results have already been published in recent years on this topic.

References

[1] Xia, Y. N., Rogers, J. A., Paul, K. E. & Whitesides, G. M. *Chem. Rev.* 99, 1823-1848, **1999**

[2] Geissler, M. & Xia, Y. N. *Adv. Mater.* 16, 1249-1269, **2004**

[3] Gates, B. D., Xu, Q. B., Stewart, M., Ryan, D., Willson, C. G. & Whitesides, G. M. *Chem. Rev.* 105, 1171-1196, **2005**

[4] Henzie, J., Barton, J. E., Stender, C. L. & Odom, T. W. *Accounts Chem. Res.*, 2006, 39, 249-257, **2006**

[5] del Campo, A. & Arzt, E. *Chem. Rev.*108, 911-945, **2008**

[6] Heule, M., Vuillemin, S. & Gauckler, L. J. *Adv. Mater.* 15, 1237-1245, **2003**

[7] Kumar, A. & Whitesides, G. M. *Appl. Phys. Lett*. 63, 2002-2004, **1993**

[8] Zhao, X. M., Xia, Y. N. & Whitesides, G. M., *Adv. Mater.* 8, 837-840, **1996**

[9] Xia, Y. N. & Whitesides, G. M. *Annu. Rev. Mater. Sci.* 28, 153-184, **1998**

[10] Martin, C. R. & Aksay, I. A. *J. Electroceram*. 12, 53-68, **2004**

[11] Rogers, J. A. & Nuzzo, R. G. *Materials Today* 50-56, **2005**

[12] Folch, A. & Schmidt, M. A. *J. Microelectromech. Syst.* 8, 85-89, **1999**

[13] Masuda, Y. *J. Ceram. Soc. Jpn.*115, 101-109, **2007**

[14] Koumoto, K., Saito, N., Gao, Y. F., Masuda, Y. & Zhu, P. X. *Bull. Chem. Soc. Jpn.* 81, 1337-1376, **2008**

[15] Huang, W. H., Li, J., Luo, C. X., Zhang, J. L., Luan, S. F. & Han, Y. C. *Colloid Surf. A-Physicochem. Eng. Asp*.273, 43-46, **2006**

[16] Huang, W. H., Li, J. A., Xue, L. J., Xing, R. B., Luan, S. F., Luo, C. X., Liu, L. B. & Han, Y. C., *Colloid Surf. A-Physicochem. Eng. Asp*. 278, 144-148, **2006**

[17] Yamauchi, Y., Imasu, J., Kuroda, Y., Kuroda, K. & Sakka, Y. *J. Mater. Chem.* 19, 1964-1967, **2009**

[18] Lee, D. H., Chang, Y. J., Herman, G. S. & Chang, C. H. *Adv. Mater.* 19, 843-847, **2007**

[19] Su, M., Liu, X. G., Li, S. Y., Dravid, V. P. & Mirkin, C. A. *J. Am. Chem. Soc.* 124, 1560-1561, **2002**

[20] Fu, L., Liu, X. G., Zhang, Y., Dravid, V. P. & Mirkin, C. A., *Nano Lett.* 3, 757-760, **2003**

[21] Salaita, K., Wang, Y. H. & Mirkin, C. A. *Nat. Nanotechnol.* 2, 145-155, **2007**

[22] Lewis, J. A. *Adv. Funct. Mater.* 16, 2193-2204, **2006**

[23] Lee, J. N., Park, C. & Whitesides, G. M. *Anal. Chem.* 75, 6544-6554, **2003**

[24] Chou, S. Y., Krauss, P. R. & Renstrom, P. J. *Science*, 272, 85-87, **1996**

[25] Chou, S. Y., Krauss, P. R. & Renstrom, P. J. *J. Vac. Sci. Technol. B*, 14, 4129-4133, **1996**

[26] Guo, L. J. *Adv. Mater*. 19, 495-513, **2007**

[27] Kim, E., Xia, Y. N. & Whitesides, G. M. *J. Am. Chem. Soc.* 118, 5722-5731, **1996**

[28] Chang, N. A., Richardson, J. J., Clem, P. G. & Hsu, J. W. P. *Small*, 2, 75-79, **2006**

[29] Bietsch, A. & Michel, B. *J. Appl. Phys.* 88, 4310-4318, **2000**

[30] Sharp, K. G., Blackman, G. S., Glassmaker, N. J., Jagota, A. & Hui, C. Y. *Langmuir*, 20, 6430-6438, **2004**

[31] Huang, Y. G. Y., Zhou, W. X., Hsia, K. J., Menard, E., Park, J. U., Rogers, J. A. & Alleyne, A. G. *Langmuir*,s 21, 8058-8068, **2005**

[32] Roca-Cusachs, P., Rico, F., Martinez, E., Toset, J., Farre, R. & Navajas, D. *Langmuir*, 21, 5542-5548, **2005**

[33] Lee, T. W., Mitrofanov, O. & Hsu, J. W. R. *Adv. Funct. Mater.* 15, 1683-1688, **2005**

[34] Odom, T. W., Love, J. C., Wolfe, D. B., Paul, K. E. & Whitesides, G. M. *Langmuir*, 18, 5314-5320, **2002**

[35] Schmid, H. & Michel, B. *Macromolecules*, 33, 3042-3049, **2000**

[36] Choi, K. M. & Rogers, J. A. *J. Am. Chem. Soc*. 125, 4060-4061, **2003**

[37] Viallet, B., Gallo, P. & Daran, E. *J. Vac. Sci. Technol. B*, 23, 72-75, **2005**

[38] Kim, W. S., Choi, D. G. & Bae, B. S. *Nanotechnology* 17, 3319-3324, **2006**

[39] Gratton, S. E. A., Williams, S. S., Napier, M. E., Pohlhaus, P. D., Zhou, Z. L., Wiles, K. B., Maynor, B. W., Shen, C., Olafsen, T., Samulski, E. T. & Desimone, J. M., *Acc. Chem. Res.* 41, 1685-1695, **2008**

[40] Truong, T. T., Lin, R. S., Jeon, S., Lee, H. H., Maria, J., Gaur, A., Hua, F., Meinel, I. & Rogers, J. A., *Langmuir*, 23, 2898-2905, **2007**

[41] Pina-Hernandez, C., Fu, P. F. & Guo, L. J. *J. Vac. Sci. Tech. B*. 26, 2426-2429, **2008**

[42] Kim, J. Y., Choi, D. G., Jeong, J. H. & Lee, E. S. *Appl. Surf. Sci*. 254, 4793-4796, **2008**

[43] Langowski, B. A. & Uhrich, K. E. *Langmuir* 21, 6366-6372, **2005**

[44] Glasmastar, K., Gold, J., Andersson, A. S., Sutherland, D. S. & Kasemo, B. *Langmuir* 19, 5475-5483, **2003**
[45] Hale, P. S., Kappen, P., Prissanaroon, W., Brack, N., Pigram, P. J. & Liesegang, *J. Appl. Surf. Sci.* 253, 3746-3750, **2007**
[46] Wigenius, J. A., Hamedi, M. & Inganas, O. *Adv. Funct. Mater*. 18, 2563-2571, **2008**
[47] Graham, D. J., Price, D. D. & Ratner, B. D. *Langmuir*, 18, 1518-1527, **2002**
[48] Roman, G. T. & Culbertson, C. T. *Langmuir*, 22, 4445-4451, **2006**
[49] Pisignano, D., Di Benedetto, F., Persano, L., Gigli, G. & Cingolani, R. *Langmuir* 20, 4802-4804, **2004**
[50] Wang, B., Oleschuk, R. D. & Horton, J. H. *Langmuir* 21, 1290-1298, **2005**
[51] He, Q. G., Liu, Z. C., Xiao, P. F., Liang, R. Q., He, N. Y. & Lu, Z. H. Langmuir 19, 6982-6986, **2003**
[52] Barbier, V., Tatoulian, M., Li, H., Arefi-Khonsari, F., Ajdari, A. & Tabeling, P. *Langmuir* 22, 5230-5232, **2006**
[53] Lee, J., Kim, M. J. & Lee, H. H. *Langmuir* 22, 2090-2095, **2006**
[54] Schwartz, R. W. *Chem. Mat*. 9, 2325-2340, **1997**
[55] Schwartz, R. W., Schneller, T. & Waser, R. C. *R. Chim*. 7, 433-461, **2004**
[56] Parikh, H. & De Guire, M. R. *J. Ceram. Soc. Jpn.* 117, 228-235, **2009**
[57] Wright, J. D. & Sommerdijk, N. A. J. M. *CRC Press, Boca Raton, FL*, **2001**
[58] Tohge, N., Matsuda, A., Minami, T., Matsuno, Y., Katayama, S. & Ikeda, Y. *Journal of Non-Crystalline* Solids, 100, 501-505, **1998**
[59] Krug, H., Merl, N. & Schmidt, H. *Journal of Non-Crystalline Solids* 147-148, 447-450, **1992**
[60] Marzolin, C., Smith, S. P., Prentiss, M. & Whitesides, G. M. *Adv. Mater*. 10, 571-574, **1998**
[61] Kim, W. S., Yoon, K. B. & Bae, B. S. *J. Mater. Chem.* 15, 4535-4539, **2005**
[62] Clem, P. G., Jeon, N. L., Nuzzo, R. G. & Payne, D. A. *J. Am. Ceram. Soc*. 80, 2821-2827, **1997**
[63] Hampton, M. J., Williams, S. S., Zhou, Z., Nunes, J., Ko, D. H., Templeton, J. L., Samulski, E. T. & DeSimone, J. M. *Adv. Mater.* 20, 2667-2673, **2008**
[64] Goh, C., Coakley, K. M. & McGehee, M. D. *Nano Lett*. 5, 1545-1549, **2005**
[65] Martin, C. R. & Aksay, I. A. *J. Phys. Chem. B*, 107, 4261-4268, **2003**
[66] Kim, J. H., Lange, F. F. & Cheon, C. I. *J. Mater. Res.* 14, 1194-1196, **1999**
[67] Harnagea, C., Alexe, M., Schilling, J., Choi, J., Wehrspohn, R. B., Hesse, D. & Gosele, U. *Appl. Phys. Lett*. 83, 1827-1829, **2003**
[68] Masuda, Y., Sugiyama, T. & Koumoto, K. *J. Mater. Chem.* 12, 2643-2647, **2002**
[69] Gao, Y. F., Masuda, Y., Yonezawa, T. & Koumoto, K. *Chem. Mat*. 14, 5006-5014, **2002**
[70] Göbel, O. F., Nedelcu, M. & Steiner, U. *Adv. Funct. Mater*. 17, 1131-1136, **2007**
[71] Zou, G., You, X. & He, P. S. *Mater. Lett.* 62, 1785-1788, **2008**
[72] Schneider, A., Su, B., Button, T. W., Singleton, L., Wilhelmi, O., Huq, S. E., Prewett, P. D. & Lawes, R. A. *Microsystem Technologies* 8, 88-92, **2002**

[73] Heule, M., Schell, J. & Gauckler, L. J., *J. Am. Ceram. Soc.*, 86, 407-412, **2003**
[74] Pisignano, D., Sariconi, E., Mazzeo, M., Gigli, G. & Cingolani, R. *Adv. Mater.*, 14, 1565-1567, **2002**
[75] Moran, P. M. & Lange, F. F. *Appl. Phys. Lett.* 74, 1332-1334, **1999**
[76] Ahn, S. J., Min, J. H., Kim, J. & Moon, J. *J. Am. Ceram. Soc.*91, 2143-2149, **2008**
[77] Seemann, R., Kramer, E. J. & Lange, F. F. *New J. Phys.* 6, 111, **2004**
[78] Seemann, R., Brinkmann, M., Kramer, E. J., Lange, F. F. & Lipowsky, R. *Proc. Natl. Acad. Sci*. USA. 102, 1848-1852, **2005**
[79] Matsuda, A., Sasaki, T., Tatsumisago, M. & Minami, T., *J. Am. Ceram. Soc*. 83, 3211-3213, **2000**
[80] Khan, S. U., Göbel, O. F., Blank, D. H. A. & ten Elshof, J. E. *ACS Appl. Mater. & Interfaces* 1, 2250-2255, **2009**
[81] Yang, P. D., Wirnsberger, G., Huang, H. C., Cordero, S. R., McGehee, M. D., Scott, B., Deng, T., Whitesides, G. M., Chmelka, B. F., Buratto, S. K. & Stucky, G. D. *Science* 287, 465-467, **2000**
[82] Su, B., Zhang, D. & Button, T. W. *J. Mater. Sci*. 37, 3123-3126, **2002**
[83] Zhang, D., Su, B. & Button, T. W. *J. Europ. Ceram. Soc*. 27, 231-237, **2004**
[84] Zhang, D., Su, B. & Button, T. W. *J. Europ. Ceram. Soc.* 27, 645-650, **2007**
[85] Schonholzer, U. P. & Gauckler, L. J., *Adv. Mater*. 11, 630-632, **1999**
[86] Bulthaup, C. A., Wilhelm, E. J., Hubert, B. N., Ridley, B. A. & Jacobson, J. M. *Appl. Phys. Lett.* 79, 1525-1527, **2001**
[87] Gobel, O. F., Blank, D. H. A. & ten Elshof, J. E. *ACS Appl. Mater. & Interfaces* 2, in press, **2010**
[88] Matsuda, A., Matsuno, Y., Tatsumisago, M. & Minami, T. *J. Am. Ceram. Soc*. 81, 2849-2852, **1998**
[89] Jeong, S., Ahn, S.-J. & Moon, J. *J. Am. Ceram. Soc*. 88, 1033-1036, **2005**
[90] Schueller, O. J. A., Whitesides, G. M., Rogers, J. A., Meier, M. & Dodabalapur, A. *Appl. Optics* 38, 5799-5802, **1999**
[91] Ro, H. W., Jones, R. L., Peng, H., Hines, D. R., Lee, H. J., Lin, E. K., Karim, A., Yoon, D. Y., Gidley, D. W. & Soles, C. L. *Adv. Mater.* 19, 2919-2924, **2007**
[92] Yang, P. D., Deng, T., Zhao, D. Y., Feng, P. Y., Pine, D., Chmelka, B. F., Whitesides, G. M. & Stucky, G. D. *Science* 282, 2244-2246, **1998**
[93] Ro, H. W., Peng, H., Niihara, K. I., Lee, H. J., Lin, E. K., Karim, A., Gidley, D. W., Jinnai, H., Yoon, D. Y. & Soles, C. L. *Adv. Mater.* 20, 1934-1939, **2008**
[94] Verschuuren, M. & Van Sprang, H., In: *Materials Research Society Symposium Proceedings Vol. 1002E*, ed. G. Gigli. Materials Research Society, Warrendale, PA, N03-05, **2007**
[95] Kim, W. S., Lee, J. H., Shin, S. Y., Bae, B. S. & Kim, Y. C. *IEEE Photonics Technol. Lett.* 16, 1888-1890, **2004**
[96] Choi, D. G., Jeong, J. H., Sim, Y. S., Lee, E. S., Kim, W. S. & Bae, B. S. *Langmuir* 21, 9390-9392, **2005**
[97] Kim, W. S., Kim, K. S., Kim, Y. C. & Bae, B. S. *Thin Solid Films* 476, 181-184, **2005**
[98] Kim, W. S., Jin, J. H. & Bae, B. S. *Nanotechnology* 17, 1212-1216, **2006**

[99] Kim, W. S., Kim, K. S., Eo, Y. J., Yoon, Y. & Bae, B. S. *J. Mater. Chem.* 15, 465-469, **2005**
[100] Alexe, M., Harnagea, C. & Hesse, D. *J. Electroceram.* 12, 69-88, **2004**
[101] Hsieh, K. C., Chen, H. L., Lin, C. H. & Lee, C. Y. *J. Vac. Sci. Technol. B* 24, 3234-3238, **2006**
[102] Chen, H. L., Hsieh, K. C., Lin, C. H. & Chen, S. H. *Nanotechnology* 19, 435304, **2008**
[103] Shi, G., Lu, N., Gao, L., Xu, H., Yang, B., Li, Y., Wu, Y. & Chi, L. *Langmuir* 25, 9639-9643, **2009**
[104] George, A., Blank, D. H. A. & ten Elshof, J. E., *Langmuir*, 25, 13298-13301, **2009**
[105] Schonholzer, U. P., Stutzmann, N., Tervoort, T. A., Smith, P. & Gauckler, L. J. *J. Am. Ceram. Soc.* 85, 1885-1887, **2002**
[106] Yi, D. K., Yoo, S. J. & Kim, D. Y. *Nano Lett.* 2, 1101-1104, **2002**
[107] Martin, C. R. & Aksay, I. A., *J. Mater. Res.* 20, 1995-2003, **2005**
[108] Auger, M. A., Schilardi, P. L., Caretti, I., Sanchez, O., Benitez, G., Albella, J. M., Gago, R., Fonticelli, M., Vazquez, L., Salvarezza, R. C. & Azzaroni, O. *Small* 1, 300-309, **2005**
[109] Deki, S., Iizuka, S., Horie, A., Mizuhata, M. & Kajinami, A. *Chem. Mat*. 16, 1747-1750, **2004**
[110] Deki, S., Iizuka, S., Horie, A., Mizuhata, M. & Kajinami, A. *J. Mater. Chem.* 14, 3127-3132, **2004**
[111] Kim, S. S., Chun, C., Hong, J. C. & Kim, D. Y. *J. Mater. Chem.* 16, 370-375, **2006**
[112] Dravid, V. P. *J. Mater. Chem.* 19, 4295-4299, **2009**
[113] Donthu, S., Pan, Z. X., Myers, B., Shekhawat, G., Wu, N. G. & Dravid, V. *Nano Lett*. 5, 1710-1715, **2005**
[114] Donthu, S., Sun, T. & Dravid, V. *Adv. Mater*. 19, 125-128, **2007**
[115] Pan, Z. X., Donthu, S. K., Wu, N. Q., Li, S. Y. & Dravid, V. P. *Small* 2, 274-280, **2006**
[116] Sun, T., Pan, Z. X., Dravid, V. P., Wang, Z. Y., Yu, M. F. & Wang, J. *Appl. Phys. Lett*. 89, 3, **2006**
[117] Pan, Z., Li, S., Wang, Z., Yu, M. F. & Dravid, V. P. *Appl. Phys. Lett*. 91, 3, **2007**
[118] Heule, M. & Gauckler, L. J. *Adv. Mater*. 13, 1790-1793, **2001**
[119] Jeon, N. L., Hu, J. M., Whitesides, G. M., Erhardt, M. K. & Nuzzo, R. G. *Adv. Mater.* 10, 1466-1469, **1998**
[120] Kim, E. & Whitesides, G. M. *J. Phys. Chem. B* 101, 855-863, **1997**
[121] Huang, W. F., Liu, Q. S. & Li, Y. *Chem. Eng. Technol*. 29, 716-723, **2006**
[122] Kim, D. S., Lee, K. C., Kwon, T. H. & Lee, S. S. *J. Micromech. Microeng*. 12, 236-246, **2002**
[123] Jeon, N. L., Choi, I. S., Xu, B. & Whitesides, G. M. *Adv. Mater*. 11, 946-950, **1999**
[124] Beh, W. S., Xia, Y. & Qin, D. *J. Mater. Res.* 14, 3995-4003, **1999**
[125] Vartuli, J. S., Ozenbas, M., Chun, C. M., Trau, M. & Aksay, I. A. *J. Mater. Res.* 18, 1259-1265, **2003**
[126] Seraji, S., Wu, Y., Jewell-Larson, N. E., Forbess, M. J., Limmer, S. J., Chou, T. P. & Cao, G. Z. *Adv. Mater*. 12, 1421-1424, **2000**

[127] Cheng, Z. Y., Wang, Z., Xing, R. B., Han, Y. C. & Lin, J. *Chem. Phys. Lett*. 376, 481-486, **2003**

[128] Yu, M., Lin, J., Wang, Z., Fu, J., Wang, S., Zhang, H. J. & Han, Y. C. *Chem. Mat*. 14, 2224-2231, **2002**

[129] Han, X. M., Lin, J., Xing, R. B., Fu, J., Wang, S. B. & Han, Y. C. *J. Phys.-Condes. Matter* 15, 2115-2126, **2003**

[130] Pang, M. L., Lin, J., Cheng, Z. Y., Fu, J., Xing, R. B. & Wang, S. B. *Mater. Sci. Eng. B: Solid State Mater. Adv. Technol*. 100, 124-131, **2003**

[131] Han, X. M., Lin, J., Fu, J., Xing, R. B., Yu, M., Zhou, Y. H. & Pang, M. L. *Solid State Sci.*6, 349-355, **2004**

[132] Han, X. M., Lin, J., Xing, R. B., Fu, J. & Wang, S. B. *Mater. Lett*. 57, 1355-1360, **2003**

[133] Park, K. H., Sung, I. K. & Kim, D. P. *J. Mater. Chem.*14, 3436-3439, **2004**

[134] Lee, D. H., Park, K. H., Hong, L. Y. & Kim, D. P. *Sens. Actuator A-Phys*. 135, 895-901, **2007**

[135] Trau, M., Yao, N., Kim, E., Xia, Y., Whitesides, G. M. & Aksay, I. A. *Nature* 390, 674-676, **1997**

[136] Wirnsberger, G., Yang, P. D., Huang, H. C., Scott, B., Deng, T., Whitesides, G. M., Chmelka, B. F. & Stucky, G. D. *J. Phys. Chem. B* 105, 6307-6313, **2001**

[137] Yang, P. D., Rizvi, A. H., Messer, B., Chmelka, B. F., Whitesides, G. M. & Stucky, G. D. *Adv. Mater.* 13, 427-431, **2001**

[138] Kim, W. S., Kim, M. G., Ahn, J. H., Bae, B. S. & Park, C. B. *Langmuir* 23, 4732-4736, **2007**

[139] de la Rica, R., Baldi, A., Mendoza, E., Paulo, A. S., Llobera, A. & Fernandez-Sanchez, C. *Small* 4, 1076-1079, **2008**

[140] Heule, M. & Gauckler, L. J. *Materials Research Society Symposium Proceedings* 687, B4.5.1 - B4.5.6, **2002**

[141] Heule, M. & Gauckler, L. J. *Sensors and Actuators B* 93, 100-106, **2003**

[142] Ahn, S. J. & Moon, J. *J. Am. Ceram. Soc*. 88, 1171-1174, **2005**

[143] Imasu, J. & Sakka, Y. *J. Ceram. Soc. Jpn*. 115, 697-700, **2007**

[144] Ahn, S. J., Lee, J. H., Kim, J. & Moon, J. *Electrochem. Solid State Lett*. 9, A228-A231, **2006**

[145] Imasu, J., Fudouzi, H. & Sakka, Y. *J. Ceram. Soc. Jpn*. 114, 725-728, **2006**

[146] ten Elshof, J.E., Khan, S.U.; Göbel, O.F. *J. Europ. Ceram. Soc.* 30, 1555-1577, **2010**

3

Fabrication and Characterization Techniques

3.1. Introduction

The first step in any soft-lithographic technique is the fabrication of a suitable master, most commonly a Si master made by common techniques e.g. photolithography, electron or ion beam lithography, nanoimprint lithography (NIL) or micro-machining. After some surface modification the master can be used to produce an elastomeric mold (stamp), most commonly made of poly(dimethylsiloxane) (PDMS) elastomer. This mold is the negative replica of the master from which it is derived. The master can be used hundreds of times for making molds. These molds or stamps can then be applied in the various soft-lithographic techniques.

In this chapter the various processes of making Si masters and PDMS molds will be described. The soft-lithographic techniques utilized in this research work will be explained. Also, the various techniques used for the analysis of structure, surface, and composition will be discussed. Finally, the techniques used to study the electrical properties of patterned films will be addressed.

3.2. Materials

3.2.1. Preparation of Master

(a). Photolithography

Masters used for micromolding in capillaries (MIMIC) and microtransfer molding (μTM) having lateral features sizes larger than 1 micrometer were fabricated via standard photolithography and deep reactive ion etching. The masters were silanized with vapor phase perfluoro trichlorosilane ($CF_3(CF_2)_6(CH_2)_2SiCl_3$) (Gelest, Inc.) prior to use in order to facilitate the detachment of PDMS from the master after curing.

(b). UV Nano-Imprint Lithography (NIL)

The basic principle of nanoimprint lithography (NIL) is to create structures by imprinting or embossing a hard stamp into a low viscosity material. Masters having patterns with features sizes of 500 nm and smaller were fabricated by NIL technique in our clean room class 10,000 (FED-STD-209 E). At first a 60 nm organic bottom anti-reflective coating (BARC) layer was coated on a double sided polished Si wafer. A UV curable imprinting material was dispensed in the form of droplets on top of the BARC

layer. Subsequently, a pre-patterned quartz stamp was pressed against each droplet in a serial manner and cured. The advantage of NIL for the fabrication of master is that there is no etching steps involved in the process.

3.2.2. Substrate Materials

The following substrates were used in this research:

a. Silicon substrates: Si (100) wafer, CZ grown, p-type, resistivity: 5-10 Ω-cm, obtained from OKMETIC;
b. Oxidized Si substrates were obtained by dry oxidation of the above mentioned Si wafers in a chamber furnace at 1100 °C in air for 5-7 h. The oxide layer thickness after thermal treatment is ca. 250-350 nm;
c. Platinized Si substrates were obtained by first depositing a 150 nm SiO_2 layer on a Si (100) wafer by dry oxidation, followed by deposition of a 40 nm thick Ti layer to improve the adhesion and then depositing a 100 nm Pt layer. These substrates were used for electrical characterization of the patterned films.

(A). Cleaning of substrate by CO_2 snow jet

The following procedure was adopted for cleaning of all substrates prior to any deposition. The substrate was fixed by means of vacuum suction on a pre-heated hot plate with a surface temperature of ca. 150 °C. Subsequently, a fine jet of CO_2 crystals was flushed on the surface at an angle of 60-70° with respect to the normal. In this way dust particles were blown away by the impact and organic impurities that adhered to the surface were dissolved. The water contact angle of a Si substrate that had been cleaned in this manner was smaller than 10°.

(B). Cleaning of substrate by oxygen plasma

After the primary cleaning step the substrates were treated with oxygen plasma (Harrick Plasma, 200W) at a pressure of 80 Pa using molecular oxygen. Quickly after snow jetting the substrates were placed in the plasma chamber for 2-5 min. After this treatment the water contact angle was smaller than 2°. The aim of oxygen plasma cleaning is to remove the organic impurities (molecules) from the surface of the substrate. The presence of these impurities may reduce the wetting of the substrate by precursor solution which may result in poor adhesion of the deposited film or pattern. Oxygen plasma treatment improves the wetting properties of the substrate by increasing its surface free energy.

3.2.3. Mold Materials

3.2.3.1. Preparation of mold

All molds were made from commercial Poly(dimethylsiloxane) (PDMS, Sylgard 184 Dow Corning GmbH, Wiesbaden, Germany). The kit consists of a base material and a cross linker, which were mixed in a 10:1 weight ratio in a glass beaker for 2-5 min. Air bubbles that had become encapsulated in the polymer in the mixing process were extracted by placing the beaker in a dessicator connected to a vacuum pump. The pressure was reduced until the bubbles started wobbling. Depending on the amount of material, all bubbles had collapsed within 10-20 min.

In the second step, a clean Si master was placed on a hot plate and the temperature was set to 40 °C. A Teflon ring of sufficient diameter (depending on the size of the master) was placed over the patterned area of the master. The liquid PDMS was poured gently onto the master and left for 12-16 h to cross-link. After complete curing the molds were peeled off carefully. The Si masters can be used more than 100 times for the fabrication of PDMS molds. The molds were cut into small blocks of 1x1 cm^2 with a surgical blade and blown with clean compressed air to remove dust and residue particles prior to use.

3.2.3.2. Modification of PDMS mold

The PDMS in as-prepared form is hydrophobic in nature. However, the surface can be modified physically and/or chemically in order to make it hydrophilic for the required applications.[1-5] The physical techniques include exposure to oxygen plasma, ultraviolet (UV) light or UV light and ozone. When the surface of the PDMS is exposed to oxygen plasma, it is converted to silica (SiO_x) as shown in Scheme 1.[1,5] The oxygen plasma breaks the C-Si bonds and removes the organic moieties from the siloxane backbone and forms an hydroxyl-functional inorganic phase.[4] Nevertheless, this hydrophilic state is unstable and the surface hydrophobicity is recovered over a period of time.[6] This hydrophobic recovery is due to the diffusion of low molecular weight chains from the bulk of the PDMS phase to the surface.[3,6]

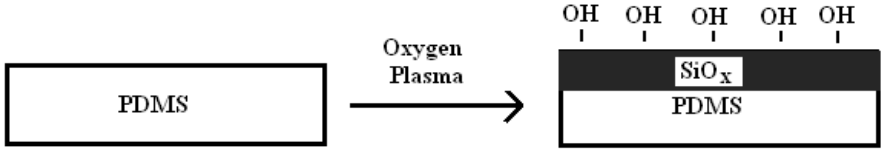

Scheme: PDMS surface functionalization by oxygen plasma treatment.

The surface properties are measured in terms of water contact angles. The as-prepared PDMS has a contact angle >110°, whereas it was <5° after treating in oxygen plasma for 2 min.

3.3. Patterning and deposition techniques

The various soft-lithographic techniques used for the fabrication of patterns in this research work are addressed in this section. Similarly, other techniques used in combination with soft-lithographic techniques will be discussed in this section as well. These techniques were applied to pattern sol-gel and suspension derived titania (TiO_2) and lead zirconate titanate ($Pb(Zr_x,Ti_{1-x})O_3$). Also sol-gel derived $LaPO_4$:Eu and $CePO_4$:Tb nano-particles embedded in hybrid silica were patterned at different length scales.

3.3.1. Micromolding in Capillaries *

Micromolding in capillaries (MIMIC) is a molding based technique in soft-lithography. The principle is based on *the spontaneous filling of a capillary network* formed by a mold and a substrate.[7] Basically, a mold having a relief pattern on its surface is brought into conformal contact with a cleaned substrate, whereby a network of interconnected cavities is established. A drop of a low viscosity fluid is placed in front of the openings of the capillaries and is sucked in by capillary action. The filling fluid may be a low viscosity pre-polymer, precursor, sol-gel, or some suspension solution. **Figure 3.1a** shows schematically the different stages in the MIMIC process. This technique is only applicable to interconnected features.

3.3.2. Microtransfer Molding*

The second molding based technique used in the present work is microtransfer molding (μTM). Here, a small drop of the precursor solution is placed on top of a patterned mold, the excess material is gently swept off with a soft elastomeric (PDMS) or steel block, the filled mold is then gently inverted on a clean substrate. The patterned material is dried (or cured) thermally, and finally the mold is removed. The technique of μTM is shown schematically in **Figure 3.1b**. The advantage of this technique is that it can pattern even isolated features. It can also be applied to pattern high viscosity materials. Further details about these two techniques are being discussed in the previous chapter.

* These techniques namely MIMIC and μTM are explained in detail in chapter 2.

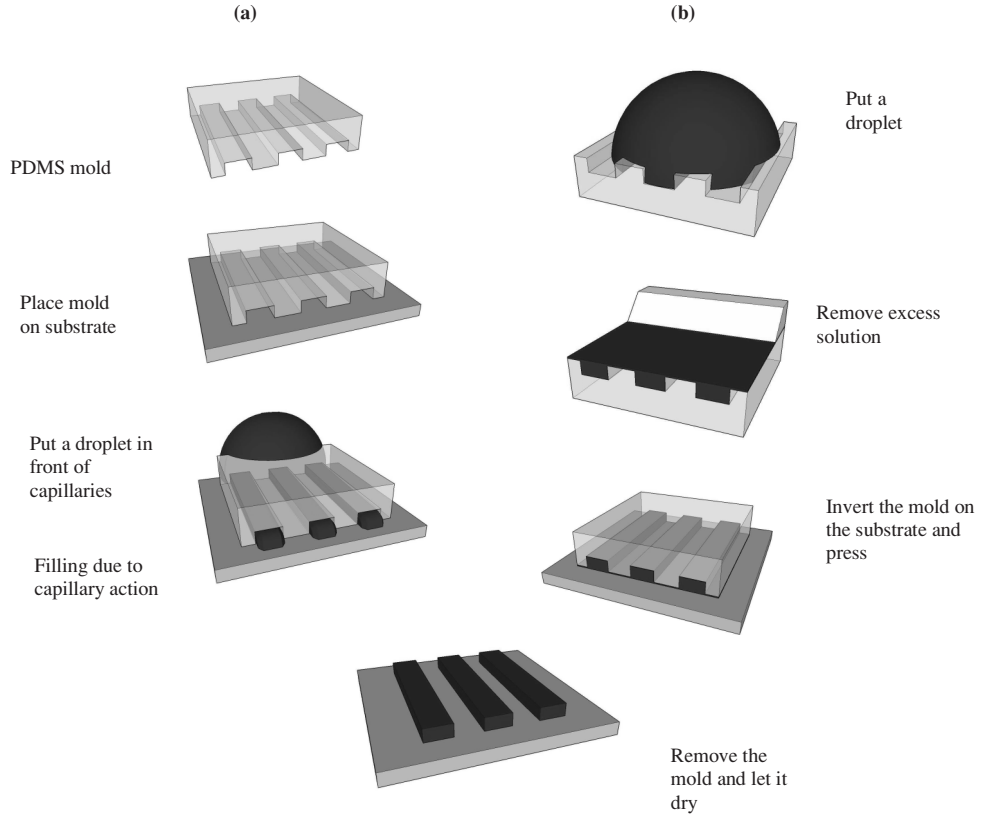

Figure 3.1: Schematic illustration of the various stages in (a) micromolding in capillaries and (b) microtransfer molding.

3.3.3. Imprint Lithography and Nano-transfer molding

For pattering at smaller scale two modified techniques called soft-imprint lithography (SIL) or soft-confocal imprint lithography (SCIL), and nano-transfer molding (NTM) have been reported.[8] They are shown in **Figure 3.2**. In SCIL process shown in **Figure 3.2a**, a drop of the sol is placed on a substrate and homogenously distributed, e.g. by a PDMS block or spin-coating with 500-1000 rpm. Then a PDMS mold is gently placed on the wet film and dried on a hot plate at 60-100 °C for 15-30 min. The lateral size of the features in the PDMS stamps used was 50-500 nm. The feature depth was 100 nm in all cases. The advantages of using a soft PDMS instead of using a rigid mold are that it provides good conformal contact, has a low reactivity with organic materials, and can be removed easily from the replicated pattern without distortion of the pattern.[9] The second technique, shown in **Figure 3.2b**, we termed it as nano-transfer molding

(NTM). It is equivalent to microtransfer molding but operates on the nanometer scale. Here the sol is poured onto a PDMS mold, distributed homogenously, transferred to the substrate, and dried under conditions similar to those in SCIL. Excess material was in both cases removed either with a soft PDMS block or with a hard material, e.g. a steel block.

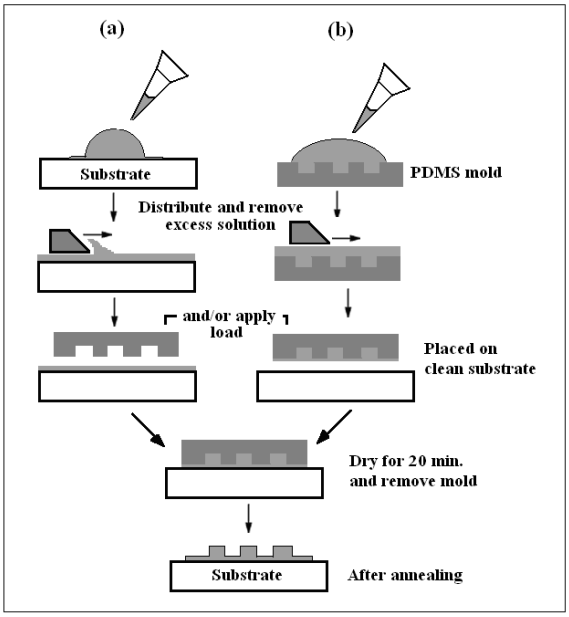

Figure 3.2: Schematic presentation of modified patterning techniques: (a) SCIL; and (b) NTM.

3.3.4. Spin Coating

Spin coating was applied to make homogenous thin films of the aforementioned solution materials. After the cleaning procedure the substrates were immediately transferred to the spin coater (WS-400 Lite Series, Laurell Technologies). The coating speed and time in most cases were 4000-5000 rpm and 30-40 s, respectively. The freshly prepared films were then subject to initial drying on a hot plate at different temperatures (depending on the material) for several minutes. This drying step was repeated after each coated layer and finally the sample was subject to the final thermal calcination step.

3.3.5. Pulsed Laser Deposition

Pulsed laser deposition (PLD) was applied to deposit electrodes on PZT films and patterns, when electrical characterization was targeted.

In PLD a high energy laser beam is focused on a target (of the source to be deposited) material inside a vacuum chamber. The electromagnetic energy of the beam is converted into thermal energy and results in evaporation of the target material. The vaporized material (in plasma plume) is deposited as a thin film on a substrate facing the target.[10]

In the present research the energy source used was a KrF (λ=248 nm) excimer laser (Lambda Physic, Compex 205) operating at frequencies between 1-30 Hz. The pulse width was about 24 ns (FWHM) and the maximum pulse energy was 650 mJ. The beam was focused by a lens having focal length of 453 mm at 248 nm projected on the target at 45° angle of incidence. The vacuum chamber was pumped down to a base pressure of 10^{-6} mbar prior to deposition. Oxygen and argon were used as deposition gases controlled by a mass flow controller (0-40 ml/min.). The deposition pressure was adjusted in between 10^{-3}-10° mbar with accuracy of 0.001 mbar.

In some cases, other techniques such as Focused Ion Beam (FIB) and sputtering were also applied to deposit the top electrodes using copper made shadow masks. The RF sputtering system (Perkin-Elmer 3, Model 2400) was used to deposit platinum (Pt) electrodes.

3.4. Characterization Techniques

In this section the main characterization techniques used in this work are addressed. These include studying the chemistry of the solution system prior to the patterning. Subsequently, characterizing the phase and surface of the patterns and thin films in the solid state form. Finally the electrical properties of the PZT derived pattern and thin film system are discussed.

3.4.1. Structural Characterization

Structural analyses of the precursor solutions were performed by small angle x-ray scattering (SAXS), while x-ray diffraction was performed on solid state materials.

3.4.1.1. Small angle x-ray scattering

In SAXS analysis, the elastic scattering of x-rays by a sample having fluctuations in electronic density between solute/solvent, or between its other components is recorded at very small angles (0.1°-10°). In this angular range, the structural information about size and shape of the particle from 0.1-50 nm can be derived for a given system. In a typical SAXS experiment, the scattering intensity I is plotted versus the scattering vector q (nm^{-1}) see **Figure 3.3**. This is related to the scattering angle θ and the wavelength λ of the incident beam by:

$$q = \frac{4\pi}{\lambda}\sin(\theta) \qquad (1)$$

At small q range the scattered intensity can be expressed by the Guinier law:

$$I(q) \propto \exp\left(-q^2 \frac{R_g^2}{3}\right) \qquad (2)$$

From the Guinier plot ($\ln I$ *vs.* q^2) the effective particle size, also known as the radius of gyration (R_g), can be determined. At large q values, all curves follow a $I \sim q^{-4}$ law; this is known as Porod law.

In the q-range between the Guinier and Porod regions, the size and shape of sols with a fractalic structure can be determined. Fractal objects are generally described in terms of three parameters, namely size of primary scatterer (R_o), fractal dimension (D_f) and correlation length (ξ).[11] R_o and ξ are also known as upper and lower cut-off lengths respectively; and ξ can also be correlated to the radius of gyration (R_g). From the ln I vs. ln q plot in the fractal range ($1/\xi << q << 1/R_o$), the value of D_f can be calculated as the negative slope of the intensity curve:

$$I \propto q^{-D_f} \qquad (3)$$

D_f is a very important parameter which describes the openness of a structure. Its value varies between 1 and 3. The more open the structure is, the smaller its D_f value becomes. The mass of objects M is related to their size R by the following equation:

$$M \propto R^{D_f} \qquad (4)$$

If the condition $\xi >> R_o$ is not fulfilled then the physical meaning of fractal becomes unclear. It is a general requirement that for a fractal system, the ratio of ξ/R_o should be equal to or larger than 10.[11] If this condition is satisfied, the scattering curve could be fitted to the Teixeira function, which describes the scattering by fractal-like objects.[12] From the best fit the parameters such as R_o, ζ and D_f could be determined. The effective particle size R_g can then be calculated from $R_g^2 = 1/2\ D_f(D_f+1)\zeta^2$.

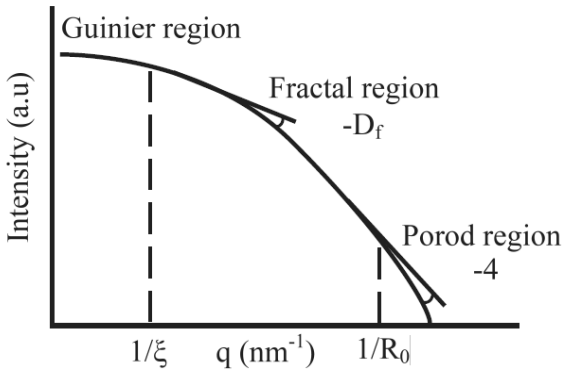

Figure 3.3: Typical SAXS curve depicting various regions; the dotted lines represent the boundaries of the fractal region, where it meets the Guinier and Porod regions.

SAXS experiments were performed by using the synchrotron radiation facilities of the Dutch-Belgian (DUBBLE) beam line BM-26B at ESRF, Grenoble.[13] The beam energy was 12 keV. The beam was focused on the corner of a 2D CCD detector in order to maximize the range of accessible q values. The samples were placed at a distance of 1.5 m from the detector and the intensity was measured for q between 0.13 and 8 nm^{-1}. A beam stop was applied to shield the detector from the direct beam and to avoid saturation of the outgoing signal. The raw data were corrected for the pixel-dependent detector sensitivity and integrated for channels with the same q values.

3.4.1.2. X-ray diffraction

For phase characterization of thin films and patterns, x-ray diffraction (XRD) analyses were performed on a powder X'pert APD (PANalytical, B.V., The Netherlands) using CuKα radiation with a wavelength of 1.54056 Å. This system uses an x-ray source operating at 50 kV and 35 mA having minimum resolution as small as 0.001°. The system is equipped with automatic slits to control the irradiated observed area on the sample.

The X'pert Highscore plus software package (PANalytical B.V., The Netherlands) coupled to ICDD database was used to analyze the data. Further, average grain sizes were calculated from the broadening of diffraction peaks when the particle size becomes smaller. This was achieved by determining the full width at half maximum (FWHM) of selected peaks. The calculations were based on the Scherrer formula.[14]

3.4.2. Surface and morphology

The following techniques were used to study the surface and morphology of substrates, molds, thin films, and patterns. Phase, elemental composition, and grain sizes were also determined in a number of cases.

3.4.2.1. Optical microscopy

Optical microscopy was performed with a Nikon Microscope (ME600, Nikon instruments Europe B.V.). Episcopic illumination with white light was used, and both bright and dark field were possible. The pictures were obtained with a Nikon digital camera connected to the system.

3.4.2.2. Scanning electron microscopy

The basic principle in Scanning Electron Microscopy (SEM) is to image the surface of the sample by scanning it with high energy electrons. In this work low resolution SEM studies were performed with a JSM-5610 (JEOL, Tokyo Japan) operating at 0.5 and 30 keV. The lateral resolution is 3.5 nm at 30 keV at a working distance of 6 mm. Topographic studies of samples were performed in the secondary electron (SE) mode.
High resolution imaging was carried out with a Leo 1550 Field emission SEM (Leo, Germany).

3.4.2.3. Atomic force microscopy

Atomic Force Microscopy (AFM), also known as Scanning Force Microscopy (SFM), is a high resolution surface characterization technique. An AFM has a cantilever with a sharp tip (probe), which is brought into close proximity to a sample surface. This leads to deflection of the cantilever according to Hooke's law. The established forces may be Van der Waals forces (attractive), Coulomb forces (attractive or repulsive) or capillary forces. Typically the signal (deflection) is measured with a laser beam reflected from the top surface of the cantilever with photodiodes. AFM measurements were performed on a Nanoscope IV instrument (Veeco, Digital Instruments, Santa Barbara, USA) in tapping mode. The resolution depends on the shape of the tip, surface roughness of the sample and instrumental settings. The surface roughness was determined from topographical data analysis.

3.4.2.4. Fluorescence microscopy

Fluorescence microscopy of patterned films was performed on a so-called inverted microscope (Leica DM IRM), connected to a digital color camera (Olympus CC-12).

3.4.2.5. Contact angle goniometry

Surface energies of substrates and molds were studied with water contact angle measurements. The sessile drop method was applied using a Dataphysics OCA15 CA system at ambient temperature.

3.4.2.6. X-ray Photoelectron Spectroscopy

XPS was performed on patterned films to obtain the surface compositional information. This was performed using a PHI Quantera Scanning ESCA Microprobe with an AlKα mocochromatic excitation source.

3.4.3. Compositional Analysis

Low energy ion scattering (LEIS) is a surface sensitive analytical technique for the characterization of chemical and structural composition of materials.

Secondary ion mass spectroscopy (SIMS) is a technique used to study the surface composition by sputtering it with a primary ion beam and collecting and analyzing the secondary ions. Compositional analyses of the patterned films were performed with LEIS and time of flight (ToF) SIMS at Tascon GmbH (Analytical Services and Consulting, Münster, Germany). These techniques are capable of providing information on the atomic and molecular structure of the top 1-3 monolayers with sensitivities down to ppm (part per millions) range, with a lateral resolution of 100 nm.

3.4.4. Electrical Characterization

3.4.4.1. Ferroelectric hysteresis

The electrical properties of PZT derived films and patterns were measured by determining ferroelectric hysteresis loops. These are also called polarization-electric (P-E) loops. This was done by using a TF2000 Analyzer (aixACCT Systems GmbH, Aachen, Germany).

3.4.4.2. Capacitance

The capacitance and leakage currents of PZT samples were measured using a Süss MicroTech (PM300, Germany) manual probe station equipped with a Keithley 4200 semiconductor characterization system. The capacitance was measured as a function of applied voltage (*C-V*) and frequency (*C-f*) in the frequency range 10 kHz-1 MHz using an AC field of 4kV/cm. The leakage current was determined by applying a DC electric field to the PZT capacitors.

References

[1] Chaudhury, M.K.; Whitesides, G.M. *Langmuir*, 7, 1013-1025, **1991**.

[2] Fakes, D.W.; Davies, M.C.; Browns, A.; Newton, J.M. *Surf. Interface Anal*. 13, 233-236, **1988**

[3] Efimenko, K.; Wallace, W.E.; Genzer, J. *J.Colloid interface Sci.* 254, 306-315, **2002**

[4] Xiao, D.; Zhang, H.; Wirth, M. *Langmuir* 18, 9971-9976, **2002**

[5] Lee, J.; Kim, M.J.; Lee, H.H. *Langmuir* 22, 2090-2095, **2006**

[6] Hillborg, H.; Gedde, U.W. *Polymer* 39, 1991-1998, **1998**

[7] Kim, E.; Xia, Y.; Whitesides, G.M. *J. Am. Chem. Soc.* 118, 5722-5731, **1996**

[8] Khan, S.U.; Göbel, O.F.; Blank, D.H.A.; ten Elshof, J.E. *ACS Appl. Mater. Interfaces*, 1, 2250-2255, **2009**

[9] Kim, W.S.; Kim, K.S.; Kim, Y.C.; Bae, B.S. *Thin Solid Films*, 476, 181-184, **2005**

[10] Chrisey, D.B. & Hubler, G.K. In Pulsed Laser Deposition of Thin Films, Hohn Wiley &Sons Inc., New York, **1994**

[11] Craievich, A. "*Small-Angle X-ray Scattering by Nanostructured Materials*" *In Handbook of Sol-Gel Science and Technology*, Vol.2, Characterization of Sol-Gel Materials and Products, Ed. S. Sakka, Springer, 161-189, **2004**

[12] Teixeira, J. *J. Appl. Cryst*. 21, 781-785, **1988**

[13] Bras, W.; Dolbnya, I.P.; Detollenaere, D.; van Tol, R.; Malfois, M.; Greaves, G.N.; Ryan, A.J.; Heeley, E. J. *Appl. Crystallogr*. 36, 791-794, **2003**

[14] Scherrer, P. *Göttinger Nachrichten* 2, 98, **1918**

4

2D and 3D Parallel Patterning of Titania with Micromolding in Capillaries

Abstract

2D and 3D TiO_2 patterns were obtained by micromolding in capillaries using sol-gel and dispersion solutions. The wet patterns were dried at 80 °C and calcined at 550 °C. The crystallographic phase, shape of patterns and shrinkage were investigated by X-ray diffraction (XRD), scanning electron microscopy (SEM) and atomic force microscopy (AFM). The patterns obtained from sol-gel solutions showed good adhesion to the substrate, uniform shapes but large shrinkage. The patterns obtained from dispersion solution have high solid content but exhibited poor adhesion and non-uniform shapes.

4.1. Introduction

Titania (TiO_2) occurs naturally in three crystalline forms: anatase, rutile and brookite. It is a metal oxide material with promising applications in thick and thin film technology, e.g., in optics,[1] dielectrics,[2] photovoltaic cells,[3] electrochromic displays,[4] antireflection coatings,[5] high-performance anodes in ionic batteries,[6] and as gas sensor material.[7-9] TiO_2 has a high refractive index ($n_{anatase}$=2.5) and good insulating properties, and as a result it is widely used as protective layer in very large scale integrated (VLSI) circuits. The high dielectric constant (ε_r= 85 at 1 MHz) allows its consideration as an alternative to SiO_2 for ultra-thin gate oxide dielectrics used in memory and logic devices.[10]

The trend towards miniaturization of electronic and optical devices stimulates a researcher to look for new and alternative fabrication techniques. The so-called soft-lithographic techniques are the result of this trend.[11] These techniques are promising tools for the easy and low cost fabrication of high tech materials. The most common feature of the various techniques is the use of a soft polymeric material, usually poly-dimethylsiloxane (PDMS),[11,12] which can be used both as a molding or stamping material. Among the molding techniques, micromolding in capillaries (MIMIC) is a promising technique.[11-13] The basic principle is based on *the formation of interconnected microchannels, which results from the conformal contact between the substrate and the mold*. Therefore, the key feature is the formation of an interconnected network for the complete penetration of the solution via capillary force. The precursor solution can be a

sol-gel, dispersion or some polymeric solution. However, the viscosity of the solution should be optimized for good filling vs. high solids content of the final pattern.

Recently, several studies have been published on the soft-lithographic patterning of TiO_2. Shi *et al.* used the solvent assisted soft-lithography (SASL) technique to pattern TiO_2 at submicrometer length scales.[14] The dimensions (width & height) of the obtained patterns were controlled by parameters such as concentration of the solution, evaporation rate, time and temperature, and not by the dimensions of the mold. Severe shrinkage associated with sol-gel based materials has also been reported. Goh *et al.* made use of embossing to produce dense arrays of pattern while using a thin layer of poly(methyl methacrylate) (PMMA) in combination with PDMS.[15] In this way the good permeability and mechanical stability were combined. After use the mold was dissolved to avoid sticking to the substrate. So far, only two-dimensional (2D) patterns have been reported, i.e. patterns consisting of a single layer of TiO_2 on a flat substrate. Three-dimensional (3D) patterns, e.g. stacked wood pile structures of TiO_2 made via soft-lithography have not yet been reported.

The present work is based on the stacked parallel patterning of TiO_2, leading to 3D dual-layer wood-pile patterns using the MIMIC technique. The precursors utilized for this purpose were a sol-gel solution and dispersion, each with its own typical solids content. Various physical factors such as degree of filling, adhesion to the substrate, shape evolution, and shrinkage of patterns derived from both sol-gel and dispersion are the main parts of the discussion. Another important aspect of the work presented here concerns the formation of undesirable residue layers. We established a new technique based on chemical modification of the mold to prevent its occurrence.

4.2. Experimental

Two types of TiO_2 solutions were prepared and utilized for patterning. These will be explained in the following sub-sections.

4.2.1. Materials

Unless otherwise specified, reagents were used as received without further purification. Titanium (IV) iso-propoxide (99.99 %), 2-methoxyethanol (>99.3 %), Polyethylene glycol 600 (>99%), acetylacetone (>99%), polyacryclic acid (MW~ 1800) were purchased from Aldrich. TiO_2 powder (99%, anatase), ammonia (25% in H_2O), octadecyl trichloro-silane (>95%) were purchased from Acros. Photocurable polyurethane (PU; NOA 73, viscosity 130 cps at 25 °C) was purchased from Norland Products. Zirconia (YSZ) grinding media was purchased from Inframat Advanced Materials. Polydimethylsiloxane (Sylgard 184) was provided by Dow Corning.

4.2.2. Sol-gel sol preparation

In a glove box (C_{water} & $C_{Oxygen} \leq 0.5$ ppm), 0.43 g of titanium (IV) iso-propoxide was mixed with 0.52 g of 2-methoxyethanol and stirred for 30 min at room temperature. To this mixture 0.3 g of acetylacetone and 0.04 g of polyethylene glycol (PEG) were added and stirred for 2 h. The sol was then filtered with a 0.2 μm Teflon filter. The viscosity of the solution amounted to ca. 2.99(7) mP·s, as measured with a microviscometer (AmVn-HT, Anton Paar GmbH). The final titania sol had a concentration of 0.6 M Ti.

4.2.3. Dispersion solution preparation

Commercially available TiO_2 powder with 80 nm particle size was used. The powder was dispersed in distilled water. In order to stabilize the dispersion, a dispersant-stabilizing agent was added, which was prepared by dissolving polyacrylic acid in water to which ammonia had been added as neutralizing agent. The solution was then ball-milled in zirconia (YSZ) grinding media with 1.5 mm diameter in a plastic bottle for 72 h. Three solutions with solids loadings of 10, 20 and 30 % by volume were prepared.

4.2.4. Modification of PDMS mold

To avoid the formation of a residue layer in the MIMIC process, the PDMS molds were modified with the following procedure.

First of all, an octadecyl trichloro-silane (OTS) was dissolved in toluene by stirring to make a homogenous solution. A 500 μl droplet of this solution was placed on a glass substrate and dried at room temperature and atmospheric pressure for 5-15 min (**Figure 4.1a**). A pre-oxidized PDMS mold was placed in the so-called inverted microcontact printing method (**Figure 4.1b**). In this way only the protruding parts of the mold reacted with the siloxane reagent on the glass surface (**Figure 4.1c**). After a specific reaction time, i.e. 15-45 min, the mold was pulled away.

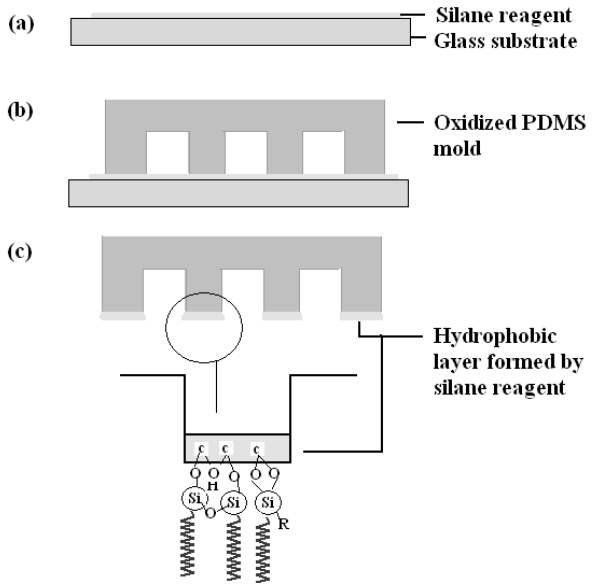

Figure 4.1: Schematic illustration of the modification steps of the mold; (a) deposition of a silane layer on a glass substrate, (b) placing of the mold on the semi-dried silane layer, and (c) hydrophobic layer formation making a hydrophobic interface and hydrophilic channels.

4.2.5. Substrate and mold preparation

A Si (100) wafer was cut with a diamond cutter into 1.5 x 1.5 cm^2 size substrate. A PDMS mold was cut to 1 x 1 cm^2 size and then blown clean with compressed air to remove dust and residual particles. The Si substrate was cleaned with a CO_2 snow jet and then with oxygen plasma for 5 min as described in Sec. 3.2.2 & 3.2.3 respectively. The PDMS mold was then treated with oxygen plasma for 2 min to increase its surface energy (hydrophilicity) and hence its adhesion to the substrate. The water contact angles of both the substrate and PDMS after oxygen plasma treatment were below 5°.

4.2.6. Analysis

Structural characterization was performed by x-ray diffraction (XRD) (Sec. 3.4.1.3). Surface analysis was carried out with a scanning electron microscope (SEM) operating between 0.5 and 30 keV (Sec. 3.4.2.2). Atomic force microscopy (AFM) analyses were performed on a Nanoscope IV instrument (Sec. 3.4.2.3).

4.3. Patterning of TiO_2 with micromolding in capillaries

4.3.1. Patterning of sol-gel derived TiO_2

The plasma treated mold was gently placed on the Si substrate. This mold has two distinct areas, i.e. lines of 3 μm and 5 μm width (w_l), and spacing between the lines of 6

and 10 μm, respectively, whereas the height was 1 μm. A tiny drop of 10-50 μl of the sol was poured at the entrance of the capillaries. After complete filling of the channels of the mold due to capillary action, the wet pattern along with the mold was placed on a hot plate at 40 °C for 10-15 min until evaporation of the solvent into the PDMS was complete. The mold was peeled off carefully without deformation of the patterned lines. The sample was further heated to 80 °C for 30 min, and finally annealed at 550 °C for 60 min.

Figure 4.2a shows sol-gel derived TiO_2 lines obtained with MIMIC. The cross-sectional profile of the lines is somewhat triangular in shape after thermal processing, as can be seen in **Figure 4.2b**. This shape is probably the result of shrinkage of the pattern upon drying. However, in contrast to other materials such as $Pb(Zr_xTi_{1-x})O_3$, or $LaPO_4$:A (A=Eu, Tb) embedded in hybrid silica (Chapter 5 & 6), no gel formation occurred, and therefore no double peak profile evolved. Other factors such as viscosity, types of solvents, pH, and precursor particle size may also affect the final shape of patterns. Nevertheless, the drying behavior is believed to be the most important factor. For 2-dimensional micropatterns, the cross-sectional shape is often less important than its lateral structure. However, in some areas of application rectangular shapes with straight angles between faces are needed, e.g. in 3D wood pile structures. Thus, it becomes important to either modify the technique or use some alternative technique that circumvents this problem.

One of the key requirements in MIMIC is that the features to be patterned should be interconnected in order for the solution to penetrate through the entire mold. A mold with two distinct areas of pillars of diameter (P_r) 800 and 1500 nm, respectively, was applied to make pit-patterned films. **Figures 4.2c and 4.2d** show such pit-patterned films of titania with a pit diameter P_d of 800 and 1500 nm, respectively. The small defects and discontinuities which occur quite regularly can be attributed to dust particles on Si or PDMS, or they may have resulted from the peel-off process of the mold. In the fabrication of miniaturized device components, the effect of contaminants and dust particles becomes more important as the feature sizes get smaller. After treating the substrate and PDMS mold with oxygen plasma, their surface energies increase, making them more attractive for contaminants. For a soft-lithographic technique one does not need clean room facilities. However, dust particles should be avoided as we observed that particles were able to deform areas as large as 10 times its actual size.

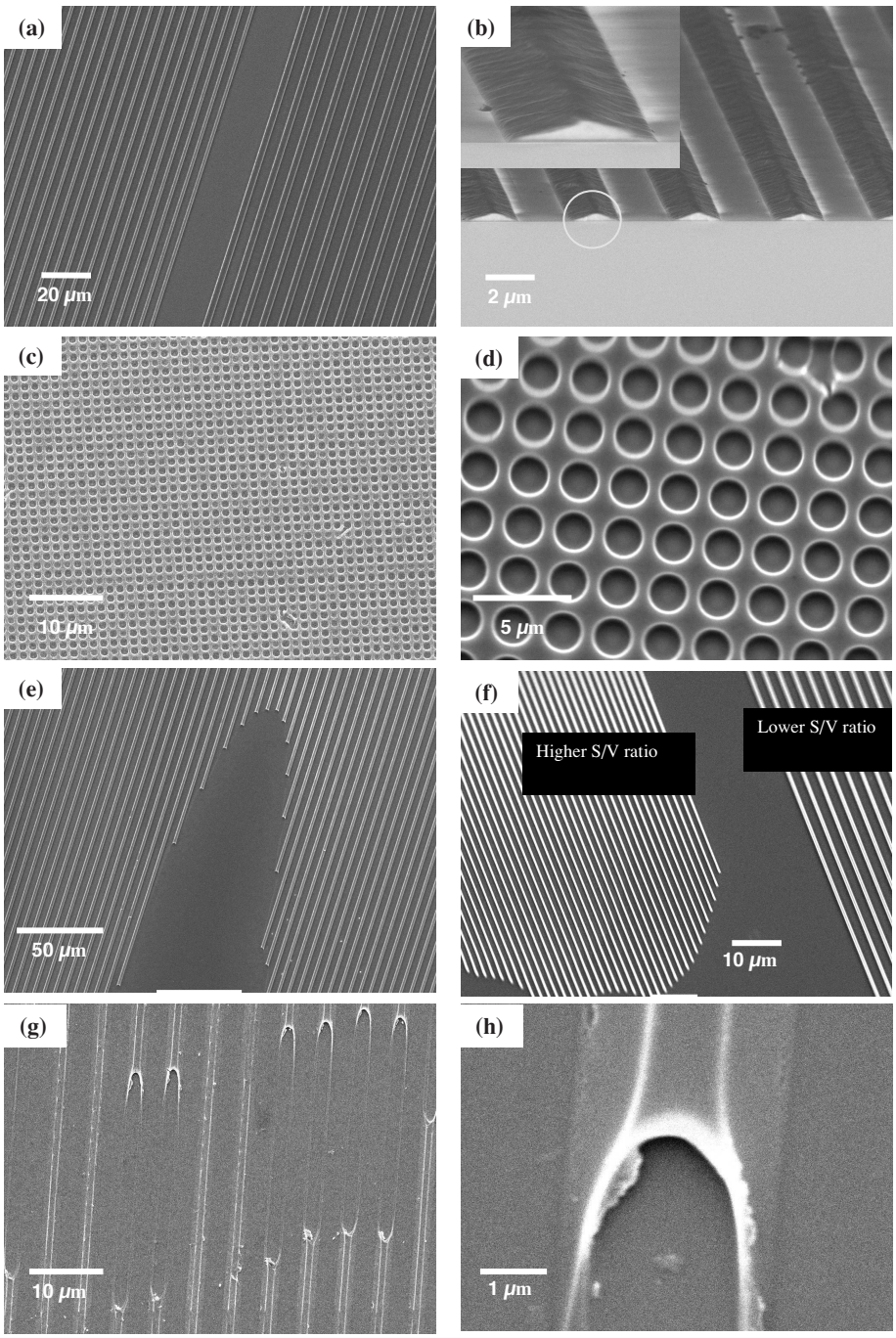

Figure 4.2: SEM images of sol-gel derived TiO_2 patterns produced with MIMIC; (a) pattern with two distinct areas, lines on the left and right have widths w_l = 3 and 5 μm, respectively; (b) line profile with w_l = 3 μm; (c) large area pit pattern with P_d = 800 nm, showing some defects; (d) pit pattern having P_d = 1.5 μm; (e) surface contamination effect in line pattern with w_l = 3μm; and (f)

effect of surface (S) to volume (V) ratio on the penetration length, line on the left and right have w_l = 800 nm and 1.6 μm, respectively; (g & h) fork-shaped ends of penetrating sols, showing that the penetration rate of sols is faster in the corners of the channels. w_l and P_d indicate line width and pit diameter, respectively.

Figure 4.2e shows the effect of a local contamination with low surface energy on the advancing of the liquid from during filling of the channels. The surface energy of the contaminant is lower than that of the penetrating solution, so that the solution cannot wet the contaminated area, and the patterning process is discontinued in every channel that contains the contaminant.

While in MIMIC process, filling of the channels and drying of the solution take place simultaneously. Kim *et al*. have derived a thermodynamic model to describe the filling of a capillary under the influence of capillary force.[16, 17] Using this equation the rate of liquid flow can be estimated from its surface tension, viscosity, cross-sectional area and length of the penetrating capillary:

$$\frac{dz}{dt} = \frac{r_H \gamma_{LV} \cos\theta}{4\eta z} = \frac{r_H (\gamma_{SV} - \gamma_{SL})}{4\eta z} \qquad (1)$$

Here r_H is the hydraulic radius (ratio of volume to surface area), γ_{SV} and γ_{SL} represent the solid-vapor and solid-liquid surface tensions, respectively, and η is the viscosity of the liquid. Similarly, z is the filled length of the channel, and t represents time.

Although the equation is derived for a tubular capillary, it provides good estimates for other shapes as well. According to Equation (1), penetration should proceed indefinitely. In practice however, the process stops after a certain period of time and/or length of penetration. This is due to the fact that as the solution penetrates into the channel, solvent from the solution diffuses into the microporous PDMS walls, so that the solids content in the entering solution increases continuously, in particular near the capillary front. As a result, the viscosity of the solution increases, reducing the penetration rate. Ultimately, the viscosity becomes so high that it prevents further penetration. **Figure 4.2f** shows the effect of surface to volume ratio of lines with different dimensions on the ultimate penetration length of the patterned lines. The lines with smaller diameter, i.e. high surface/volume (S/V) ratio dried faster than the wider ones. As a result, the penetration length of narrow channels was found to be smaller than that of wider ones.

Heule *et al*. reported on the patterning of powder-based tin oxide (SnO_2) patterns by MIMIC.[18] The formation of fork-shaped spikes was attributed to the faster penetration of the solution in the corners of the channels. We observed the same phenomenon while patterning sol-gel based TiO_2 lines. However, it only occurred when the mold was left on the substrate for longer periods of time, i.e. 60 min or more. Examples are

shown in **Figure 4.2g & 4.2h**. Another possible reason could be the lack of supply of solution to further fill the capillaries. Incomplete filling could thus lead to the formation of these spikes.

Structural analysis

The diffraction spectra of a sol-gel derived TiO_2 patterned film on a Si (100) substrate is shown in **Figure 4.3**. All peaks correspond to the anatase phase of TiO_2 and to the Si (100) substrate. The film was initially dried at 40 °C for 10 min and then at 80 °C for 30 min. Subsequently they were annealed at 550 °C at a heating and cooling rate of 5 °C/min, and holding time of 60 min.

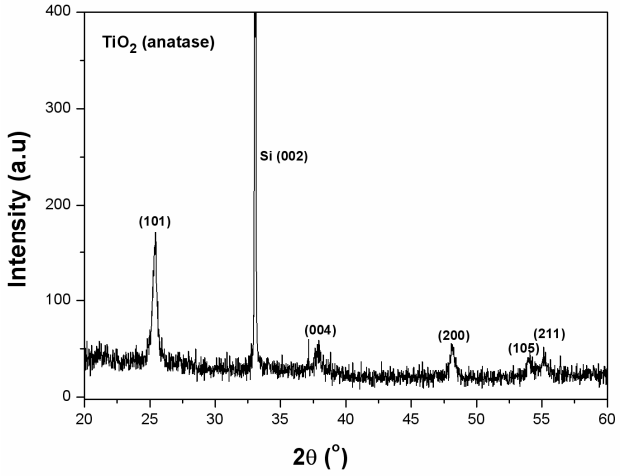

Figure 4.3: *θ-2θ* scan of sol-gel derived TiO_2 pattern on Si (100) substrate; annealed at 550 °C for 60 min.

4.3.2. Topographic study of patterns - Shrinkage & cracking

The MIMIC technique requires solutions with a low viscosity for fast and complete penetration throughout the entire network of channels. To ensure a sufficiently low viscosity, the solids content should remain low. Depending on the material, this results in huge volumetric shrinkage of the patterns during drying and thermal annealing.[19,20] This reduces the fidelity of the resulting patterns. Furthermore, in most applications some kind of functionalization of the patterned surface is necessary, for example the deposition of top electrodes onto a pre-patterned film. Thus, it is necessary for such patterns to have a rectangular shape. As the discussion above indicated, shrinkage reduces the control over the final shape in MIMIC processes.

Another important aspect is crack generation in patterned films. Films that are first heated to elevated temperatures and then cooled to room temperature will sense intrinsic stresses; i.e. compressive and/or tensile stress. This intrinsic stress normally originates from one or more of the following reasons: (a) volumetric shrinkage upon thermal annealing, (b) differences in coefficients of thermal expansion between substrate and film, (c) phase transformations, or (d) clamping of the film to the substrate. Intrinsic stress can ultimately result in the cracking of thin films and patterns. Cracking has two major stages; first crack initiation, and crack propagation. It is interesting to note that the tendency to cracking was considerably smaller in MIMIC-patterned films than in spin-coated thin films. This is because cracks can propagate in all direction in thin films to release internal stresses. However, in patterned lines or similar structures with micrometer-scale lateral dimensions in at least one direction, developed stresses can relax in the direction that is perpendicular to both the plane of substrate, and the main axis of the line. In other words, since all patterned features (lines, pillars) are isolated from each other, a crack that is initiated in one feature cannot propagate to another, provided that the patterned features are not connected via a thick residue layer. As far as cracks are formed, they are mostly the result of in-plane tensile stresses that occur in the main direction of the lines. The crack planes that occur are therefore oriented perpendicular to this direction.

Figures 4.4a and 4.4b show examples of shrinkage and cracking phenomena of multiple and single TiO_2 lines. As can be observed the cracks in a line do not propagate through the entire pattern, but run mostly in the direction perpendicular to the main direction of the line. Similarly, **Figures 4.4c and 4.4d** show the effects of shrinkage of pit-patterned films. However, the predominant shrinkage takes place in vertical rather than in lateral direction.[19,20] This is due to the fact that the patterned film is clamped to a substrate in the lateral directions, and is free to move in the vertical direction. For these TiO_2 patterns a total volumetric shrinkage of ca. 97% was found.

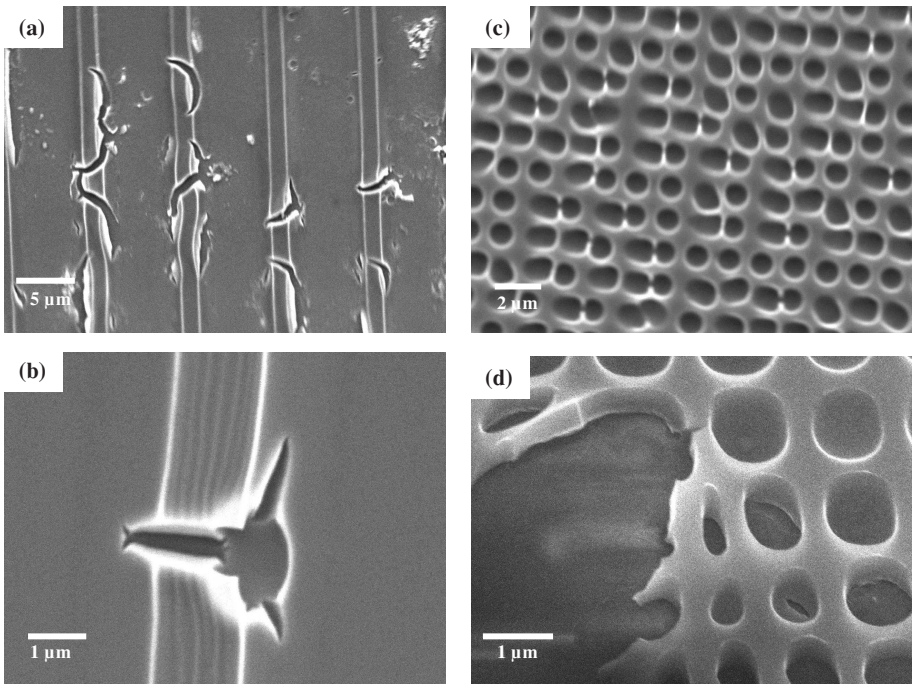

Figure 4.4: Sol-gel based TiO_2 patterns obtained with MIMIC showing cracks that are due to shrinkage after thermal processing of (a & b) line patterns; and (c&d) pit patterns.

4.3.3. Dispersion Derived TiO_2 Patterns

In order to avoid severe shrinkage and obtain denser and more regularly shaped patterns, MIMIC was also applied to dispersion-based TiO_2 with solids contents of 10, 20, and 30% by volume. Among these the dispersion with 10 vol.% solids loading yielded better patterns than the other two dispersions. Dispersions with solids contents above 10 vol.% showed a poorer quality of channel filling, because the larger viscosities of these solutions hampered easy penetration into the channels. The dispersions were prepared as described in section 4.2.3. **Figures 4.5a and 4.5b** show SEM pictures of TiO_2 line patterns with a line width of 3 µm derived from dispersions with 10 vol.% titania. **Figure 4.5c** shows an AFM topographic image of this line pattern. The cross-sectional profile of the lines derived from dispersions was found to be comparatively more rectangular than those derived from sol-gel, although they were not completely rectangular either. Furthermore, the solids mass per unit surface area in the final patterns was higher than in comparable patterns derived from sol-gel precursors. The dispersions with higher solids contents showed a decreased penetration rate and length because of their high viscosity. The rate of filling decreases as the viscosity increases and because of the continuous drying of dispersions during the MIMIC process. These

observations were found to be in agreement with the work of Heule *et al.*,[18] although they used molds with semi-circular shaped channels.

Figure 4.5.d & 4.5e show SEM pictures of a pit-patterned film with P_d of ca. 3 µm after thermal treatment. **Figure 4.5f** shows the AFM picture of a pit with P_d of ca. 1.5 µm. Some coarse grains/particles were observed at the edge of the pits. We noticed two drawbacks in dispersion-based solutions. Firstly, the adhesion of the patterns to the silicon substrate was poor in comparison with sol-gel derived films. Secondly, the patterns were much more porous and needed higher sintering temperatures (ca. 800 °C or higher) for densification. Very high processing temperatures limit the use of substrates that are not stable at higher temperature. Thirdly, the surface roughness of patterns derived from dispersions was also higher, since the particles in solution agglomerated, leading to larger and coarser particles.

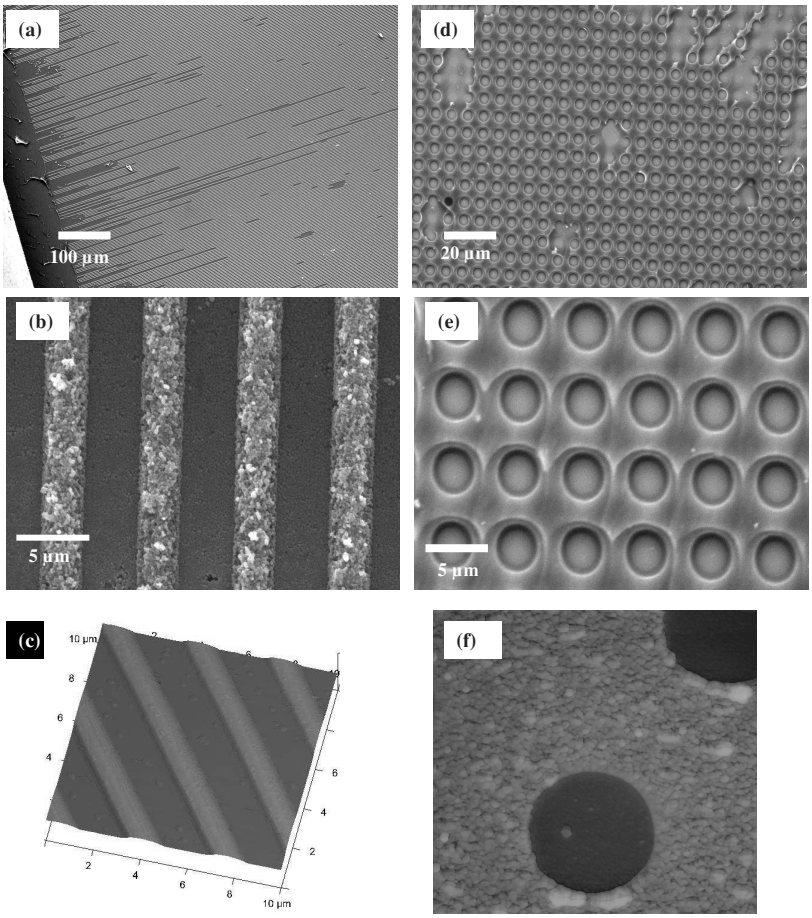

Figure 4.5: SEM and AFM images of 10 vol. % dispersion based TiO_2 lines patterned with MIMIC; (a): large area pattern of lines; (b): close-up from (a) showing the shape of lines with w_l

of 3 μm; (c): AFM image of the same line pattern; (d) large area pit-patterned film; (e): close-up of pit pattern with P_d =1.5 μm; (f) AFM image of pit-patterned film having P_d =1.5 μm.

4.3.4. Dispersion Derived 3D TiO_2 Patterning

As discussed in the introduction of this chapter, 3D wood pile patterns may find application in photonics for wave-guiding and photonic crystals. The titania dispersions were used to make stacks of 2 layers of TiO_2 lines by applying MIMIC. **Figure 4.6a** depicts the schematic procedure adopted for patterning these 3D structures. The first layer was patterned with conventional MIMIC as described in 3.3.1. The pattern was dried at 80 °C for 1 h. Then, a thin film of polyurethane (PU) was spin-coated on top with 1500 rpm. The PU film was cured by exposure to UV light with a wavelength of 350 nm for 2 h. Subsequently, the PU film was treated in oxygen plasma for 5-10 min, in order to improve its adhesion to the PDMS mold for the next layer to be deposited. A fresh PDMS mold was also treated in oxygen plasma for 5 min and placed very carefully on top of the PU film in such a way that channels of the mold were oriented perpendicular to the lines of the first layer. Then a second layer was patterned on top of the PU film using MIMIC. Finally, after drying the buried PU film was degraded by annealing the sample at 550 °C in air for 2 h. This yielded a 3D wood pile pattern with line width w_l of ca. 4 μm, as shown in **Figures 4.6b** and **4.6c**. In principle, the same procedure is expected to be applicable to stack a third or more layers. However, defects and errors that occur in one layer will be transmitted to the layers above. Thus, increasing the number of layers also promotes the number of defects in the final pattern, especially in the upper layers. Furthermore, the weight of the mold while placing it on top of the green body may also produce defects. It was found that the adhesion of the second layer to the underlying PU-titania substrate was weaker than the adhesion of the first layer to the substrate. The adhesion was improved by oxygen plasma treatment of the polymer film for 5 min prior to deposition of the second layer.

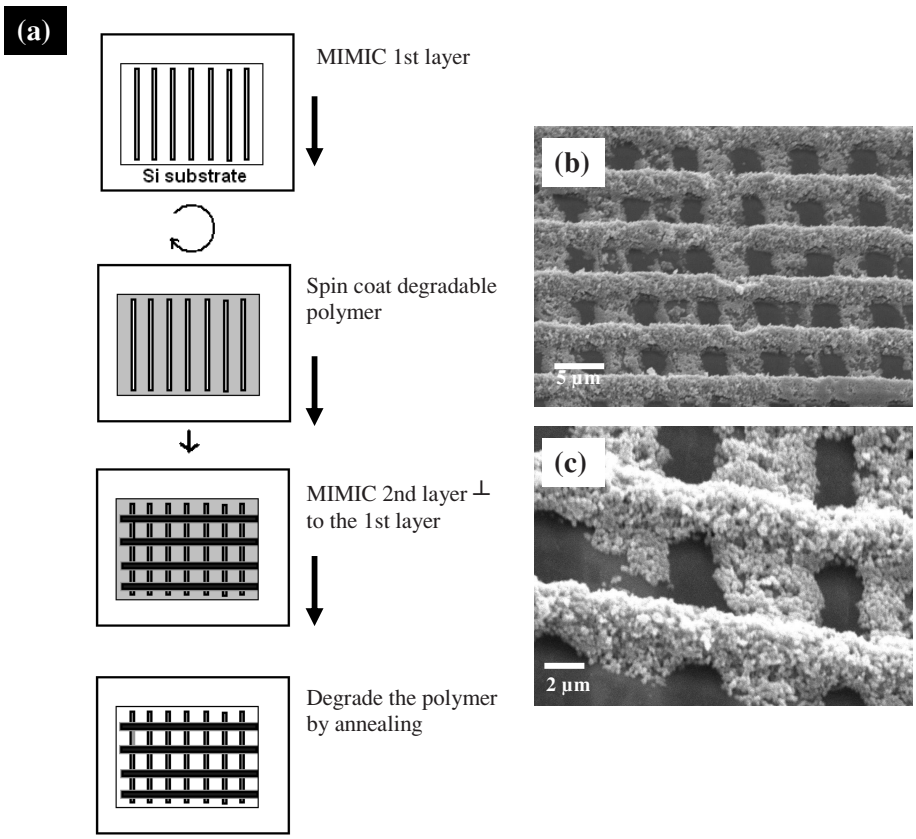

Figure 4.6: **(a)** Schematic illustration of the MIMIC procedure for 3D patterning; **(b & c)** TiO_2 3D wood pile patterns with line width w_l = 4 µm.

4.3.5. Residue layer formation and how to prevent it by stable modification of PDMS mold

In order to improve the adhesion between substrate and mold, their surface energies were increased by oxygen plasma treatment. The mechanism of surface energy increase has been explained in Sec. 3.2.3.2. It leads to a measurable decrease of the water contact angle, and therefore, to an increase of the capillary force on the penetrating solution. This will increase the penetration rate and final penetration length when all other variables remain the same. The surfaces of the substrate and the mold are not perfectly flat. On nanoscopic level they show surface roughness. These irregularities may prevent confocal contact in some local areas, leading to the formation of very small pores between substrate and mold (**Figure 4.7a)**. According to Equation (1), the penetration rate (dZ/dt) is proportional to the radius of the capillary. This implies that the narrower the channel is, the larger will be the capillary force that it exerts. Thus, the capillary force exerted by the very small pores between substrate and mold is much

higher than the capillary force exerted by the micrometer-sized capillaries and channels. This inevitably leads to the formation of an unwanted thin layer underneath the mold, which is called a "residue layer". Theoretically, a residue layer may form when the size of the precursor entities in solution is smaller than the size of the small pores. The thickness of the residue layer is typically between 5-50 nm. On the other hand, if the surface energies of substrate and mold are not increased, the contact angle of the precursor solution inside the channels is unfavorable. This prevents the formation of a residue layer, but also reduces the penetration length of the liquid, and leads to incomplete filling of the mold. To have sufficient penetration without formation of a residue layer, alternative measures should be taken.

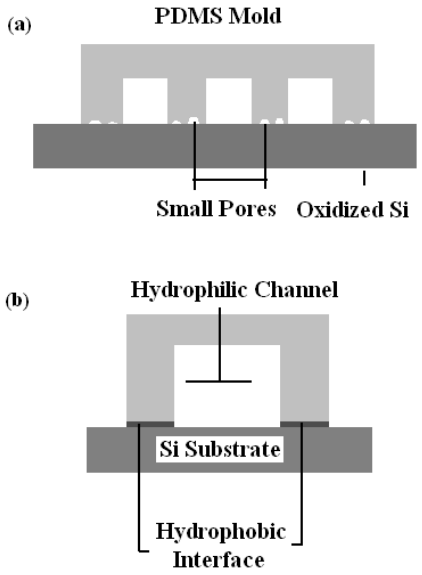

Figure 4.7: Schematic illustration of (a) pore formation at the interface between mold and substrate, and (b) modified mold with hydrophobic interface and hydrophilic channel.

When MIMIC is being used, an ideal configuration would be to have a mold with a comparatively hydrophobic interface in areas where it makes contact with the substrate, and hydrophilic micro-capillaries. This is schematically shown in **Figure 4.7b**. To fabricate such a mold, we adopted the experimental procedure described in section 3.2.4.

Figure 4.8 shows SEM micrographs of TiO_2 lines made by MIMIC. As can be seen in **Figure 4.8a**, the use of a chemically unmodified plasma-treated mold led to formation of a residue layer between the lines. **Figure 4.8b** shows the effect of

modifying the mold with octadecyl trichloro-silane (OTS). The residue layer was reduced to a large extent and only small traces of residue layer could still be observed. In this case the mold had been oxygen plasma treated for 2.5 min prior to silane layer deposition. Even better results were obtained when the mold was plasma-treated for 5 min prior to silanization, as is shown in **Figure 4.8c**. No residue layer was observed at any location. The quality and reproducibility of lines that can be made with these molds depends on many factors which will be explained in the following.

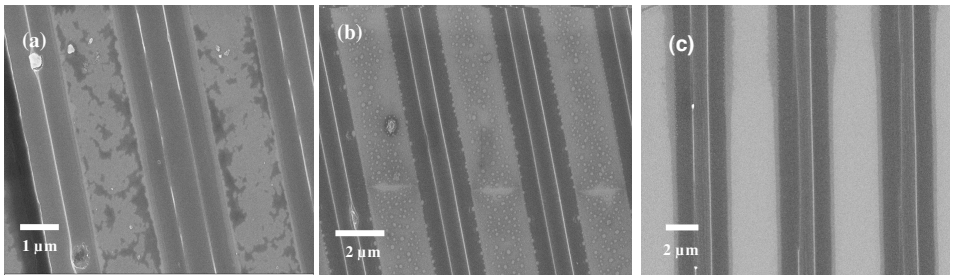

Figure 4.8: SEM micrographs of MIMIC made TiO_2 line patterns using (a) a non-silanized mold; (b) a mold that was silanized after 2.5 min of oxygen plasma treatment; (c) a mold that was silanized after 5 min of oxygen plasma treatment.

The following factors were found to have significant effects:

I. ***Oxygen plasma treatment***

The duration of oxygen plasma treatment to increase the surface energy of the PDMS mold prior to silanization is of prime importance. Molds that had been plasma-treated for a too long period of time became so hydrophilic that the OTS diffused to the inner walls of the channels, making them hydrophobic. On the other hand, when the molds were plasma-treated for a very short period of time (<2 min), then incomplete filling of the capillary channels occurred during the patterning step. It was found that an oxygen plasma treatment of 5 min yielded water contact angles smaller than 3°. This period of treatment gave good results. Very thin or no residue layers were observed in combination with complete filling of capillaries.

II. ***Concentration of silane***

Another important factor is the concentration of the organosilane (OTS) in the solvent toluene. The optimum concentration of OTS in toluene in this experiment was found to be $2.02 \cdot 10^{-5}$ M. Concentrations below this value resulted in the formation of a non-uniform residue layer, whereas higher concentrations reduced the penetration length. This is because higher concentration makes the channels of the mold hydrophobic through diffusion, and thus reduces the penetration length during MIMIC.

III. ***Time of contact between mold and silane***

The time of contact of the oxidized mold with the silanized glass substrate is also of importance. Very long contact times resulted in diffusion of organosilane to the capillaries, making them more hydrophobic and increasing the contact angle, thereby reducing the capillary force. Short contact times resulted in some residue layer, because no good or an incomplete OTS layer was formed. Contact times of 5-45 min were applied in our experiments. A contact time of 15 min gave the best results.

In summary, modification of the protruding parts of the mold worked well to avoid residual layer formation. The balance between capillary filling and residue layer formation can be established by optimizing the oxygen plasma treatment, the amount and concentration of organosilane, and the time of contact between mold and silane.

4.4. Conclusions

Micromolding in capillaries was successfully used to form 2D and 3D TiO_2 patterns on Si substrates. Two types of liquids, namely sol-gel solution and dispersions were used as precursors and both were found to have their own advantages and limitations. The sol-gel derived patterns were much denser and showed good adhesion to the substrate. However, the large shrinkage and non-uniform shape after drying and thermal annealing limits their use in 3D pattern fabrication. In contrast, patterns derived from dispersions showed less or no shrinkage and their shapes changed less than the sol-gel derived patterns. Nevertheless, their adhesion to the substrate was poor. They were also more porous, and needed higher sintering temperatures for full densification. This limits their use to pattern substrates that are not stable at high temperatures.

Another important aspect of the MIMIC technique is the formation of an unavoidable residue layer between molded features. Chemical modification of the protruding features of the PDMS mold can be applied to avoid its occurrence.

Nevertheless, MIMIC has a large potential for the fabrication of a variety of materials from their respective solutions with little or small changes in the process parameters.

The 2D patterns may find application in gas sensors, where large surface area patterns are needed. The 3D wood pile patterns could be important in photonics, e.g. as waveguides and photonic crystals.

References

[1] Yoldas, B.E.; O'Keeffe, T.W. *Appl. Opt.* 18, 3133, **1979**

[2] Es-Souni, M.; Oja, I.; Krunk, M. *J. Mater. Sci. Mater. Elec.* 15, 6, 341, **2004**

[3] O'Regan, B.; Grätzel, M.; *Nature*, 353, 737-740, **1991**

[4] Dinh, N.N.; Oanh, N.Th.T. Long, P.D.; Bernard, M.C.; Goff, A.H-Le. *Thin Solid Films*, 423, (1), 70-76, **2003**

[5] Jin, P.; Mia, L.; Tanemura, S.; Xu, G.; Tazawa, M.; Yoshimura, K. *Appl. Surf. Sci.* 212-213, 775-778, **2003**

[6] Jung, H-G.; Sung, Woo Oh, S.; Ce, J.; Jayaprakash, N.; Sun, Y-K. *Electrochem. Comm.* 11, 756-759, **2009**

[7] Ferroni, M.; Carotta, M.C.; Guidi, V.; Martinelli, G.; Ronconi, F.; Richard, O.; Van Dyck, D.; Van Landuyt, J. *Sensors and Actuators*, B68, 140-145, **2000**

[8] Bonini, N.; Carotta, M.C.; Chiorino, A.; Guidi, V.; Malagu, C.; Martinelli, G.; Paglialonga, L.; Sacerdoti, M. *Sensors and Actuators*, B68, 274-280, **2000**

[9] Göpel, W.; Rocker, G. *Phys. Rev. B* 28, 3427-3438, **1983**

[10] Fukuda, H.; Maeda, S.; Salam, K.M.A.; Nomura, S. *Jpn. J. Appl. Phys*. 41, 6912-6915, **2002**

[11] Xia, Y.; Whitesides, G.M. *Angew. Chem. Int. Ed.* 37, 550-575, **1998**

[12] Duineveld, P.C. *Langmuir*, 18, 9554-9559, **2002**

[13] Kim, E.; Xia, Y.; Whitesides, G.M. *J. Am. Chem. Soc.* 118, 5722-5731, **1996**

[14] Shi, G.; Lu, N.; Gao, L.; Xu, H.; Yang, B.; Li, Y.; Wu, Y.; Chi, L. *Langmuir*, 25, (17), 9639-9643, **2009**

[15] Goh, C.; Coakley, K.M.; McGehee, M.D. *Nano Lett*. 5, 8, **2005**

[16] Kim, E.; Whitesides, G.M. *J. Phys. Chem. B*, 101, 855-863, **1997**

[17] Kim, E.; Xia, Y.; Whitesides, G.M. *Nature*, 376, 581-584, **1995**

[18] Heule, M.; Schell, J.; Gauckler, L.J. *J. Am. Ceram. Soc.* 86, 407-412, **2003**

[19] Khan, S.U.; Göbel, O.F.; ten Elshof, J.E.; Blank, D.H.A. *ACS Appl. Mater. Interfaces,* 10, 2250-2255, **2009**

[20] Vartuli, J. S.; Özenbas, M.; Chun, C. M.; Trau, M.; Aksay, I. A. *J. Mater. Res. 18*, 1259–1265, **2003**

5

Patterning of Luminescent Nano-crystalline $LaPO_4$:Eu and $CePO_4$:Tb Particles Embedded in Hybrid Organosilica

Abstract

Eu^{3+} doped $LaPO_4$ and Tb^{3+} doped $CePO_4$ luminescent nanoparticles embedded in hybrid organosilica were patterned by soft-lithography. The patterns were annealed at 300 ^oC in nitrogen environment for 30 minutes after initial drying at room temperature. They were characterized with optical and photoluminescence (PL) microscopy, x-ray diffraction (XRD), and scanning electron microscopy (SEM). Compositional analyses were carried out with x-ray photoelectron spectroscopy (XPS), Low energy ion scattering (LEIS), and secondary ion mass spectroscopy (SIMS). The luminescence intensities were found to be low either due to low concentration of nanoparticles, and/or to some quenching phenomenon.

5.1. Introduction

Oxide materials doped with lanthanide ions comprise a class of materials that have great technological importance in areas such as phosphor lamps, displays, sensors, lasers, and optical amplifiers.[1-3] At nanometer scale these materials have high surface-to-volume ratio and enhanced structural, electronic, and optical properties in comparison to the bulk phase. Generally, oxide materials are known to be good hosts for lanthanide ions, since they provide good quantum yields. For example, lanthanum orthophosphate ($LaPO_4$) is an excellent host for ions such as europium, cerium, and terbium in the fabrication of photoluminescent materials.[3,4]

At present the most common technologies used for the deposition of these materials are electrophoretic deposition,[5-7] screen printing,[8] pulsed laser deposition,[9,10] and traditional photolithography.[11] In fact, the patterning techniques used for phosphor screens are known to have a great effect on the resolution of flat panel displays.[12]

Soft-lithographic techniques[13] could be used as alternative techniques, when simplicity, ease of use and cost effectiveness is targeted. They are cheap, easy and simple and most importantly, they need no clean room conditions or complicated and lengthy processing steps. So far, relatively little work has been reported on the use of soft-lithographic techniques for the patterning of luminescent materials. Yu *et al.*

applied micromolding in capillaries (MIMIC) to pattern a Pechini sol-gel based nanocrystalline YVO_4:A (A=Eu^{3+}, Dy^{3+}, Sm^{3+}, Er^{3+}) phosphor films.[12] Pisignano *et al*. employed mechanical lithographic techniques to print 1D patterns of light emitting materials embedded in organic films.[14] They reported that patterned films exhibited enhanced luminescence (by more than a factor of two) as compared to non-patterned films. Similarly, Han and co-workers[15] applied the technique of MIMIC to sol-gel based phosphor patterned lines having various line widths. The patterned and non-patterned films exhibited the same optical properties.

Here the use of MIMIC (Sect. 2.2.3 & 3.3.1) and μTM (Sec. 2.2.1 & 3.3.2) for the patterning of two types of luminescent nano-particles embedded in hybrid organosilica is reported. The patterning methods were applied to obtain the 2D line patterns and 3D wood pile structures. The same techniques can also be utilized to pattern other complex oxides and composite materials from liquid solutions.

5.2. Experimental

5.2.1. Materials

Unless otherwise stated, reagents were used as received without further purification. The organosilane precursor 1,2-bis(triethoxysilyl)ethane (99.999%) abbreviated as BTESE, nitric acid (65%), polyoxyethylene 20 cetyl ether (Brij 58), and ethanol (99.8%) were all purchased from Aldrich. N, N-dimethylformamide (99.8%) (DMF) was purchased from Merck.

5.2.2. Synthesis of luminescent lanthanide phosphate nano-particles

Two types of luminescent nano-particles (NPs), namely $LaPO_4$:Eu and $CePO_4$:Tb, having particle diameters (Φ) of 5-8 nm, were used for patterning in the present work. The synthesis route adopted was according to Riwotzki *et al*. and was scaled down to 10 mmol and slightly modified.[16]

In short, to a solution of lanthanide chloride hydrate salts (10 mmol) in methanol (50 mL), tris(2-ethylhexyl) phosphate (TEHP, 60 mL) was added. Under reduced pressure (10 mbar at 60 °C), methanol and water were evaporated. Depending on the lanthanide ions used for the synthesis, the remaining solution sometimes remained slightly colored.

In parallel, a solution of crystalline phosphoric acid (980 mg, 10 mmol) in tris(2-ethylhexyl) phosphate (30 mL) and tri-n-octylamine (TOA, 13.1 mL, 30 mmol) was prepared. The dissolved acid solution was heated to 80 °C, and water and oxygen were removed by the vacuum. The solution was flushed with argon three times before the lanthanide-ion solution was added. Again, the flask was evacuated and flushed with argon three times before the mixture was heated to 200 °C for 20 h in order to minimize the oxidation of cerium(III) to cerium(IV). During the reaction, the temperature

decreased by 30 °C to 170-175 °C. The heating was stopped and the colloidal solution was cooled to room temperature. Then, the solution was added to methanol (400 mL) in a separating funnel to precipitate the nanocrystals as white solid.

Preparation of nano-particles solution embedded in hybrid silica

Solution a): 10 mg of the $LaPO_4$:Eu NPs were dissolved in 5 ml of DMF and stirred at 100 °C for 1 h. In case of $CePO_4$:Tb the NPs were dissolved in ethanol and stirred for 1 h at room temperature. When needed, the amount of solvent was varied for the adjustment of viscosity.

Solution b): Aqueous nitric acid (0.5 ml concentrated HNO_3 in 1.8 ml of water) was added dropwise to 1.8 ml of 1,2-bis(triethoxysilyl)ethane (BTESE) and 5.0 ml of ethanol while stirring in an ice bath. The mixture was refluxed for 2-3 h at 60 °C.

Solutions of various concentrations were made by mixing solutions *a* and *b* in various proportions. The viscosity was adjusted by adding small amounts of Brij 58 to the final solution and stirring for 2-3 h. The viscosity of the final solution was measured to be 4.210 mPa·s.

5.3. Results and Discussion

5.3.1. Patterning of $LaPO_4$:Eu by Micromolding in Capillaries

Micromolding in capillaries (MIMIC) as described in Sec. 2.2.3. & 3.3.1 was applied to pattern $LaPO_4$:Eu nano-particles (NPs) embedded in hybrid organosilica. The Si substrates and PDMS molds were cleaned with snow jet and/or oxygen plasma for a period of time as described in Sec. 3.2.3.2. **Figure 5.1** shows SEM and AFM images of line and pit patterned films. The complete filling of the capillaries took 10-15 min. The wet patterns were then left for 10-60 min (with the mold) at 80 °C on a hot plate in order to evaporate the solvents, and were annealed at 300 °C for 30 min in nitrogen. **Figure 5.1a** shows an example of such a line pattern having a line width (w_l) of 6 μm and spacing between the lines (s_l) of 12 μm. The adhesion of the filled mold to the substrate after drying was found to be stronger than for TiO_2 patterns lines (chapter 4). In some cases the strong adhesion resulted in detachment of a residue layer from the mold and stayed on the substrate. An example is shown in **Figure 5.1b**, where the darkest lines, which are mostly located in the lower part of the picture, are the residue lines of PDMS, while the less dark lines between the PDMS residues are actual patterned organosilica lines. The resulting shapes of the organosilica pattern are not perfect replicas of the master from which they are obtained, as can been seen in **Figure 5.1c**. However, compared to the patterned TiO_2 lines (chapter 4), the organosilica lines were comparatively different in shape. **Figure 5.1d** shows an AFM image that illustrates the surface roughness between the patterned features due to PDMS residues.

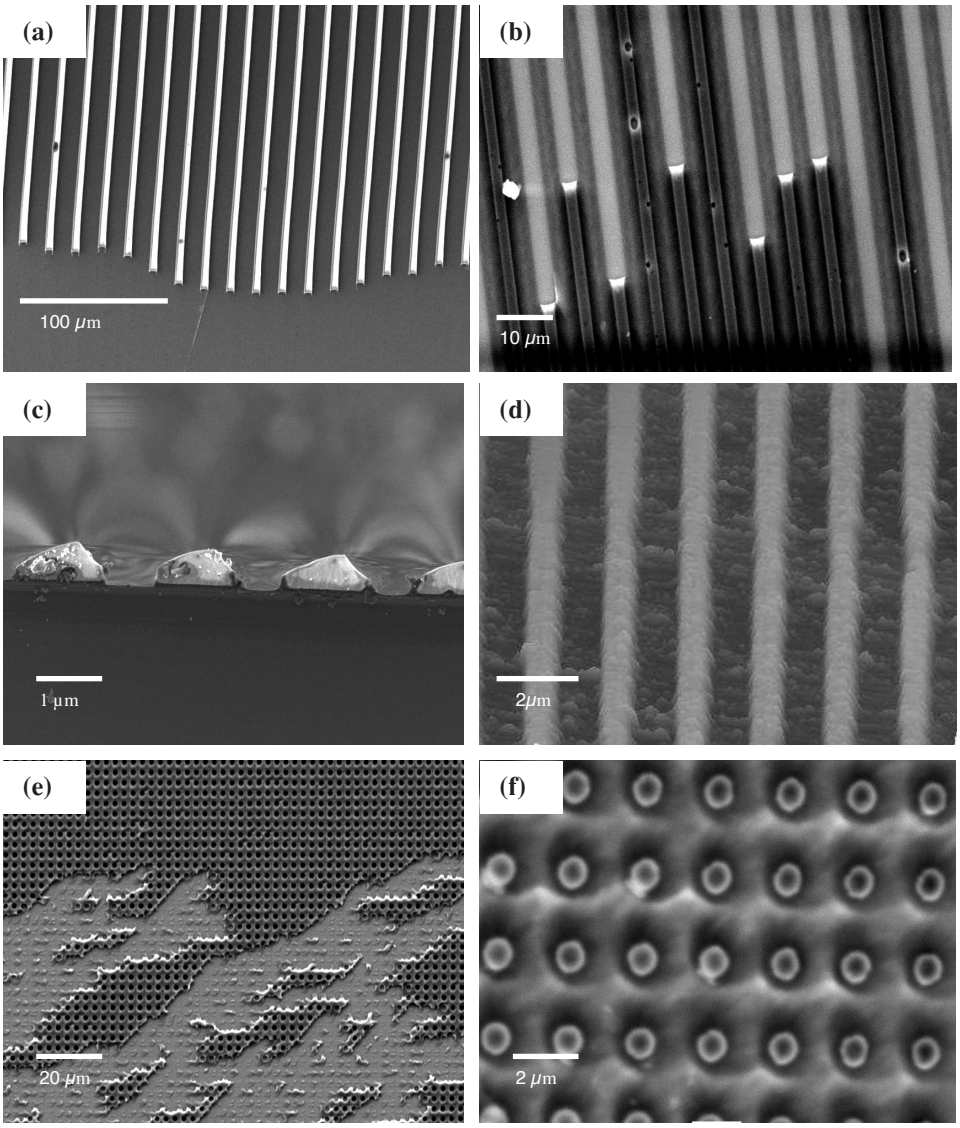

Figure 5.1: SEM and AFM images of $LaPO_4$:Eu NPs embedded in hybrid organosilica and made with the MIMIC technique. (a) SEM image of line patterns having w_l=6 μm & S_l=12 μm; (b) SEM image of a non-annealed line pattern showing patterned lines and PDMS residue; (c) Cross-sectional SEM image of 1.5 μm patterned lines; (d) AFM image of 1 μm wide lines showing surface roughness due to residual PDMS layer; (e) SEM image of pit-patterned film having P_d= 800 nm, depicting the detachment of the pattern due to strong adhesion of the film to the mold; and (f) pit pattern showing white PDMS residues inside the pit pattern. Here w_l, s_l, and P_d mean the width of the lines, spacing between the lines, and diameter of the pit, respectively.

The strong adhesion between mold, pattern and substrate can have two consequences. It may either result in the detachment of PDMS from the mold and its adhesion to the substrate (**Figure 5.1b**), or in the detachment of the patterned film from the substrate. An example of the latter effect is shown in **Figure 5.1e**, where a pit-patterned film was removed together with the mold. This problem can be solved by careful adjustment of the surface energy of the mold by varying the time of plasma treatment, as shown elsewhere.[17] The white areas inside the holes in the pit-patterned film in **Figure 5.1f** also shows the residue layer.

5.3.2. Patterning of $LaPO_4$:Eu by Microtransfer Molding

As discussed in the previous section the adhesion of MIMIC-patterned films was too strong that it resulted in the partial detachment (removal) of the patterned material. In order to circumvent this problem we applied microtransfer molding (μTM). A tiny drop of solution containing NPs was gently placed on a PDMS mold after it had been treated with oxygen plasma for 20-60 s. After removing the excess material from the protruding parts of the mold with a clean PDMS or steel block, the mold was placed and pressed carefully onto a clean Si substrate. Mold and pattern were then placed on a hot plate at 80 °C for 10-30 min to solidify the wet pattern. **Figure 5.2a&b** show line patterns having w_l of 6 μm made with μTM. Similarly, **Figure 5.2c** shows an AFM height image of the shape of the pattern. The shape profile is more rectangular than those derived from MIMIC.

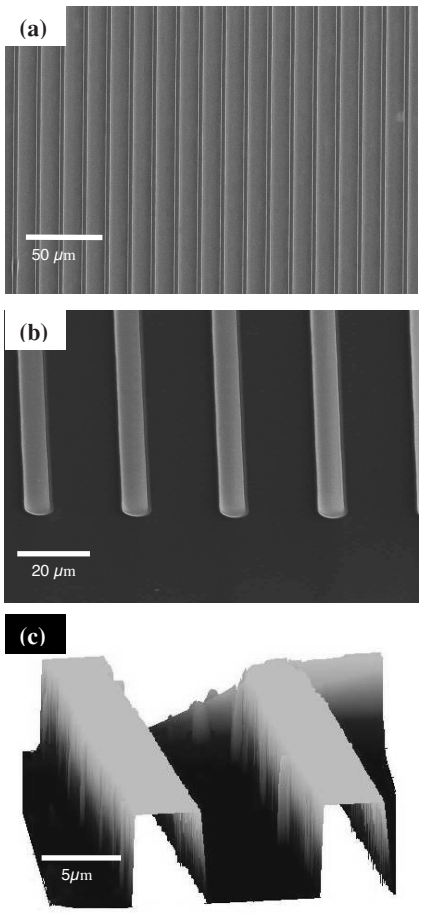

Figure 5.2: Images of $LaPO_4$:Eu lines having w_l=6 μm & s_l=12 μm patterned with μTM; (a&b) SEM images; and (c) topographic AFM. The shape of the line is more rectangular than those derived from MIMIC.

The main reason that the shape of the pattern is replicated well with μTM is probably that the channels of the mold are filled prior to replication, and exposed to air, to which solvents can evaporate faster and more homogeneously than through the mold as in MIMIC.

5.3.3. Patterning of $CePO_4$:Tb NPs

MIMIC and μTM were applied to pattern $CePO_4$:Tb NPs of various dimensions and shapes. **Figure 5.3a** shows a MIMIC-made line patterned film having w_l of 6 μm. The filling length of the channels was higher and the evaporation was comparatively faster than that of $LaPO_4$:Eu NPs which were stabilized in DMF, since ethanol evaporates

faster than DMF. Furthermore, DMF was observed to be less compatible with PDMS, since it degraded the polymer when it was left in contact with PDMS for longer periods of time. **Figure 5.3b** shows a μTM-derived line patterned film having w_l 3 μm before annealing. Residue PDMS lines between the actual patterned lines can be observed. This was found to happen when the PDMS mold was treated in oxygen plasma for more than 30 s. Longer plasma treatment times increase the surface energy of the mold by oxidizing PDMS to amorphous SiO_x, which is brittle. The surface energy increased the bonding strength between mold and substrate, and the brittleness of the oxidized PDMS layer.

Molds treated within oxygen plasma for shorter periods of 20-30 s were found to be suitable for replication of features (**Figure 5.3c**). On the other hand, a mold treated with plasma for a too short period of time reduces the adhesion of the patterned material with the substrate. In that case the patterned material may detach from the substrate. An example is shown in **Figure 5.3d**, where the displacement of line patterns and their detachment from the substrate can be observed.

An advantage of μTM over MIMIC is the possibility of patterning isolated features. Examples of patterned isolated pillars having diameters (P_r) of 800 and 1500 nm are shown in the lower and upper part of **Figure 5.3e**. In **Figure 5.3f** the residue layer between the patterned features is visible. This occurs when the excess solution was not completely removed from the mold prior to their registration onto the substrate.

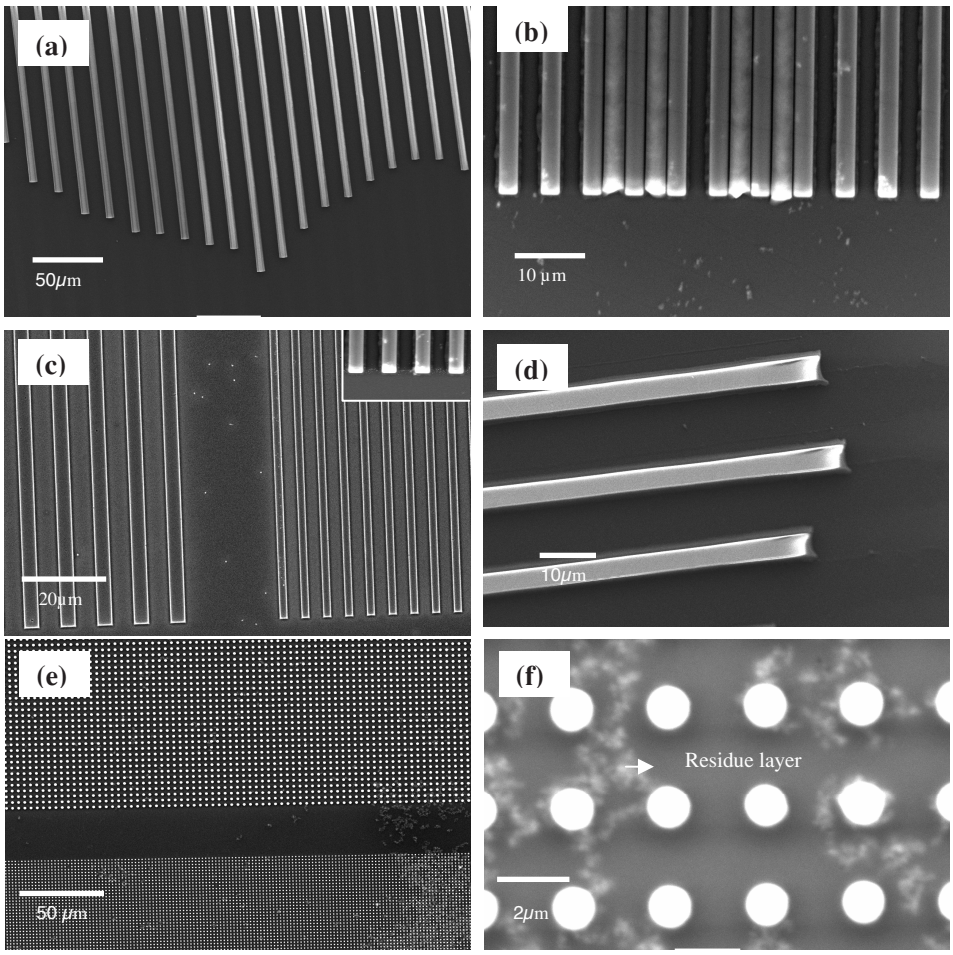

Figure 5.3: SEM images of $CePO_4$:Tb fluorescence NPs in hybrid silica; (a) line pattern made with MIMIC having w_l=6 μm; (b) line pattern made with μTM showing residue of PDMS lines between the patterned lines as a result of strong adhesion; (c) line pattern made with μTM having w_l=5μm (left) and w_l=3μm (right); (d) μTM derived line pattern showing displacement and detachment of the lines due to poor adhesion to the substrate ; (e) μTM derived pillars pattern having diameter of P_r=800 nm (lower part), and P_r=1500 nm (upper part); and (f) pillar pattern showing the residue layer between the pillars.

5.3.4. Important aspects of microtransfer molding

Although μTM has many advantages over MIMIC, the adhesion of μTM-patterned features to the substrate is weaker than of MIMIC-derived ones. When patterning line structures the excess solution should be removed at right angle to the lines. Otherwise, it may cause the removal of the solution from the lines and results in the formation of partially filled M-shaped lines. See **Figure 5.4a**.

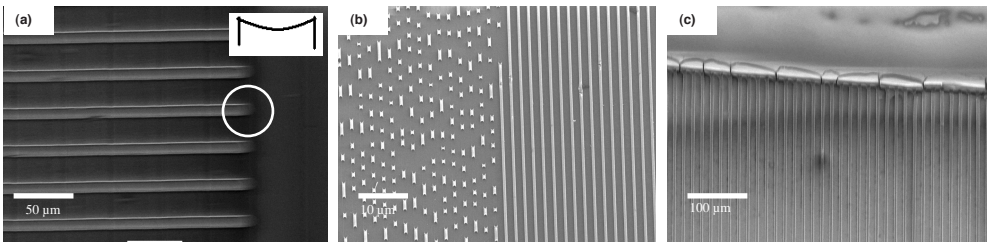

Figure 5.4: SEM images showing the effects of various processing variables in µTM (a) removal of the excess material in a direction parallel to the lines results in M-shaped lines; (b) application of strong force during the removal of excess material may result in incomplete filling of features of the mold; (c) reservoir (bulk) of excess material at the edge of the patterned lines resulting from incomplete removal of excess solution.

The force exerted on a cleaning block to remove excess solution from the mold is also of importance. Application of too large force may cause the partial or complete removal of solution from the patterned area, and lead to incomplete pattern replication. An example is shown in **Figure 5.4b** (left), where the broken lines resulted from too large forces on the mold. The force applied with a hard material such as steel should be smaller than that of a soft material such as PDMS. Finally, the excess materials should be removed thoroughly from the mold, or it will be transferred to the substrate and may affect the pattern (**Figure 5.4c**).

5.3.5. 3D type Patterning

Two techniques were also applied to pattern the organosilica-embedded NPs in a 3D layer-by-layer fashion. The applied patterning procedure was similar to the one discussed in Sec. 4.3.4 for TiO_2. While the MIMIC derived patterns showed good adhesion to the substrate, the final line shapes were not perfectly rectangular; this is an undesirable feature in 3D patterning. Formation of a residue layer is another limitation of MIMIC, even though absence of residue layers was one of the underlying reasons to develop MIMIC in the first place. In some cases both techniques were also combined to make 3D patterns. **Figure 5.5a** shows a µTM derived 3D patterns of hybrid organosilica-embedded $LaPO_4$:Eu NPs having w_l of 6 µm. Some residue layers can be seen in **Figure 5.5b** near the area of detachment of the 2nd layer.

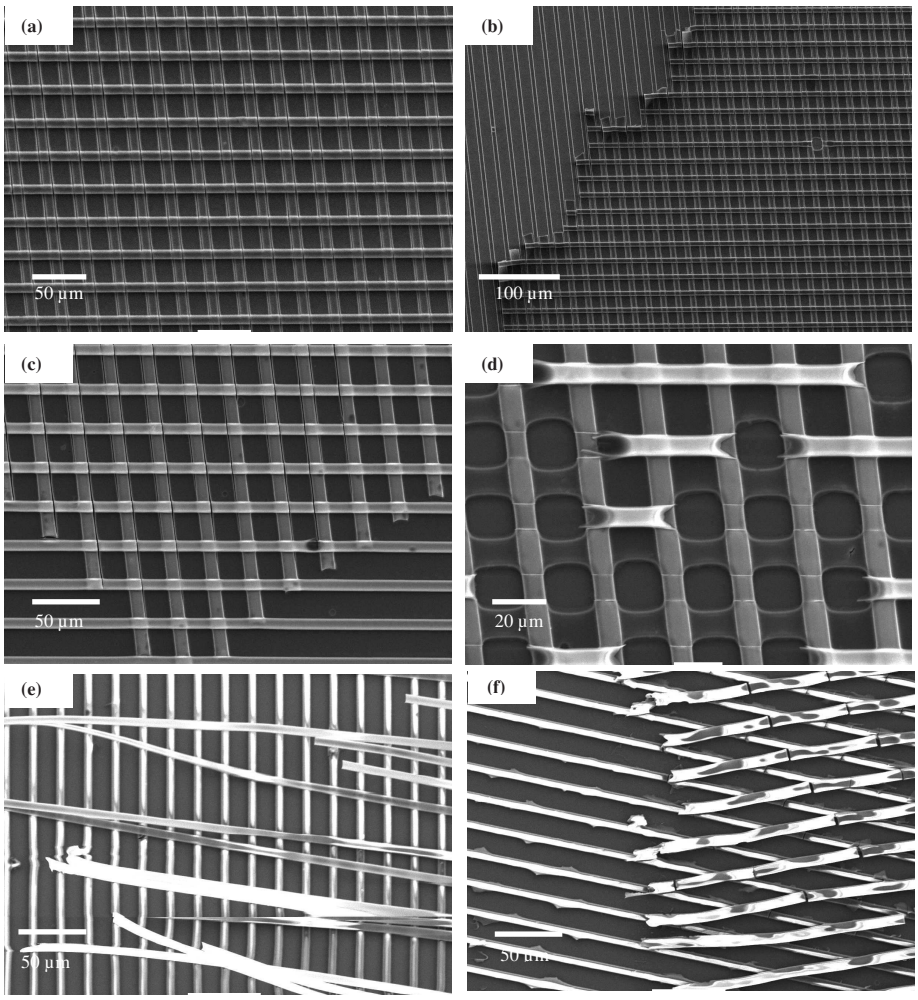

Figure 5.5: SEM images of 3D patterns. (a) µTM-derived dual layer pattern; (b) Detached second layer of a 3D pattern; (c) 3D pattern showing some cracks ; (d) Effect of incomplete drying of the second layer on pattern coherence and adhesion; (e) Dual layer pattern where first layer was made with MIMIC and second layer with µTM; (f) µTM-derived dual layer patterns. The lines are at ca. 120° with respect to the others. Fractures are visible at the points of contact.

Figure 5.5c shows the 3D pattern of $LaPO_4$:Eu embedded organosilica derived from µTM showing small cracks at the point of contact of two layers. Prior to the deposition of the second layer in µTM, the wet solution in the channels should be dried for a period of time, i.e. partially gelled. Otherwise, it may penetrate into the underlying layer and result in defected pattern (**Figure 5.5d**). This should be done before the solution bond to the mold channels, since in that case it might not transfer to the substrate. The time period may vary for different materials and solvents, however, in

the present scenario a time interval of 2-3 min was found to be the optimum. The adhesion of the μTM derived second layer to the underlying layer was found to be weak as compared to those derived from MIMIC. Eventually, this leads to detachment of the top layer, as illustrated in **Figures 5.5e**. The second layer was also deposited under other angles to see if that might improve the adhesion of the second layer, but this also resulted in cracked lines, see **Figure 5.5f**. The cracking of lines probably result from stresses that occur due to shrinkage of the second layer when the pattern dries.

5.3.6. Photoluminescence Microscopy

Eu has maximum luminescence (fluorescence) at λ = 393 nm, whereas for $LaPO_4$:Eu the best excitation is at 260 nm.[1-5] **Figure 5.6a&b** show the photoluminescence (fluorescence) micrographs of a $LaPO_4$:Eu patterned film made by MIMIC. These patterned films were studied with optical microscopy using an excitation wavelength of 260-300 nm. The photoluminescence intensity, however, was very low as can be seen in the figure. X-ray photoelectron spectroscopy (XPS) was performed to study presence of the NPs in the patterned films. However, the results (not presented here) did not show indications for the presence of NPs in the patterned lines. The following possible reasons can be sum up about the reduced luminescence intensities.

Firstly, that the NPs are not present in the upper layers of the patterned lines, since XPS can give information upto 20 Å with an exponential decay towards the depth. The sensitivity of XPS is limited to 0.1-0.2 at%, depending on material. Lower concentrations will not be detected.

Furthermore, the microscope lenses were made from glass, which absorbs UV light. Thus, the microscope itself may have reduced the observed intensity drastically. A mercury lamp (λ=254 nm) was also tried, but the intensity remained low. The excitation and emission wavelengths may also be affected by the matrix material. The hybrid organosilica matrix may reduce the optical yield by several orders of magnitude. Other reasons might include quenching effects such as phonon emission, where the energy of the excited state is consumed in the form of vibrational energy. Nevertheless, a detailed investigation into this effect is not within the scope of this research work. **Figure 5.6c** shows optical micrograph of a MIMIC-patterned film of $CePO_4$:Tb. The color spectrum indicates the presence of a residue layer, and the color contrast is indicative of thickness variation. The dark spots are small dust particles.

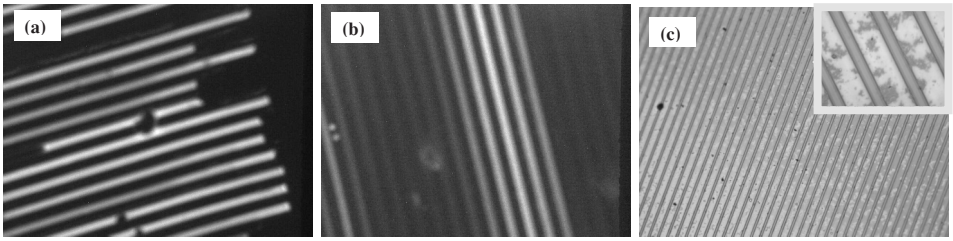

Figure 5.6: (a&b) PL micrographs of $LaPO_4$:Eu line patterns with w_l=4 µm, excited with 260 nm UV light, showing reduced luminescence intensity; and (c) optical micrograph of a $CePO_4$:Tb patterned film with w_l= 6µm, depicting residues and color contrast due to thickness variations of a few nanometers.

5.3.7. Low Energy Ion Scattering Analysis

To look in more detail to the surface composition than is possible with XPS, compositional analyses of other three representative samples were done with the low energy ion scattering (LEIS) technique (section 2.4.2.7). LEIS can register lower element concentrations, but only in the upper atomic layer. One of the samples (M1), shown in Figure 5.1a, is a MIMIC derived line patterned film of $LaPO_4$:Eu NPs. The second sample (M2) is shown in Figure 5.3a, and is a MIMIC made $CePO_4$:Tb patterned film. The third sample (T1) is shown in Figure 5.2. It is a µTM-made $LaPO_4$:Eu line patterned film. Henceforth, these samples will be represented by M1, M2 and T1, respectively.

LEIS was performed using helium for the identification of low mass elements, followed by neon scattering for the identification of high mass elements. This way the composition of the first atomic layer was studied by ion scattering. **Figure 5.7 a&b** show the He and Ne LEIS spectra of the above three samples.

In samples M1 and M2, no rare earth elements were detected. A likely reason is that the concentration of NPs is below the detection limit, at least in the top most layer. Since LEIS is sensitive only to the top atomic layer and cannot detect elements below a few atomic layers. On the other hand, Sample T1 showed the presence of lanthanum (La) in the outermost monolayer. The difference between the samples lies only in the use of the applied patterning technique, which suggests that the NPs are not present in the upper top layer of MIMIC-derived samples. Major differences resulting from the two soft-lithographic techniques are related to differences in filling behavior, and differences in evaporation rates of solvent, etc. These may affect the concentration of NPs in the upper most regions of the patterned lines.

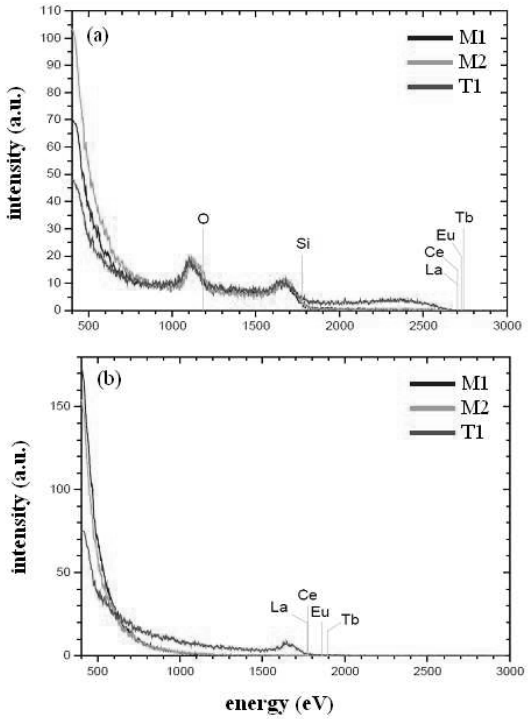

Figure 5.7: LEIS spectra of (a) He and (b) Ne scattering of $LaPO_4$:Eu NPs (M1) patterned by MIMIC; $CePO_4$:Tb NPs (M2) patterned by MIMIC; and $LaPO_4$:Eu NPs (T1) patterned by μTM. All lines were made with same mold having w_l =6 μm, and NPs were embedded in hybrid organosilica.

5.3.8. Secondary Ion Mass Spectroscopy Analysis

Time of flight (TOF) secondary ion mass spectroscopy (SIMS) was performed on the same samples as mentioned in the above section.

In all three samples clear signs of SiOH compounds were detected. Sample T1 showed the presence of La and Eu along with the phosphates (**Figure 5.8a**). However, for sample M1 neither La nor Eu could be detected (**Figure 5.8b**). Similarly, for sample M2, a limited amount of Ce and Tb was detected (**Figure 5.8c)**. Furthermore, no phosphates were found in the two samples (b&c). Aliphatic and aromatic hydrocarbons were detected in these two samples. The aromatic compounds probably may have resulted from the initial synthesis of the NPs, and therefore indirectly suggests their presence in the materials under investigation here.

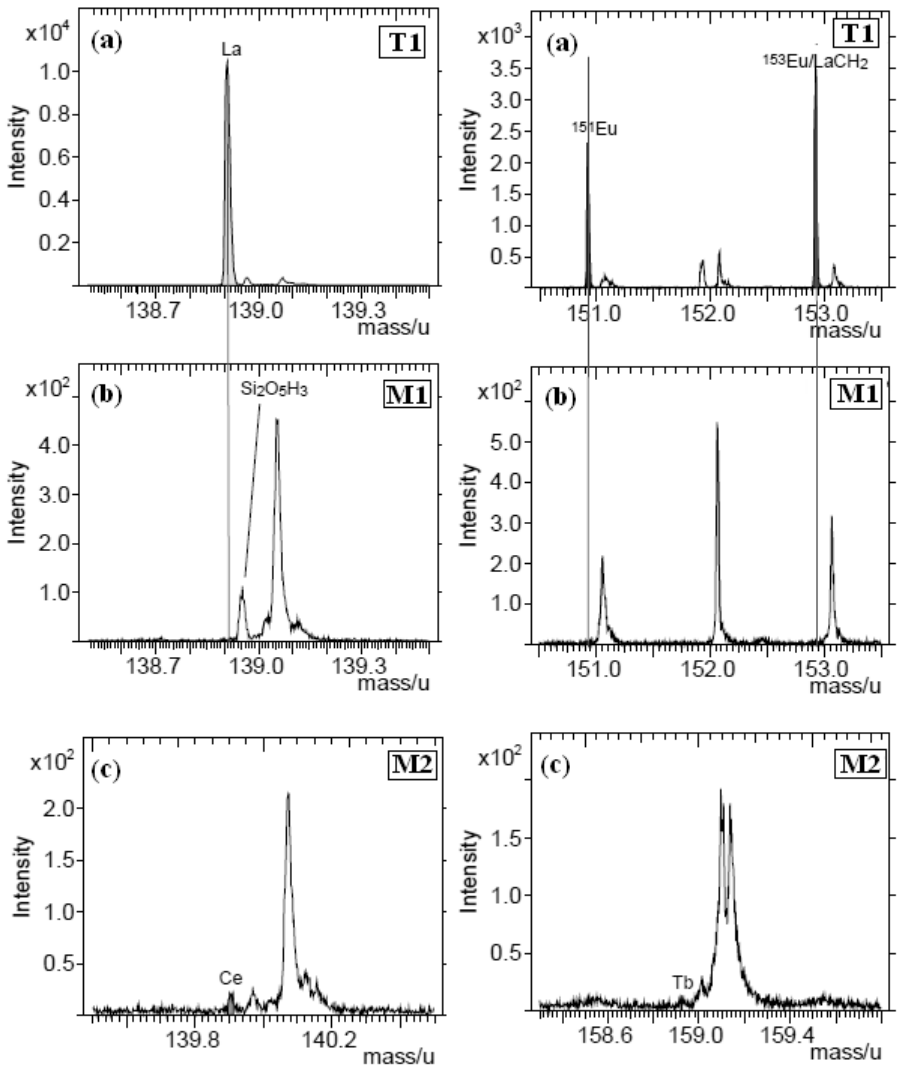

Figure 5.8: ToF-SIMS spectra of (a) T1: ($LaPO_4$:Eu NPs lines by μTM); (b) M1: ($LaPO_4$:Eu NPs patterned by MIMIC) ; and (c) M2: ($CePO_4$:Tb NPs patterned by MIMIC).

On the basis of compositional analysis with LEIS and SIMS, some indications for the reasons for the reduced intensities observed with PL microscopy can be deduced. Firstly, the NPs are not near to the surface region. The path that photons have to travel to escape from the organosilica matrix is therefore relatively long, this affect the degree of absorption by the organosilica matrix. Furthermore, the sample patterned with μTM showed the presence of NPs very near to the external surface. This suggests that the patterning technique also has an influence on the location of NPs in the matrix material

in the given pattern. Silica is known to be a good host material for such kinds of particles; however, quenching effects cannot be ignored.

5.4. Conclusions

MIMIC and μTM techniques were applied successfully to pattern $LaPO_4$:Eu and $CePO_4$:Tb NPs embedded in hybrid silica. The shape of the patterned lines derived from MIMIC was found to be different than those derived with μTM. The adhesion of the patterned material to the substrate and to the mold was found to be higher than that of titania as discussed in the previous chapter. Furthermore, the adhesion of MIMIC derived patterns to the substrate and the underlying pattern was stronger than that of μTM made patterns. This is probably due to the fact that the residue layer in MIMIC is thicker, which improves bonding to the substrate. Also, in MIMIC the bonding is stronger due to the fact that in μTM the sol is gellified (semi-dried) before it is transferred. On the other hand, the shape of patterns is better replicated with μTM than with MIMIC.

Photoluminescence properties in the encapsulated NPs were studied. Their intensities were low. This may be either due to some quenching effects, and/or due to the fact that the NPs are buried away from the external surface. Other possibility could be that their amount is low. Nevertheless, the experiments show that both techniques can be used to pattern similar or other complex materials with these techniques.

References

[1] Meyssamy, H.; Riwotzki, K.; Kornowski, A.; Naused, S.; Haase, M. *Adv. Mater.* 11, 10, **1999**

[2] Stouwdam, J.W.; Van Veggel, F.C.J.M. *Nano Lett*. 2, 733-737, **2002**

[3] Riwotzki, K.; Meyssamy, H.; Schnablegger, H.; Kornowski, A.; Haase, M. *Angew. Chem. Int. Ed.* 40, 3, **2001**

[4] Li, W.; Lee, J. *J. Phys. Chem. C* 112, 11679-11684, **2008**

[5] Stouwdam, J.W. *Lanthanide-Doped Nanoparticles as the Active Optical Medium in Polymer-Based Devices*, PhD Thesis, ISBN 90-365-2011-8, University of Twente, **2004**

[6] Sluzky, E.; Hesse, K. *J. Electrochem. Soc.* 126, 2742, **1989**

[7] Talbot, J.B.; Sluzky, E.; Kurinec, S.K. *J. Mater. Sci*. 39, 771-778, **2004**

[8] Santana-Aranda, M.A.; Meléndez-Lira, M. *Appl. Surf. Sci.* 175-176, 538-542, **2001**

[9] Korzenski, M.B.; Lecoeur, Ph.; Mercey, B.; Raveau, B. *Chem. Mater.* 13, 1545-1551, **2001**

[10] Lecoeur, Ph.; Korzenski, M.B.; Ambrosini, A.; Mercey, B.; Camy, P.; Doualan, J.L. *Appl. Surf. Sci*. 186, 403-407, **2002**

[11] Bohannan, E.W.; Gao, X.; Gaston, K.R.; Doss, C.D.; Leventis, S.L.; Leventis, N.J. *J. Sol-Gel Sci. Tech.*. 23, 235-245, **2002**

[12] Yu, M.; Lin, J.; Wang, Z.; Fu, J.; Wang, S.; Zhang, H.J.; Han, Y.C. *Chem. Mater.*

14, 2224-2231, **2002**

[13] Xia, Y.; Whitesides, G.M. *Angew. Chem. Int. Ed*. 37, 550-575, **1998**

[14] Pisignano, D.; Raganato, M.F.; Persano, L.; Gigli, G.; Visconti, P.; Barbarella, G.; Favaretto, L.; Zambianchi, M.; Cingolani, R. *Nanotechnology*, 15, 953-957, **2004**

[15] Han, X.M.; Lin, J.; Fu, J.; Xing, R.B.; Yu, M.; Zhou, Y.H.; Pang, M.L. *Sol. State Sci.* 6, 349-355, **2004**

[16] Riwotzki, K.; Meyssamy, H.; Kornowski, A.; Haase, M. *J. Phys. Chem. B*, 104, 2824-2828, **2000**

[17] Khan, S.U.; Göbel, O.F.; ten Elshof, J.E.; Blank, D.H.A. *ACS Appl. Mater. Interfaces,* 10, 2250-2255, **2009**

6

Sol-gel derived Lead Zirconate Titanate: Processing, Patterning and Characterization

Abstract

The sol-gel route for fabrication of lead zirconate titanate films is a widely employed method in thin film technology. To produce good quality films and patterns with high fidelity, the fabrication of PZT by a sol-gel process was investigated, and various processing steps were studied. Sol-gel based PZT solutions were prepared and converted into thin films and patterns with spin coating and soft-lithographic techniques, respectively. Structural and compositional analysis of the films and patterns was performed with XRD, and surface and topography were studied with HRSEM and AFM. The ferroelectric and dielectric properties of the film derived were also investigated.

6.1. Introduction

Lead zirconate titanate (PZT) is a perovskite-type ferroelectric material. Ferroelectrics are characterized by their spontaneous polarization, the direction of which can be reversed by external electric field. These properties stem from the non-centrosymmetric crystal structure. The high piezoelectric and pyroelectric coefficients of PZT make it a good candidate for commercial applications. These applications include, for example, infrared (IR) sensors, high frequency piezoelectric transducers, and surface acoustic wave devices.[1-4] Because of the high dielectric constant, and polarization hysteresis, it is considered as a good candidate for non-volatile random-access memory (NVRAM) devices.[5,6] Films of PZT can be derived from both physical and chemical methods. The chemical solution deposition (CSD) methods consist of sol-gel and metal organic deposition (MOD).[7-10] The advantages of using these methods are many fold; e.g. good control over composition, low capital cost, and ease of process integration with semiconductor technology. Most commonly precursor solutions are deposited as thin films, which are then transformed from amorphous into crystalline phase by thermal treatment.

However, the reproducibility of high quality PZT films in terms of microstructure, composition and properties is complicated. It has been reported that the solution preparation conditions have significant influence on the microstructure, orientation and electrical properties, and substantial research is dedicated to investigate the factors affecting the processing of PZT films.[11-16] Another important area is the integration of

PZT films in electric devices such as dielectrics, transducers, capacitors, and micro-electromechanical systems (MEMS). Conventional photolithography is generally not compatible with ceramic materials. The use of various subtractive steps involved, such as wet etching with HF limit with the use of materials such as PZT. Alternative techniques that are simple, cheap, and may have high throughput, and most importantly, are compatible with such materials should be adopted. Ferroelectric PZT has been patterned with soft-lithographic techniques on different length scales.[17-20] The present work on PZT has three main objectives: (1) preparation of highly reproducible solutions, (2) patterning with different soft-lithographic molding techniques, and comparison of the resulting structures, and (3) electrical characterization of derived films and patterns. Evolution of the shapes of patterns, effect of shrinkage, and cracking phenomena related to the evolution of the PZT phase will be discussed.

6.2. Experimental

6.2.1. Materials

All chemicals were used as received, unless otherwise stated. Metal alkoxides were stored and mixed in a glove box (MBRAUN, Siemens) with water and oxygen concentrations below 1 ppm. Lead(II) acetate trihydrate (99 %), titanium(IV) isopropoxide (99.99 %), 2-methoxyethanol (>99.3 %), poly(ethylene glycol) (M.W. 600) were all purchased from Aldrich. Zirconium(IV) n-propoxide (70 % w/w in n-propanol) and ethylene glycol (99%) were purchased from Alfa Aesar. Glacial acetic acid (99.8 %), acetyl acetone (>99%) were obtained from Merck.

6.2.2. Substrate and mold material

The substrates used were Si(100), oxidized Si, and platinized Si (PZT/Pt/Ti/SiO_2/Si). The type and their preparation are discussed in section 2.2.2. The molds applied were of 4, 6, 8, 10 and 12 μm widths having aspect ratios of 1, 1.5, 2, 2.5, and 3 respectively.

6.2.3. Solution Synthesis: State of the Art

A number of chemical solution processing methodologies for the fabrication of lead zirconate titanate (PZT) solution have been reported in literature.[7-10] Most common techniques involve the use of a lead salt and zirconium/titanium alkoxide precursors. The preparation procedure adopted in the present work will be explained below. In all cases the molar ratio of Zr/Ti was kept at 52:48 and the final concentration of the PZT solution was 0.6 M.

Solution A: This solution was prepared according to Yi *et al.*[21] This recipe is based on the use of acetic acid and water and is the most widely adopted method for the preparation of PZT thin films. First of all, lead acetate trihydrate was dissolved in acetic acid at 80 °C for 15 min and then refluxed at 105 °C for 3 h. To this solution

stoichiometric amounts of Zr-n-propoxide and then Ti-isopropoxide with the right molar ratios were added and stirred for 30 min. To this solution water was added such that the final concentration of the PZT sol was 0.6 M.

Solution B: This solution was prepared according to the method of Schwartz *et al.* It is known as the inverted mixing order (IMO) process.[22,23] Here the order of mixing is slightly reversed. First a Ti-alkoxide solution was added to Zr-alkoxide upon which an exothermic reaction took place. To this acetic acid was added and ultrasonicated, followed by addition of a solution of lead acetate in methanol refluxed at 105 °C. Finally, methanol and water were added.

Solution C: An amount of 6 µl of ethylene glycol and 3 ml of acetyl acetone were added to 10 ml of solution **A**, and the mixture was stirred overnight.

Solution D: In a glove box, optimum amounts of Zr-n-propoxide and Ti-iso-propoxide were mixed separately in 2-methoxyethanol and stirred for 24 h to stabilize the solutions. Lead acetate tri-hydrate was dissolved in acetic acid at room temperature and refluxed at 105 °C for 2-3 h to remove all remaining water. To compensate for the loss of lead during thermal processing, 15 mol% excess Pb was added. The Zr and Ti propoxide solutions were mixed together and stirred for another 2 h and finally mixed with the lead acetate solution inside a glove box at room temperature. Finally, 10 µl poly(ethylene glycol) was added to 10 ml of the solution and stirred for 2-3 h. All solutions were filtered with a 0.2 µm Teflon filter and stored at room temperature.

Thin films were prepared by spin coating four layers of each solution at 4000 rpm on a Si(100) substrate. The films after deposition were pyrolyzed immediately on a hot plate at 280-400 °C for 5 min and finally annealed at 650 °C for 30 min in a conventional furnace with 5°C/min heating/cooling rates. Patterning was done by applying micromolding in capillaries (MIMIC) and microtransfer molding (µTM) techniques, as discussed in detail in Chapters 2 & 3.

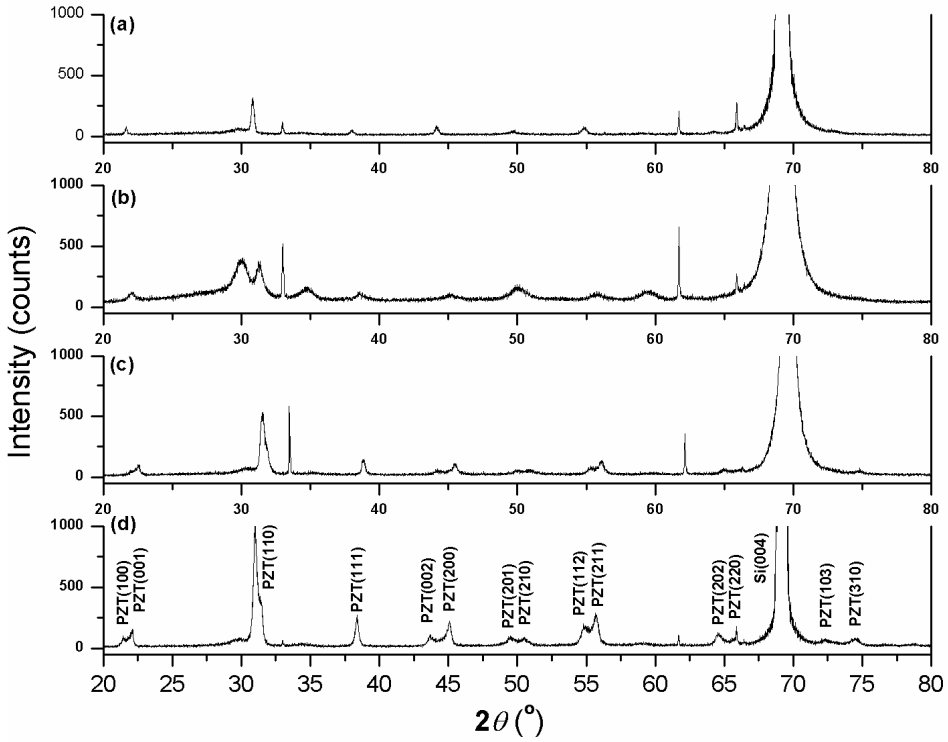

Figure 6.1: XRD diffractograms of PZT thin films obtained from solutions A (a), B (b), C (c) and D (d). Four layers were spin coated at 4000 rpm on a Si(100) substrate, pyrolyzed on a hot plate at 280-300 °C, and finally annealed at 650 °C for 30 min.

6.3. Results and Discussions

6.3.1. PZT thin films and patterns

6.3.1.1. Cracking

Figure 6.2a shows a cracked PZT thin film pyrolyzed at 200 °C for 5 min and annealed at 650 °C for 30 min. The film was made from solution A. The predominant cracks formed during the low temperature processing step on the hot stage. Other factors such as fast solvent evaporation and poor adhesion, and differences in thermal expansion coefficients between film and substrate may have contributed as well.

Cracking could be reduced or even completely stopped by pyrolyzing the samples at higher temperatures, e.g. 400 °C. An example is shown in **Figure 6.2b,** where the cracking of the film was completely avoided. The surface morphology indicates a columnar grain structure. The film was derived from solution D. This suggests that by using a suitable and stable solution and combining it with appropriate thermal processing high quality films can be produced containing cracks.

Patterning the films with some soft-lithographic technique is another way to reduce the tendency to cracking. First of all, cracks cannot propagate easily through a patterned film, since the lines and other objects are often isolated from each other. Secondly, the lateral stresses in micrometer-sized drying or annealing line and dot patterns are much lower than in two-dimensional films. **Figure 6.2c & d** show MIMIC-derived line patterned films, pyrolyzed at 200 °C and 400 °C, respectively, and then annealed at 650 °C. Both line patterns were derived from solution A. The width of the patterned lines (w_l) is 6 μm in both cases. It can be seen in Figure 6.2d that the patterned line has no cracks.

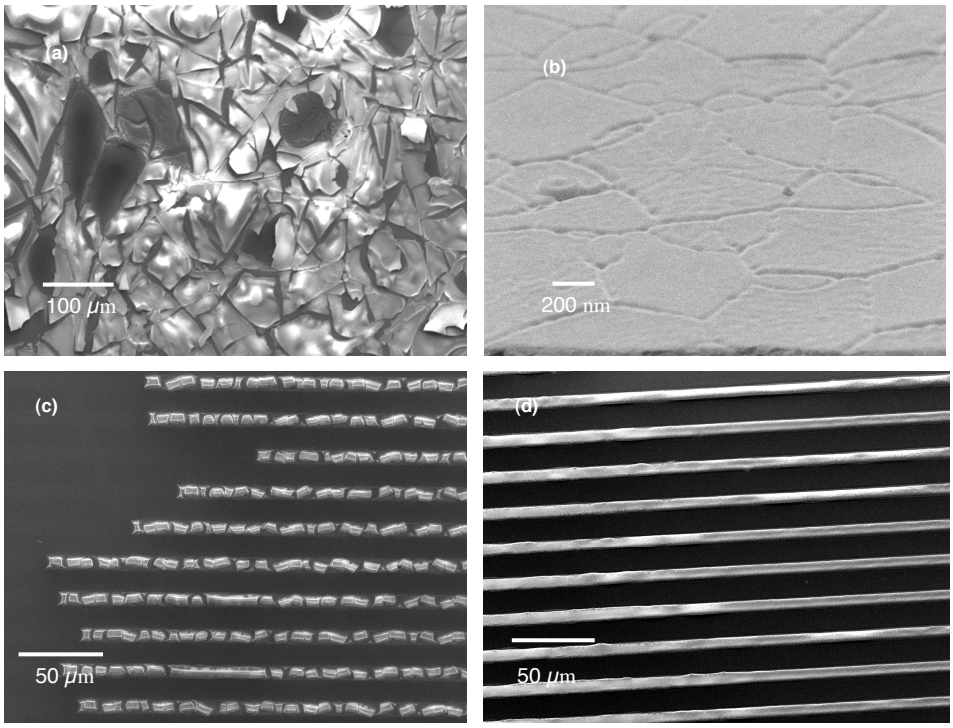

Figure 6.2: SEM micrographs of films and patterns after thermal annealing at 650 °C for 30 min. (a) and (b) show spin-coated PZT thin films: (a) solution A and pyrolyzed at 200 °C; (b) solution D and pyrolyzed at 400 °C; (c) and (d) show MIMIC-patterned lines made from solution A with w_l=6 μm. Patterns were pyrolyzed at (c) 200 °C, and (d) 400 °C.

The results suggest that not only the technique has a role but also the thermal processing route affects cracking in patterns. It can be concluded that good PZT thin films and micropatterns can be realized by using different precursor solution methods and thermal processing procedures.

6.3.1.2. Other aspects

Other factors were also found to have significant effects on the surface, texture, and shape of films and patterns. For example, it has been reported in literature that platinized Si substrates ($Pt/Ti/SiO_2/Si$ shortly Pt-Si) promote textured or columnar growth.[24,25] Chen *et al*.[26] found that the formation of an intermetallic phase Pt_xPb at the PZT/Pt interface promotes the (111) orientation of PZT. A change in the texture of films and patterns was also observed in the present research when films were deposited from solution D on Pt substrates. An example is given in **Figure 6.3a**. It depicts a 4-layer spin-coated film deposited at 4000 rpm on a Pt-Si substrate. The film was pyrolyzed at 400 °C for 5 min after the deposition of each layer and finally annealed at 650 °C for 30 min. The resulting film shows a textured appearance, indicating the role of the substrate on the film.

Microtransfer molding (μTM) was applied to make patterned films on a Pt-Si substrate from solution D. The same thermal protocols were applied as for thin films. **Figure 6.3b** shows an example of a pillar patterned film having a diameter (P_r) of 800 nm. Here, too, the texture of the film is different from the non-plantinized substrate. The results indicate that PZT films and patterns have a tendency to form more granular-textured films on Pt-Si. Brooks *et al*. reported that by thermal annealing in nitrogen environment the films grew in a columnar fashion.[25] In our experiments, we annealed all samples in air and only textured structures were observed.

Experiments were also done to make PZT thin films and patterns from hybrid dispersion solutions, consisting on a preformed PZT-like solid phase in a PZT solution. Hybrid dispersion solutions have higher solids content than the standard sol-gel solutions. This has an effect on the cracking tendency of films, and on the shape evolution of features of patterns, since the degree of shrinkage upon drying and thermal annealing is smaller. Hybrid dispersions were made by drying PZT solution D at room temperature for 24 h. The formed gel was then ground to a fine powder. The powder was mixed with fresh PZT solution and stirred overnight. **Figures 6.3c & 6.3d** show a thin film and a MIMIC-derived line pattern derived from the hybrid solution. The thin film was made by spin coating 3 layers at 4000 rpm, followed by heat treatment at 400 °C for 5 min after each layer. The same solution was converted to patterned lines by MIMIC with a mold having line features w_l=4 μm and aspect ratio of 1. The thin films showed high surface roughness, as can be seen in Figure 6.3c. Similarly, the patterned lines in Figure 6.3d showed residues from fine powder between the lines. However, the lines showed no indication of cracks.

Another important aspect of PZT based solutions concerns aging. The role of solution aging on the final films and their electrical properties has been reported in literature.[27,28] In all acetylacetone-based solutions one can even observe a change in

color of the solution, where it changes from light yellow (fresh sol) to orange and finally to dark orange after several weeks. We observed the formation of small crystals in some cases, as can be seen in **Figure 6.3e**. They are indicated by an arrow, and they resulted from a solution made in a similar way as solution C. We did not study the composition of these crystals; they could either be Pb and/or Zr-based crystals. In most cases they are not visible with the bare eye. An example of a line pattern having width (w_l) of 4 μm derived from such a solution by MIMIC is shown in **Figure 6.3f.** The rough edges are clearly visible in the figure.

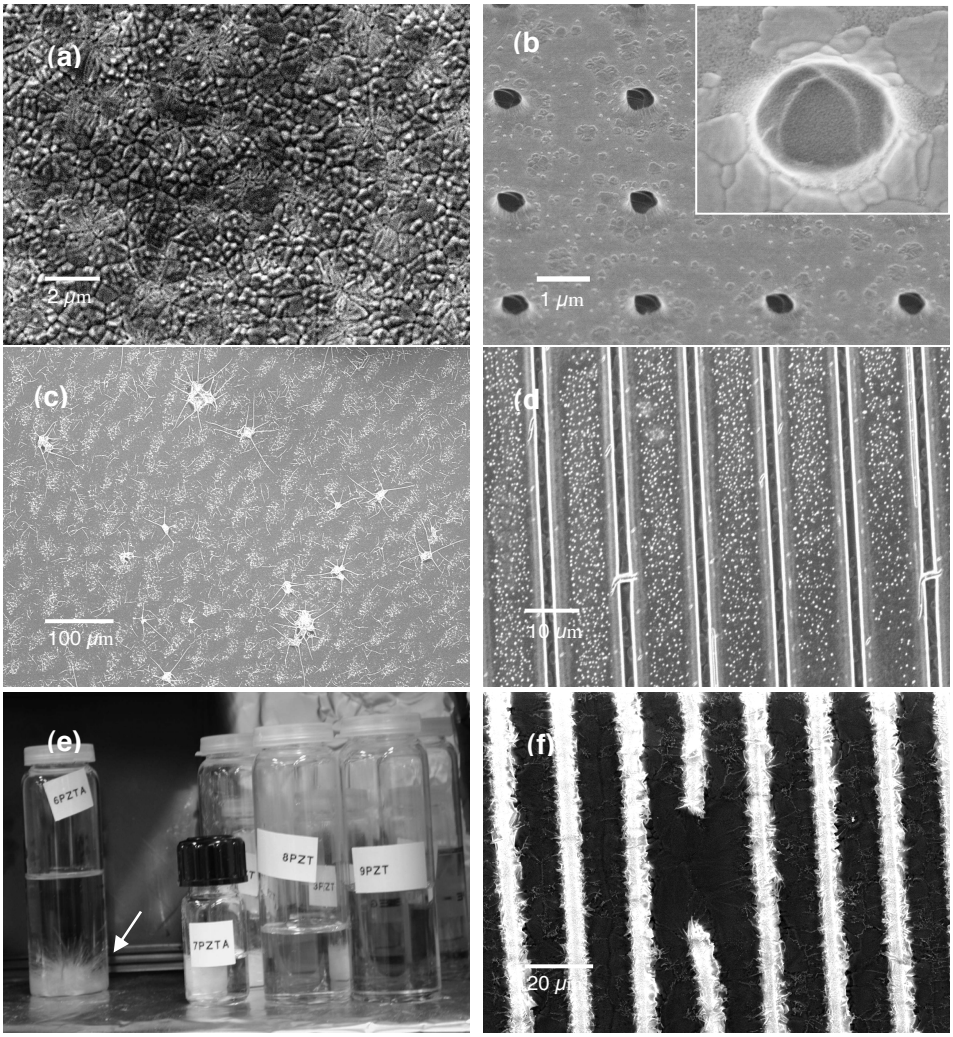

Figure 6.3: SEM micrographs of (a) spin coated film derived from solution D on a Pt-Si substrate; (b) μTM made pillar patterned film on Pt-Si substrate having P_r= 800 nm; (c) film derived from sol-gel and powder hybrid solution; (d) MIMIC derived line pattern having w_l=4

μm; (e) aging effects in sol-gel solution C; crystals at the bottom in the solution are indicated by an arrow; and (f) MIMIC derived line pattern with w_l=4 μm from such a solution; irregularities resulted from small crystallites in the solution. All samples were annealed at 650 °C for 30 min with 5°C/min heating /cooling rates.

6.3.2. Double-peak topographic study

A). High resolution electron microscopy

The shape formation of patterned features of titania and photoluminescent NPs embedded in hybrid silica have been discussed in the previous chapters. Also the comparison of the shapes derived from the two techniques, MIMIC and μTM, has been addressed. Here the shape formation of PZT lines will be discussed. Interestingly, the shape of PZT lines is unlike the aforementioned two types of materials. While for the other materials the thickness of the lines was higher at the centre and lower at the edges (Chapter 4 & 5), for PZT it is higher at the corners and lower at the centre. This type of shape is known as the double peak profile and has been reported in literature by Martin *et al.* [18]. They presented two hypotheses to account for the formation of such kind of cross-sectional profiles. Firstly, it may result from preferential wetting of sharp corners by the precursor liquid. Thermodynamically this drives liquid menisci to adopt round profiles and will result in the minimization of total surface energies. The second reason is the enhanced drying at the corners of capillaries because of the locally higher surface-to-volume ratio.

The double peak topographies were further studied in the present work. Most samples discussed here were annealed in conventional furnace at 650 °C for 10 min with a heating/cooling rate of 5°C/min, some were annealed in a microwave oven at the same temperature. As discussed earlier, double-peak topographies are undesirable for certain areas of application. Moreover, the ideal situation is generally to form an exact (negative) replica of the master structure, and have complete control over the replication process. We observed the double peak profile both in MIMIC and μTM experiments with PZT solutions. **Figure 6.4a** shows a MIMIC-derived line pattern having a width w_l of 10 μm and heated to 80 °C, followed by heating to 400 °C, for 2-3 min at both temperatures. **Figure 6.4b** shows a μTM derived pattern with a feature width w_l of 12 μm after the same heat treatment. It is obvious that the solution preferably wets the corners of the mold in order to reduce the total surface energy.

To study the effect of non-uniform drying in the channel as reported by Martin *et al.* [18] the following experiment was performed. A PDMS mold with a line pattern w_l of 6 μm was soaked overnight in a mixture of 2-methoxyethanol and acetic acid in an 8:1 volume ratio. The soaked mold was used to pattern PZT with μTM. By soaking the mold was saturated with solvents that are used to prepare a PZT sol. As a result, the overall rate of solvent loss from drying sols is reduced. Drying gradients inside the

capillary are therefore smaller, so that relative differences in rate of solvent loss between bulk, surface and corner areas should be diminished. This should then ideally result in lines with a more rectangular shape. The shape profile derived from the pre-soaked mold was compared with a pattern that was obtained with the same technique, but with a dry mold. Both samples were initially dried on a hot plate at 80 °C, first with the mold for 20 s, and then for another 7 min after removal of the mold. The cross-sectional shape profiles are shown in **Figure 6.4c** and **Figure 6.4d**. The former was obtained with the un-soaked mold and the latter one with the soaked mold. Interestingly, the double peak profile occurred in both samples. However, the patterned lines derived with the soaked mold showed more porosity at the interior of the line. This indicates that some solvent remained trapped inside the lines and when pyrolyzed the sudden evaporation results in a more porous structure. However, the sample derived with the un-soaked mold shows uniform porosity through the entire cross-section. In this case, since the mold was not saturated with solvents, they could diffuse easily from the patterned lines into the mold.

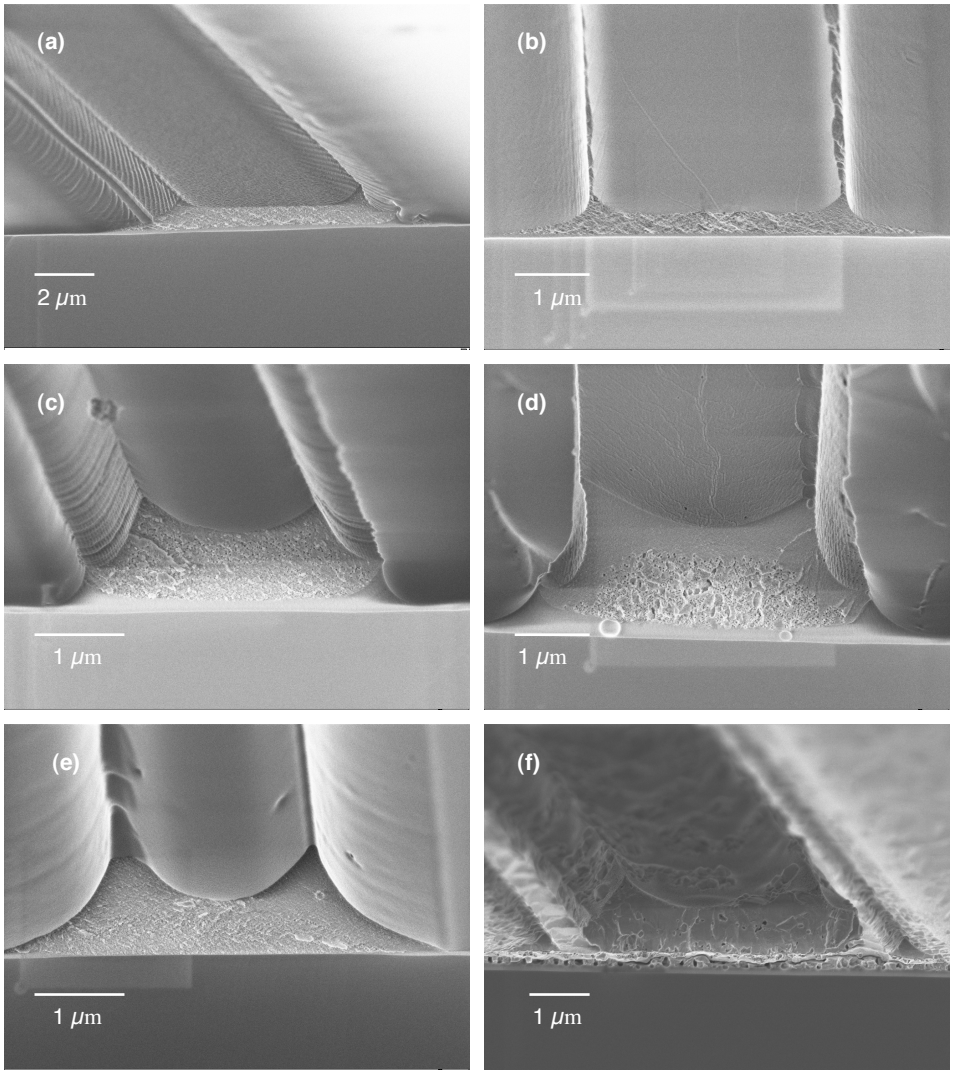

Figure 6.4: SEM cross-sectional profiles of (a) MIMIC pattern with w_l=10 μm; (b) μTM made with w_l=12 μm; (c); MIMIC derived line patterns with w_l=6 μm using a dry mold; (d) MIMIC derived line patterns with w_l=6 μm using a soaked (wet) mold; (e) shape profile of a sample directly placed and annealed in a microwave furnace at 650 °C for 30 min; and (f) profile of a line on a Pt-Si substrate. All samples were annealed at 650 °C for 30 min.

To study the effect of heating rate on cross-sectional profile, a μTM made sample of the same line width after treatment at 80 °C for 3 min and at 400 °C for 2 min was directly placed in a microwave oven at 650 °C for 30 min. The shape profile of the line is shown in **Figure 6.4e.** The resultant shape profile was found to be relatively different from those that had been annealed in a conventional furnace. For the microwave sample the vertical collapse of the roof of the patterned line was more pronounced, and

the edges were less sharp. However, the lines have a fine grained structure and less porosity than the patterns annealed in a conventional furnace.

Finally, to study the role of the substrate on the cross-sectional shape, MIMIC was applied on a Pt-Si substrate using a 6 μm mold. The thermal protocol was the same as used for the sample shown in Figure 6.4a. The SEM micrograph of the line profile is shown in **Figure 6.4f**. As discussed in a previous section the Pt-Si substrate promotes textured or preferential orientation of the PZT phase. In accordance with those findings, also here the line has a rougher and more textured appearance. Furthermore, the line was detached from the substrate at the corners, indicating comparatively poor adhesion as compared to bare Si substrates.

B). Atomic force microscopic study

The double peak profiles were further studied with atomic force microscope (AFM) in tapping mode. Two samples were patterned by MIMIC and μTM from a mold having width and height of 8 and 4 μm, respectively. After initial drying at room temperature for a couple of min the samples were placed on a hotplate at 80 °C for 3 min with the mold on, and subsequently at 430 °C for 2 min after removal of the mold. Finally the patterns were annealed in a conventional furnace at 650 °C for 30 min. **Figure 6.5a** shows the cross-sections of these patterned lines, where M and U refer to MIMIC and μTM, respectively. The volumetric shrinkage of the patterns was calculated by Riemann's summation method. A total volumetric shrinkage of 84% and 76% was calculated for the MIMIC and μTM derived samples, respectively. Clearly, the MIMIC derived patterned line has high shrinkage in both vertical and horizontal direction. However, it is also more symmetric than the μTM derived line. Therefore, it may be concluded that MIMIC derived PZT line patterns are denser than μTM pattern and show good symmetry.

Another set of experiments was performed to see the effects of heating rates. Two samples were patterned by MIMIC with a mold having width and height of 8x4 μm (**Figure 6.5b**). After patterning both samples were placed on a hot plate at 80 °C for 3 min with mold, followed by 7 min without the mold at 430 °C. Sample C was annealed in a conventional furnace at 650 °C for 30 min with heating/cooling rates of 5 °C. Sample M was directly placed in a microwave furnace for 30 min at a preset temperature of 650 °C. A total of 82% and 89% volumetric shrinkage was calculated for samples M and C, respectively. This indicates that the sample annealed in the microwave oven is more porous than the one annealed in a conventional furnace. Obviously, the sample annealed in a conventional furnace experienced a longer sintering time.

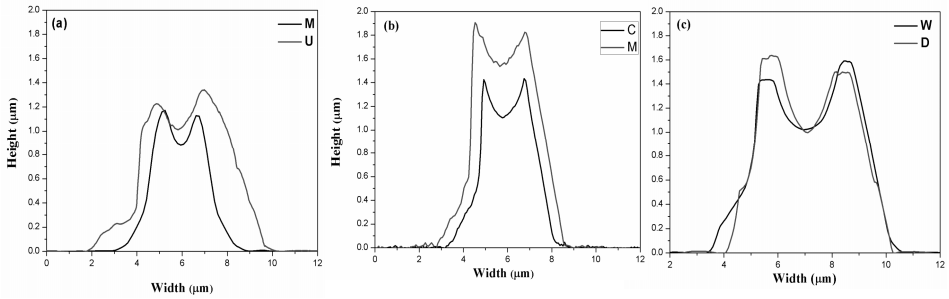

Figure 6.5: AFM cross-section profiles of (a) MIMIC (M) and μTM (U) derived line patterns from a mold with line width of 8 μm, after annealing in a conventional furnace at 650 °C for 30 min; (b) MIMIC derived patterns of line width of 8 μm annealed in a conventional furnace (C) and in a microwave furnace (M) for 30 min at 650 °C; (c) μTM made line patterns derived with a soaked mold (W) and a dry mold (D) having line width of 6 μm and annealed in a conventional furnace at 650 °C for 30 min.

The samples shown in Figure 6.4c&d were also analyzed with AFM and their cross-sections are shown in **Figure 6.5c**. The height profiles W and D represent patterns obtained with the soaked (wet) mold and un-soaked (dry) mold, respectively. The total volumetric shrinkage was found to be 74% and 70% for the W and D, respectively. The line pattern obtained with dry mold showed relatively less shrinkage than the wet mold. However, the difference is not very significant. It shows that soaking the mold in solvents does not have a significant effect on the degree of shrinkage, or the shape of lines. The only difference is that a dry mold yields a more uniform and finer porosity through the entire patterned area, whereas the soaked mold gives high porosity and large pores at the interior part of the pattern.

6.3.3. Electrical Properties

One of the objectives of the patterning of PZT was to compare its electrical properties to that of a spin coated film. However, the deposition of a top electrode on line patterned film was found to be difficult. Three techniques were applied to deposit top electrodes, namely sputtering, focused ion beam (FIB) and pulsed laser deposition (PLD). However, none of these methods yielded a good top electrode. In sputtering and PLD, the alignment of a shadow mask can easily disrupt the patterned lines, since oxides are very brittle. Also the depositing flux can be deposited only on top of patterned lines and not at edges and corners, as schematically illustrated in **Figure 6.6a**. Electrodes that had been deposited this way gave no electrical signal. Similarly, since FIB is a very localized deposition technique with highly localized energy input, depositing top electrodes by FIB resulted in the etching of the PZT patterned lines.

The ferroelectric and dielectric properties of the spin coated thin films were investigated after deposition of Pt top electrodes by PLD. A 4-layered PZT film having

a thickness of ca. 360 nm was produced by spin-coating sol-gel solution D on a Pt-Si substrate, as described in Section 6.2. A SEM micrograph of the surface morphology is shown in **Figure 6.2 b**, and the cross-sectional view of the film is shown in **Figure 6.6b**. The films obtained from this solution had outstanding electrical properties in comparison to the other solutions, as will be explained below.

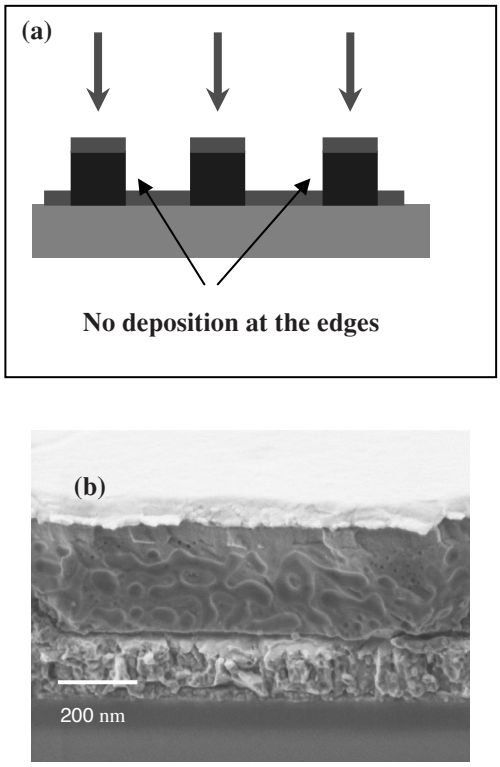

Figure 6.6: (a) Schematic illustration of a top electrode deposition on patterned lines; and (b) SEM micrographs of a sol-gel derived PZT film on a Pt-Si substrate cross-sectional view.

6.3.3. a. Polarization analysis

Platinum (Pt) top electrodes of 200 μm^2 area were deposited by pulsed laser deposition (PLD) to study the electrical properties. **Figure 6.7a** shows typical P-E hysteresis loops for a PZT/Pt/Ti/SiO_2/Si film. The P-E loops shown are measured at a frequency of 1 kHz. The loop at high voltage showed good symmetry. The saturation and remnant polarization were found to be 48 $\mu C/cm^2$ and 12.36 $\mu C/cm^2$ at 20 V, and 47 $\mu C/cm^2$ and 18.2 $\mu C/cm^2$ at 10 V, respectively.

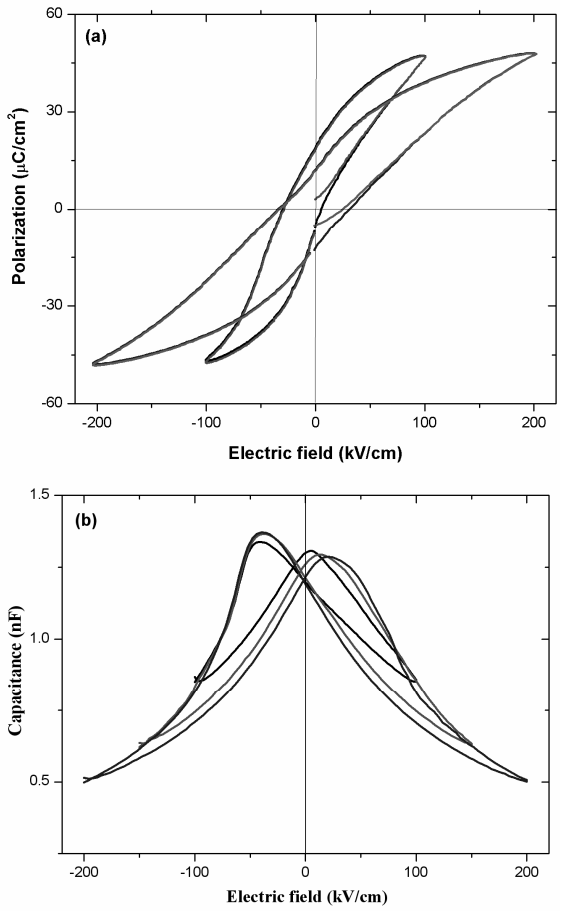

Figure 6.7: (a) Ferroelectric hysteresis loops of PZT/Pt/Ti/SiO_2/Si thin film at 1 kHz frequency; and (b) capacitance versus applied electric field of a PZT thin film capacitor at 10 kHz.

6.3.3. b. Capacitance analysis

The capacitance behavior of the above sample was measure with dc field at ±200 kV/cm, back and forth at a frequency of 10 kHz. **Figure 6.7b** shows the capacitance vs. applied electric field (C-V) loops of "butterfly"-type curves, typical for ferroelectric materials. It is interesting to note that the shape of the butterfly is not completely symmetric. This is probably due to differences in thermal treatment of the top and bottom electrodes. Unlike the top electrode the bottom electrode was heat treated along with PZT film at 650 °C.

6.4. Conclusions

Sol-gel based PZT solution synthesis techniques were investigated. The solution preparation route and mixing order have a large effect on film quality. Patterned films showed comparatively little or no cracking in comparison with the spin coated films. The cross-sectional shape of the patterned lines was investigated in detail. The results indicate that the solution has a tendency to preferential wetting of the corners of the mold, resulting in double peak profiles. This is independent of patterning method, pretreatment of the mold, or thermal annealing process. The electrical properties of films derived from various solutions were investigated.

References

[1] Scott, J.F.; Paz de Araujo, C.A. *Science*, 246, 1400-1405, **1989**

[2] Scott, J.F.; *Science*, 315, 954-959, **2007**

[3] Lesaicherre, P.; Yamamichi, S.; Takemura, H.; Yamaguchi, H.; Tokashiki, K.; Miyasaka, Y.; Yoshida, M.; Ono, H. Int. Ferroelectrics 11, 81-100, **1995**

[4] Dawber, M.; Rabe, K.M.; Scott, J.F.; *Rev. Mod. Phys.* 77, 1084-1124, **2005**

[5] Scott, J.F.; *Phys. World* 8, 46-50, **1995**

[6] Paz de Araujo, C.A.; Taylor, G.W. *Ferroelectrics*, 116, 215-228, **1991**

[7] Schwartz, R.W. Chem. Mater. 9, 2325-2340, **1997**

[8] Fukushima, J.; Kodaira, K.; Matsushita, T.J. *Mater. Sci*. 19, 595-598, **1984**

[9] Budd, K.D.; Dey, S.K.; Payne, D.A. *Brit. Ceram. Soc. Proc*. 36, 107-121, **1985**

[10] Dey, S.K.; Budd, K.D.; Payne, D.A. *IEEE Trans. UFFC* 35, 80-81, **1988**

[11] Schwartz, R.W.; Voigt, J.A.; Tuttle, B.A.; Payne, D.A.; Reichert, DaSalla, R.S. *J. Mater. Res.* 12, 444-456, **1997**

[12] Lakeman, C.D.E.; Payne, D.A. J. Am. Ceram. Soc. 75, 3091-3096, **1992**

[13] Schwartz, R.W.; Boyle, T.J.; Lockwood, S.J.; Sinclair, M.B.; Dimos, D.; Buchheit, C.D. Int. Ferroelectrics, 7, 259-277, **1995**

[14] Kushida, K.; Udayakumar, K. R.; Krupanidhi, S. B.; Cross, L.E. *J. Am. Ceram. Soc*. 76, 1345-1348, **1993**

[15] Khaenamkaew, P.; Muensit, S.; Bdikin, I.K. Kholkin, A.L. *Mat. Chem. Phy*. 102, 159-164, **2007**

[16] Yu, S.; Yao, K.; Shannigrahi, S.; Eng Hock, F.T. *J. Mater. Res*. 18, 737-741, **2003**

[17] Seraji, S.; Wu, Y.; Jewell-Larson, N.E.; Forbess, M.J.; Limmer, S.J.; Chou, T.P.; Cao, G. *Adv. Mater*. 12, 1421-1424, **2000**

[18] Martin, C.R.; Aksay, I.A. *J. Phys. Chem. B* 107, 4261-4268, **2003**

[19] Martin, C.R.; Aksay, I.A. *J. Electroceram.* 12, 53-68, **2004**

[20] Vartuli, J.S.; Özenbas, M.; Chun, C-M.; Trau, M.; Aksay, I.A. *J. Mater. Res*. 18, 1259-1265, **2003**

[21] Yi, G.; Wu, Z.; Sayer, M. *J. Appl. Phys*. 64, 2717-2724, **1988**

[22] Assink, R.A.; Schwartz, R.W. Chem. Mat. 5, 511-517, **1993**

[23] Schwartz, R.W. Assink, R.A.; Headly, T.J. Ferrelectric Thin Films II, edited by Kingon, A.I.; Myers, E.R.; Tuttle, B. *Mat. Res. Soc. Symp. Proc*. 243, 245-254, **1992**

[24] Huang, Z.; Zhang, Q.; Whatmore, R.W. *J. Mater. Sci. Lett.* 17, 1157-1159, **1998**

[25] Brooks, K.G.; Reaney, I.M.; Klissurska, R.; Huang, Y.; Bursill, L.; Setter, N. *J. Mater. Res.* 9, 2540-2553, **1994**

[26] Chen. S.; Chen, I. *Ferroelectrics* 152, 25-30, **1994**

[27] Zhang, Q.; Huang, Z.; Whatmore, R.W. *J. Sol-Gel Sci. Tech*. 23, 135-144, **2002**

[28] Huang. Z.; Zhang, Q.; Whatmore, R.W. *J. Sol-Gel Sci. Tech*. 24, 49-55, **2002**

7

In-situ Small Angle X-ray Scattering Study of the Structural Evolution of Sol-Gel Derived Lead Zirconate Titanate Thin Films: from Liquid Phase Sols to Thermally Annealed Condensed Phases

Abstract

An in-situ small angle x-ray scattering study (SAXS) study of the structure and structural evolution of sol-gel derived lead zirconate titanate (PZT) sols and drying thin films is reported. The structure and reactivity of hydrolyzed and non-hydrolyzed PZT solutions was investigated at room temperature and 60 °C. The reactivity of 0.3 M PZT stock solutions with water at room temperature was limited, yielding structures with a radius of gyration of 0.65 nm after 48 h of ageing under water-rich conditions. Growth occurred within minutes at 60 °C, although the radius of gyration of the entities in these sols also remained below 1 nm, even when a large excess of water was added. Upon drying hydrolyzed thin films at room temperature and 60 °C, loss of solvent and the formation of agglomerates consisting of 1.5-2 nm sized particles were observed. SAXS analyses of as-dried and thermally annealed thin films showed indications for grain growth with increasing annealing temperature, in agreement with TEM analysis.

7.1. Introduction

Because of its wide range of applications a lot of research in the past decades has been dedicated to the fabrication and characterization of lead zirconate titanate ($PbZr_{1-x}Ti_xO_3$; PZT) thin films.[1-4] PZT is technologically important because of its large remnant polarization, low coercive field, and high piezoelectric coefficients. There are two major routes for the fabrication of thin films, namely by physical and wet-chemical techniques. The physical techniques include metal-organic chemical vapor deposition (MOCVD),[5,6] sputtering,[7,8] and pulsed laser deposition.[9,10] The chemical solution deposition techniques (CSD)[11] include the sol-gel route,[12,13] metal-organic deposition (MOD),[14,15] and chelate synthesis.[12] Among the latter, the sol-gel technique has attracted considerable attention because of its simplicity, low cost, good compositional control and its ability for large area film fabrication.[16]

Typical sol-gel solutions consist of metal alkoxides and/or metal carboxylate precursors, solvents, water and catalyst. It is well known that the nature of the sol has a profound effect on the microstructure, orientation and electrical properties of the films.[12,16] Although the precursor chemical structure strongly effects the densification and crystallization of PZT films, relatively few details are known about the structural evolution in different steps of the sol-gel process. The structural chemistry of PZT sols has been studied by various analytical techniques, such as nuclear magnetic resonance (NMR),[17-21] Fourier transform infrared (FTIR),[19,20] gas chromatography-mass spectroscopy (GC-MS),[18] photon correlation spectroscopy (PCS)[21-23] and small angle X-ray scattering.[21-23]

It is known that the properties of sols are controlled by factors like the nature of the metal-carrying reagent, solvent, reagent concentration, water concentration, method of water addition, catalyst, and solution preparation/reaction conditions.[11,12,24,25] For multicomponent (mixed metal) systems such as PZT, prehydrolysis of less reactive alkoxides is sometimes employed to improve compositional uniformity. As soluble oligomers instead of precipitates can only be formed under very water-lean conditions,[25] a key point is to restrict the amount of water and to control the way in which it is added. Assink *et al.* reported that acetic acid acts as a key chelating agent, affecting the reactivity and promoting esterification reactions that result in many alkyl acetate esters as byproducts. This suggests the formation of metal acetates and/or metal alkoxy acetates due to (partial) exchange of alkoxy ligands by acetate.[17] Detailed knowledge regarding the nature of precursor species in PZT solutions during hydrolysis, condensation, and upon drying after film formation is scarce. An extended x-ray absorption fine structure (EXAFS) study of commonly used PZT sols showed that the constituent solvent/modifiers such as acetic acid and acetylacetone have an effect on the degree of homogeneity in the distribution of Pb and Zr, but no Pb-Zr correlations could be determined in any of the samples.[26] It is however believed that most metal alkoxides and metal carboxylates can form oligomeric solutions in appropriate solvents. Well-known examples are $Ti_6(O^iPr)_{10}(OOCCH_3)_4O_4$, $Ti_6(O^iPr)_8(OOCCH_3)_8O_4$ and $Zr_4O(OPr)_{10}(CH_3COCH_2COCH_3)$.[11,12] Several polyoxometalate complexes of lead and titanium or zirconium precursors in similar solvents have also been reported, e.g., $PbTi_2[(\mu_4\text{-}O)(OOCCH_3)(OCH_2CH_3)_7]_2$, $Pb_4Zr_4(\mu\text{-}O_2CR')_8(O^iPr)_{16}(OH^iPr)_2$, $Pb_2Ti_4(\mu\text{-}O_2CR')_4(OR)_{16}$, $Pb_2Ti_3(\mu_4\text{-}O)(\mu_3\text{-}O)(\mu\text{-}O_2CC_7H_{15})_2(\mu\text{-}O^iPr)_6(O^iPr)_4$, $PbZr_3(\mu_4\text{-}O)(OAc)_2(O^iPr)_{10}$ and several others.[27-31] In all these complexes the number of lead ions is smaller than or equal to the number of transition metal ions. Moreover, they all formed in the absence of water, i.e., without the hydrolysis step that is typical for initiating sol-gel processes.

In the drying stage of sol-gel films the situation becomes even much more complex, as complexation reactions and evaporation take place simultaneously, and they

influence each other to a large extent.[24,25,32] For instance, loss of solvent due to physical drying concentrates a solution and increases the solution viscosity and reaction rate of species that are present in that solution. If more than one solvent is used, differences in the relative rates of evaporation of solvents at a given temperature leads to a gradually changing matrix for the particles in the sol, which may affect their solubility and reactivity, and lead to phase separation. Moreover, water is a volatile reagent that may actually be evaporated before it is being consumed in a thin film drying process. Obviously, this has a large effect on the final structure of the as-dried thin film. At present, our knowledge is not sufficient for a complete understanding of the system, from initial sol synthesis to final film or nanopattern fabrication. Neutron scattering studies have shown that alkoxide-based sol-gel processing are incapable of producing compositionally homogeneous samples and that this is due to compositional segregation that occurs early on during sol-gel processing, and is not eliminated in the high temperature heat treatment.[33] We therefore wanted to elucidate some aspects of the development of morphology of PZT in various steps of the sol-gel process.

The present work describes an in-situ Small Angle X-ray Scattering (SAXS) study of the structure and structural evolution of PZT sols on a nm-length scale. Sol evolution, thin film deposition and subsequent drying and thermal annealing steps were investigated. In particular, we focused on the structural evolution of a solution composition that has been used successfully by us to imprint PZT nanopatterns with a lateral resolution below 200 nm by soft lithography,[34] and is based on the combined use of acetic acid and 2-methoxyethanol as solvents. Similar solutions have been reported to yield relatively chemically homogeneous sols.[26] It is not possible in practice to investigate the multi-dimensional variable space of a sol-gel process completely. We therefore chose to investigate only a limited number of solutions and process conditions, in order to get insight into structures, phases and dimensions that typically evolve, and the processes that occur on the nanoscale.

In SAXS experiments the elastic scattering of x-rays by a sample that has local fluctuations in its electronic density is recorded at very small angles. Restricting further discussion to colloidal solutions and powders, structural information about entities with dimensions of 0.1-50 nm can be derived from this angular range.[35] In a typical SAXS experiment, the scattering intensity *I(q)* is plotted versus the scattering vector q (nm^{-1}), which is related to the scattering angle θ and the wavelength λ (nm) of the incident beam by:

$$q = \frac{4\pi}{\lambda}\sin\theta \qquad (1)$$

At sufficiently small q the scattering intensity of nanoparticle solutions can be expressed by the Guinier law:[35,36]

$$I(q) = I(0)\exp\left(-q^2\frac{R_g^2}{3}\right) \qquad (2)$$

From the Guinier plot (ln I vs. q^2) the effective particle size in solution, also known as the radius of gyration (R_g), can be determined from the slope. Equation (2) holds when $qR_g<1$. The scattering intensity at zero angle is given by:

$$I(0) = N(\Delta\rho)^2 V^2 \qquad (3)$$

where N is the number of particles, $\Delta\rho$ the electron density difference between particle and surrounding medium (solvent), and V the volume of the particle.

This study can be divided into three parts. The first part discusses the chemistry and structure of PZT sols at room temperature and at 60°C, including their reactivity with water. The second part describes a number of in-situ drying experiments of sol-gel PZT thin films. Similar drying experiments were performed at room temperature and 60°C. The third part is an ex-situ study of grain growth in as-dried thin films upon thermal annealing.

7.2. Experimental Section

7.2.1. Synthesis of PZT sols

Lead(II) acetate trihydrate (99 %, Aldrich), zirconium(IV) *n*-propoxide (70 % w/w in *n*-propanol, Alfa Aesar) and titanium(IV) isopropoxide (99.999 %, Aldrich) were used as precursor materials. Glacial acetic acid (99.8 %, Merck) and 2-methoxyethanol (>99.3 %, Aldrich) were used as solvents, stabilizers, and chelating agents. Initially, three stock solutions were made. A Pb-acetate solution was prepared by dissolving lead acetate trihydrate in acetic acid and subsequent refluxing at 105 °C for two hours to remove all remaining water. The other two solutions, based on titanium isopropoxide and zirconium *n*-propoxide, respectively, were dissolved in 2-methoxyethanol and stirred in a glove box under nitrogen. All stock solutions were stirred at room temperature for 24 h. They were then stored at room temperature. The concentration of individual stock solutions was 0.6 mol/dm^3. Prior to experiments, the stock solutions were mixed in the appropriate molar ratios and stirred for 5-10 min. The molar ratio of lead to zirconium to titanium was always kept at 100:52:48, giving a concentration of the final PZT solution of 0.3 mol/dm^3.

7.2.2. SAXS Experiments

SAXS experiments were performed on the Dutch-Belgian beamline (DUBBLE) BM-26B of the ESRF in Grenoble, France.[37] The beam energy was 16 keV. The beam was focused at the corner of a 2D gas-filled multiwire proportional CCD detector in order to maximize the range of accessible q (scattering vector) values. The samples were placed at a distance of 1.5 m from the detector and the intensity was measured in the range $0.13 < q < 8.0$ nm^{-1}. The raw data were corrected for the pixel-dependent detector sensitivity and integrated for channels with the same q values. Experiments were performed on three types of samples described below, in order to study various aspects of the structural evolution of PZT thin films.

The data were analyzed using Guinier analysis (Equation (2)) and the Scatter software package.[38] Guinier analysis was carried out in the range $0.7 < q^2 < 1.5$ nm^{-2}, where the condition $qR_g < 1$ is satisfied for all samples. All experimental data at q>6.05 nm^{-1} have a larger error than at smaller scattering vectors, because the number of detector elements with which the intensities in this q-range are measured is smaller than below 6 nm^{-1}. A small discontinuity can be observed in some of the experimental curves around this q-value.

7.2.2.1. PZT sols

To study the structure of PZT sols and the constituent stock solutions, small quantities of solutions were contained in a borosilicate glass capillary (Ø =1.5 mm, glass no. 14, Hilgenberg, Malsfeld, Germany) and measured at room temperature. The scattering intensity from a capillary containing only the corresponding solvent was subtracted from the overall intensity signal, whereby a correction was made for the fact that the concentration of solvent in a PZT sol is lower than in the pure solvent. The scattering data were collected for periods of typically 3-5 min at room temperature. To investigate the growth of sols at elevated temperatures after addition of water due to hydrolysis/condensation, SAXS data were collected on sols in borosilicate glass capillaries (Ø =1.0 mm, glass no. 14, Hilgenberg, Malsfeld, Germany) that were mounted into a Linkam heating stage, which was heated to 60 °C. Measurements were done with 3-5 min intervals for time periods of typically 60 min.

7.2.2.2. Drying films

The setup that was used to follow the evolution of drying thin films is schematically illustrated in **Figure 7.1**. PZT sols were contained in a Kapton foil that was mounted on an aluminum rotor head with a diameter of ca. 11 cm. The rotation speed of the rotor head was 100 rpm, which ensured a homogenous distribution of liquid film over the surface of the Kapton foil. The incident x-ray beam entered the chamber from the right side under a shallow angle with respect to the plane of the paper, as shown in the figure.

The beam scattered on the rotating Kapton-supported drying film on the left, and exited the chamber through a mica window at the left. The scattering intensity was recorded at regular time intervals at room temperature and 60 °C. Correction for the background signal was carried out by subtracting the scattering intensity of the empty chamber, *i.e.* Kapton foil under the same conditions. We thus monitored the scattering intensity of the PZT sol including the solvent matrix.

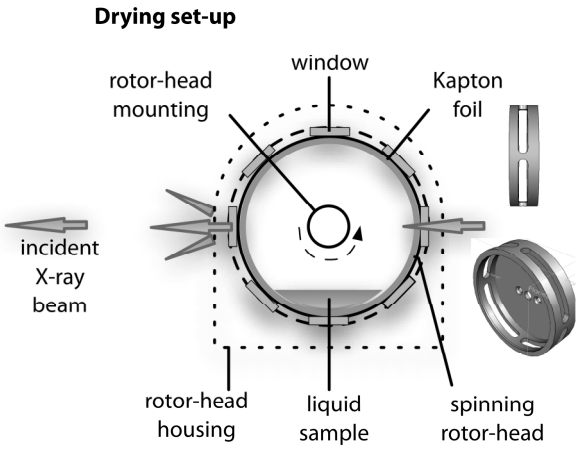

Figure 7.1: Schematic illustration of the setup used to study drying thin films by in situ SAXS.

7.2.2.3. Thermally annealed PZT

PZT films were dried at room temperature for 24 h. One was used as it is, the other materials were thermally annealed in air at 350, 450 and 550 °C, respectively, for 30 min. The heating and cooling rates were 5 °C/min. After the heat treatment, the material was placed on a Kapton foil and mounted in such a way that the foil was perpendicular to the incident x-ray beam. The scattering curve of bare Kapton foil was recorded and subtracted from the total intensity of the PZT sample.

7.2.3. TEM and XRD experiments

Transmission electron micrographs (TEM) of the four powder samples described in section 7.2.2.3 were made using a Philips CM30 FEG TEM. The acceleration voltage was 300 kV. The point-to-point resolution was less than 2 Å. Analyses were performed on amorphous and polycrystalline powder samples deposited on a carbon coated copper grid.

X-ray diffraction (XRD) was carried out on a Philips diffractometer PW3020 (Software XPert Data Collector 2.0e, Panalytical B.V., Almelo, the Netherlands).

7.3. Results and Discussion

7.3.1. Reactions of PZT sols with water

The effect of hydrolysis on the structural evolution of PZT sols was studied on a series of PZT stock solutions with gradually increasing concentrations of water. **Figure 7.2a** shows the ln I – ln q plots of a series of samples with equivalent PZT concentrations of 0.2-0.3 M after ageing for 48 h at room temperature. The data were corrected for the relative number of transmitted photons, such that the intensities can be compared. Interestingly, the scattering curves of unhydrolyzed and hydrolyzed PZT sols with a $[H_2O]$: [Zr+Ti] ratio below 5 showed very clear correlations at $q > 2.7$ nm^{-1}. These peaks indicate the formation of a well-defined structure or series of structures in solution. Interestingly, the structure did not evolve when the $[H_2O]$: [Zr+Ti] ratio was 9 or higher. In the non-hydrolyzed PZT solution, a considerable amount of white precipitate formed during ageing. The precipitate was isolated, dried and subjected to SAXS. The scattering curve of the precipitate is shown in Figure 7.2a. The same correlations as in the sols with low water concentration emerged as very pronounced signals. This strongly suggests that the precipitate contains the same structure or structures that caused the peaks at $q > 2.7$ nm^{-1} in the scattering curve of the sols.

At present, the nature of the structure of the precipitate remains unclear. It is difficult to interpret the scattering curve in terms of a molecular model, since the number of peaks that are visible in the curves is limited, and it is not clear if they belong to only one or to more than one type of structure. In view of the fact that the structure was seen to evolve only when Pb and Zr/Ti stock solutions had been mixed, and when water was absent or only available in limited concentrations, it may be that that they are polyoxometalate complexes or precipitated phases thereof, which contain both lead and titanium or zirconium. Little literature on the molecular structure of PZT precursor solutions in 2-methoxyethanol and/or acetic acid is available, let alone of water-containing PZT sols. Preferential homocondensation of zirconium species has been reported, but seems to depend on the preparation route and solvents/modifiers used.[26] Available data by the group of Hubert-Pfalzgraf on similar systems suggests that there is a tendency for Pb, Zr and Ti atoms to cluster into polyoxometalate structures $Pb_nM_mX_q$, with M=Ti or Zr, and X oxygen-coordinating ligands.[25,27-31] Values of n and m are 2-4, with $n \leq m$, p and q >>10 in all polyoxometalates of which the structure has been reported till date. We may assume that it is possible that similar clusters and structural motifs develop in the PZT sols studied here. The results shown in Figure 7.2a may suggest that similar structures evolved in the non-hydrolyzed PZT solution. Their formation appears to be avoided when sufficient water is available for sol-gel type hydrolysis and concentration reactions, leading to growth of particles.

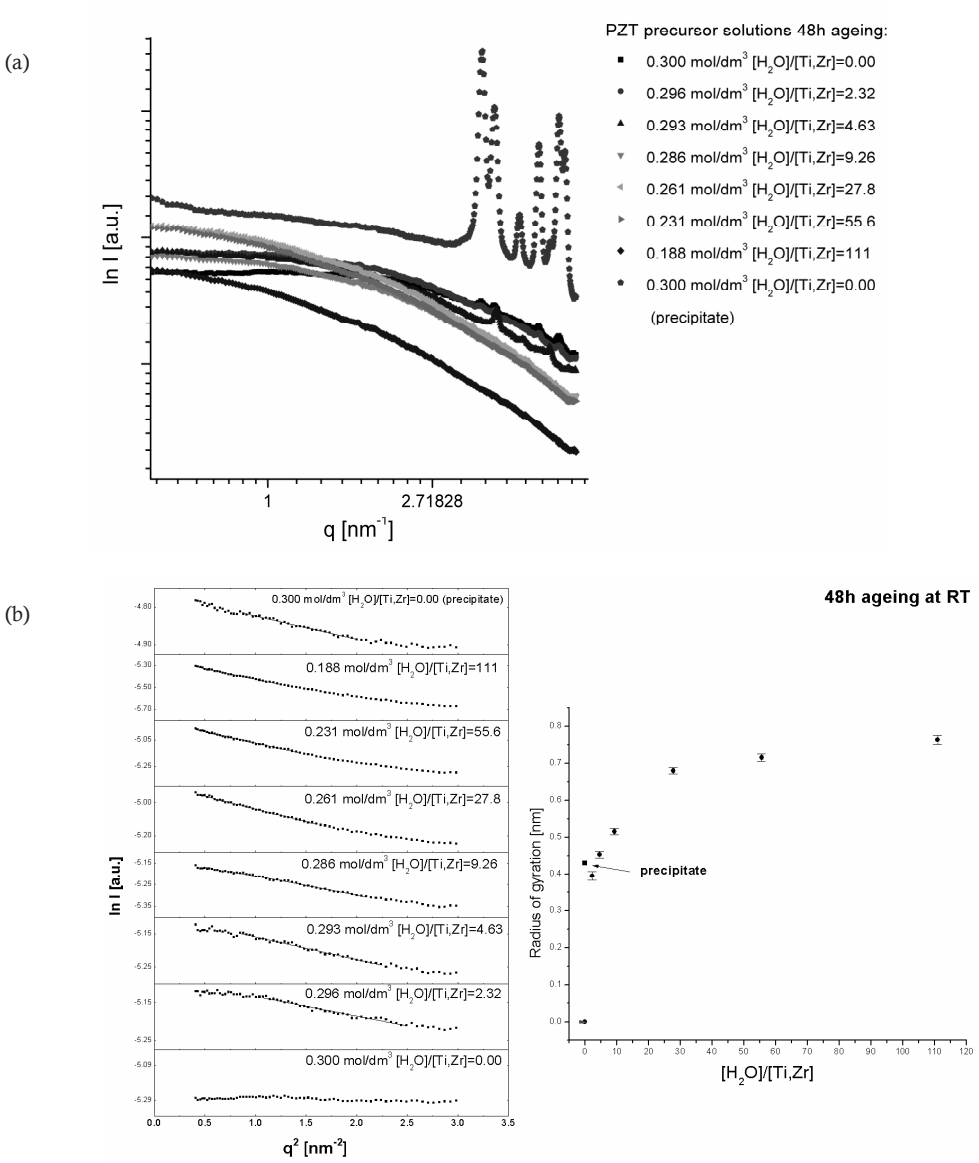

Figure 7.2: Renormalized scattering curves of stock solutions: (a) ln I - q representation of non-hydrolyzed and hydrolyzed PZT sols after 48 h ageing at room temperature; the scattering curve of the precipitate that was isolated from the non-hydrolyzed sol is also shown; (b) Guinier representation of the same scattering curves in the range $0.5 < q^2 < 3$ nm^{-2}; shown to the right is the corresponding radius of gyration as function of the water to PZT molar ratio.

Guinier plots of the same series of hydrolyzed PZT solutions after 48 h ageing at room temperature are shown in **Figure 7.2b**. The data are plotted only in the q-range

where Equation (2) is valid. From the slopes of the curves, the radii of gyration R_g were calculated via Equation (2). The values of R_g are plotted versus [H_2O] : [Zr+Ti] in Figure 7.2b. The radius of gyration increases sharply from near zero to R_g ~0.5 nm with increasing water concentration when [H_2O] : [Zr+Ti] < 10. At higher water concentrations, the further increase of R_g levels off quickly, to reach R_g = 0.75 nm when [H_2O] : [Zr+Ti] = 111. The level-off effect is probably due to the effect of dilution of the reacting sol by water. The addition of water increases the rate of hydrolysis, but the accompanying effect of dilution suppresses condensation as it lowers the concentration of PZT precursor material in the condensing sol. Since the rate of condensation is roughly proportional to the square of concentration, the effect of dilution becomes dominant at high water concentrations. A radius of gyration was also calculated from the scattering curve of the precipitate. It is in the same size range as the species in the sols.

It is noted that the radii of gyration presented here are at the lower limit of what can be determined with Guinier analysis and the calculated gyration radii should therefore be taken with some care. However, the results clearly show that growth of the sol is promoted by the presence of water, and the rate of condensation at room temperature is limited. Only (sub)nanometer-size clusters or particles seem to evolve in the sol-gel process under these conditions, despite the relative excess of water that had been added. This can be attributed to the stabilizing effect that coordinating solvents like 2-methoxyethanol and acetic acid may have on the reactivity of metal alkoxides with water.[39]

Under the assumption that the sol consists of isolated spheres of radius R_0 in solution, R_g and R_0 are related via[40]

$$R_g = R_0 \sqrt{\frac{3}{5}} \qquad (4)$$

Thus, the true diameter $2R_0$ of the spherical particles after one hour of growth was approximately 2 nm.

The reactivity of the PZT stock solution with water was also investigated at 60 °C. PZT sols were mixed with water, resulting in [H_2O] : [Zr+Ti] ratios of 9.3 and 27.8, respectively. The capillaries were then heated rapidly to 60 °C and SAXS curves were collected for an hour with time intervals of 5 min. The evolution of the radius of gyration of these samples with time was determined using Equation (2) in the q-range where qR_g < 1. The best fits to the data are shown in **Figure 7.3a and 7.3b** by drawn lines in the interval where the condition for Guinier analysis is met. As can be seen, the

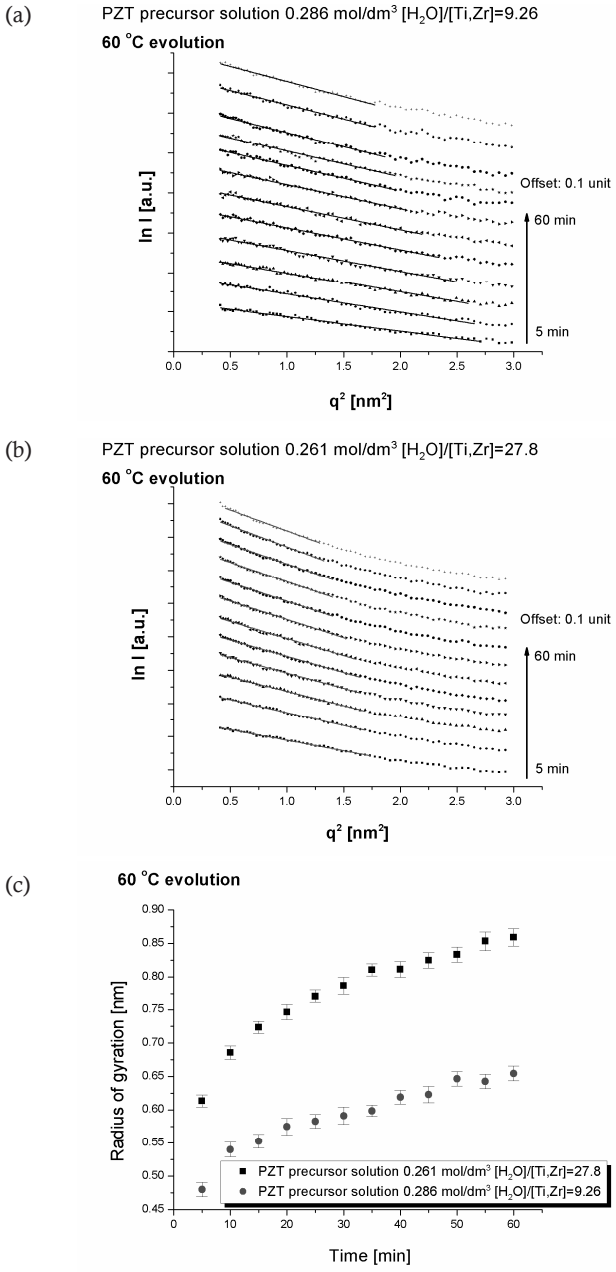

Figure 7.3: (a) Guinier plots ln $I - q^2$ of scattering curves of PZT sols with $[H_2O]$: [Zr+Ti] = 9.26 after 5-60 min of reaction; (b) Guinier plots ln $I - q^2$ of scattering curves of PZT sols with $[H_2O]$: [Zr+Ti] = 27.8 after 5-60 min of reaction. Best fits to the data in the range where $qR_g < 1$ are indicated by drawn lines. All curves have an offset relative to each other on the intensity axis. (c) Evolution of radius of gyration R_g of PZT sols at 60 °C as function of time, with $[H_2O]$: [Zr+Ti] = 9.25 and 27.77, respectively.

value of R_g increased with time. This indicates the occurrence of some growth process. The PZT sol with [H_2O] : [Zr+Ti]= 9.3 grew to R_g ~ 0.65 nm over 60 min, and when [H_2O] : [Zr+Ti] was increased to 27.8, R_g increased to ~0.85 nm in the same time interval. Growth also proceeded after that period. Irrespective of the actual nature and structure of the sol, the data show that the growth rate is strongly dependent on temperature, and also on water concentration. The trends in the growth curves in **Figure 7.3c** suggest that particle growth took place primarily within the first minutes after mixing. The growth rate levels off after that period, and is only modestly dependent on the water concentration in the solution.

7.3.2. Drying of PZT thin films

To study the structural evolution of PZT sols after their deposition into thin films, we performed in situ SAXS experiments on drying thin films on Kapton foil at temperatures of 23°C and 60°C directly after mixing of the reactants. Scattering data were collected at regular time intervals. The contribution of the Kapton foil to the total scattering intensity was subtracted from the raw data. Thus, the entire drying thin film solution including solvents was monitored. **Figure 7.4** shows representative background-corrected scattering curves of a PZT sol without water, and a hydrolyzed PZT solution with a [H_2O] : [Zr+Ti] molar ratio of 9.3. Because of the dynamic nature of the process, the signal to noise ratio in the experimental scattering curves is smaller than in the previous sections and no quantitative analyses were therefore performed on the data.

The overall shape of both curves remains the same during the drying process, but the intensity can be seen to decrease. This decrease is explained by the occurrence of physical drying, i.e., decreased absorption of radiation due to loss of solvent. Furthermore, a local intensity maximum developed around q = 3.8 - 4.2 nm^{-1}. The maximum was slightly more pronounced in the hydrolyzed sol. The local maximum can be explained by the occurrence of processes such as spinodal decomposition, or the agglomeration of primary entities, e.g., titanium alkoxide-based clusters or titanium oxohydroxide precipitates of more or less similar size. In view of the fact that we never obtained transparent gels from the PZT sols, spinodal decomposition is not very likely in this case. Clustering of similarly sized entities into larger agglomerates also yields an x-ray scattering curve with a maximum in intensity at a certain q^*, that is associated with the size of the primary particles. A semi-quantitative estimate of the correlation length d^* in real space associated with q^* is

$$d^* = 2\pi/q^*. \qquad (5)$$

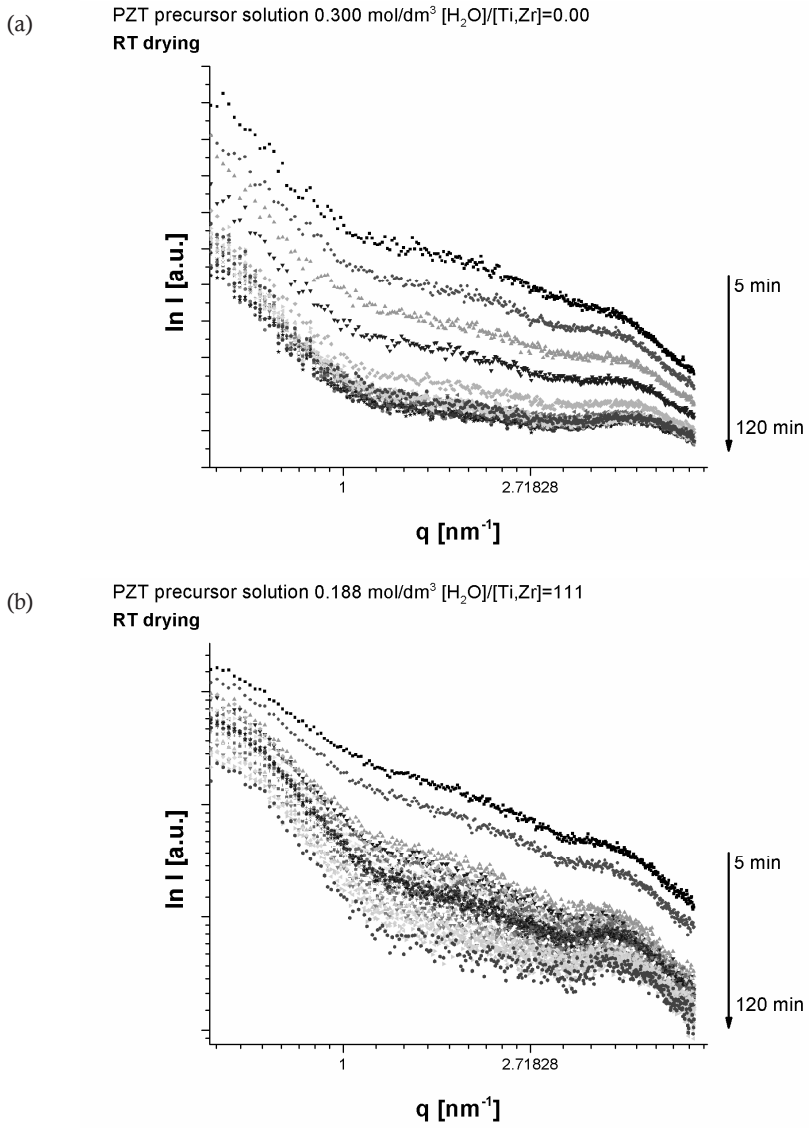

Figure 7.4: Scattering curves showing the scattering intensity of drying thin films at room temperature. Background signal from Kapton foil was subtracted from the total scattering curves. (a) 0.3 M PZT solution without water; (b) 0.19 M PZT sol with $[H_2O]$: [Zr+Ti] = 111. Absolute scattering intensities are shown.

The peak around q^*=3.8 – 4.2 nm^{-1} corresponds with an agglomerate that consists of randomly close-packed particles with dimensions in the range d^* = 1.5 – 1.7 nm. Interestingly, this size is reasonably close to the diameter of non-agglomerated particles in solution as found after 48 h of ageing at room temperature. It is therefore most likely that the drying process at room temperature consists of physical evaporation of solvent,

leading to more and more concentrated sols, up to the point where the particles finally agglomerate into larger randomly close-packed structures. A very similar diffuse peak located at q~4 nm^{-1} has also been observed in another SAXS study on sol-gel derived mixed silica-titania powder, and it was attributed to preformed particles with a diameter of ~1.5 nm.[41]

The same in situ drying experiments were also performed at 60 °C. **Figure 7.5** shows the corresponding scattering profiles of non-hydrolyzed and hydrolyzed PZT sols. Similar trends can be observed as at room temperature. Also the size of the agglomerating entities is similar, irrespective of hydrolysis ratio or temperature. It is most likely that that particles that emerged in the non-hydrolyzed PZT sol, had formed by absorption of moisture from air into the drying film.

All these experiments suggest that small particles with a maximum size of ~2 nm are formed in PZT sols upon hydrolysis and condensation. These particles agglomerate into larger randomly close-packed structures upon removal of the solvent matrix by physical drying. There are no indications in the present data for the occurrence of phase separation or occurrence of chemical heterogeneity during or after drying. Chemical heterogeneity has been observed with neutron scattering studies in annealed PZT powders, when it was found that the Zr/Ti ratio varied widely at different locations in the samples.[33] Furthermore, EXAFS studies of partially heat-treated PZT made from a 2-methoxyethanol based recipe indicated chemical heterogeneity on the atomic level, with predominant Pb-O-Pb, Zr-O-Zr and Ti-O-Ti linkages present in the powder.[42] On the other hand, EXAFS on similar powders derived from metal *n*-butoxides also indicated predominant Zr-O-Zr linkages, although Pb-O-Zr linkages were observed in all samples.[43] Our SAXS data cannot discern between these situations, as they provide structural rather than chemical information on the system.

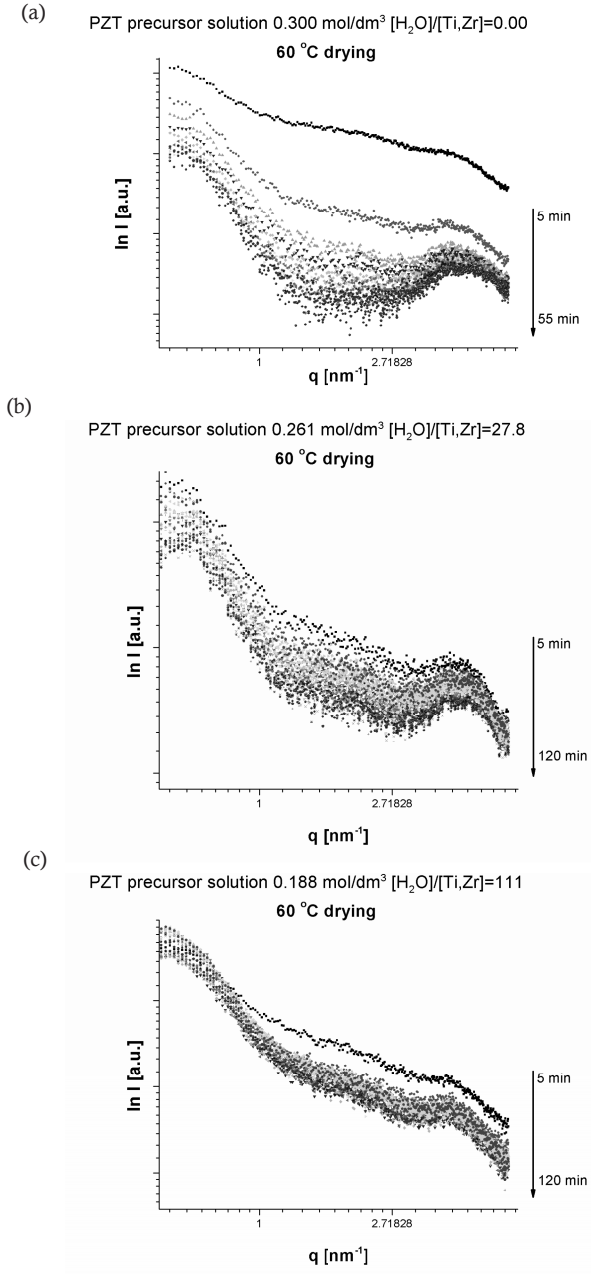

Figure 7.5: Scattering curves of drying thin films at 60 °C. Background signal from Kapton foil was subtracted from the total scattering curves. **(a):** 0.3 M PZT solution without water; **(b):** 0.26 M PZT sol with $[H_2O]$: [Zr+Ti] = 27.8; **(c):** 0.19 M PZT sol with $[H_2O]$: [Zr+Ti] = 111. Absolute scattering intensities are shown.

7.3.3. Thermal annealing of PZT thin films

The scattering curve of a room temperature-dried PZT powdered film after background subtraction is shown in **Figure 7.6**. The as-dried PZT film shows no variation of intensity with q, indicating a completely amorphous film without internal structure or local chemical inhomogeneity causing electron density contrast $\Delta\rho$. The other curves showed indications for the presence of structural features on the length scale covered these experiments and were fitted to a model. The model we adopted consists of a distribution of spherical grains that are spatially organized in a disordered, liquid-like manner. The structure factor of a Percus-Yevick-type lattice was assumed for this purpose,[44] and fitted using the Scatter program.[38] The intensity of the curve of PZT annealed at 350 °C was very weak and it was not possible to make a fair fit of the model to the data. Other more complicated models did not yield positive results either and will therefore not be discussed further. The model could be fitted very well to the scattering curves of the samples that were annealed at 450 and 550 °C. The curves with the best fits are shown as drawn lines in **Figure 7.6**.

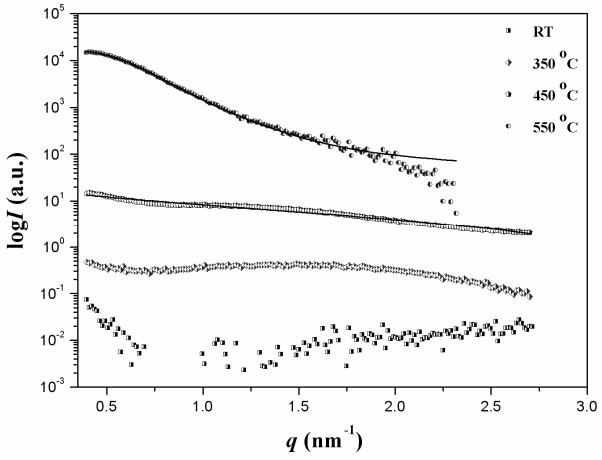

Figure 7.6: SAXS curves of heat-treated PZT films. Background signal from Kapton foil was subtracted from the total scattering curves. The scattering curves have an offset relative to each other on the intensity axis. "RT" indicates film as dried at room temperature for 24 h; other curves are PZT films after annealing at 350, 450 and 550 °C, respectively. Model fits to the curves of 450 and 550°C annealed PZT are indicated by drawn lines.

The diameter of the grains calculated from the best fits are 2.2 and 7.5 nm, respectively. The standard deviation of the calculated grain size distribution was small, i.e., σ~0.2 nm, but could not be determined precisely. The results indicate that grain growth. A

factor that also contributes to the data is the loss of organics at 350-500 °C due to the annealing in air.

We also investigated the same annealed PZT powders with TEM analysis. Representative TEM pictures are shown in **Figure 7.7**. The samples dried at room temperature and annealed at 350 °C looked completely amorphous, and no grain size could be determined. The TEM picture of the powder treated at 450 °C showed some indications for emerging crystallinity, but grain size could not be estimated. The SAXS data suggest a grain size of ~2 nm at this temperature. The sample annealed at 550 °C showed well-developed crystallinity and the grain size could be estimated to be 7 ± 2 nm. This is in close agreement with the results of the theoretical fit to the SAXS data.

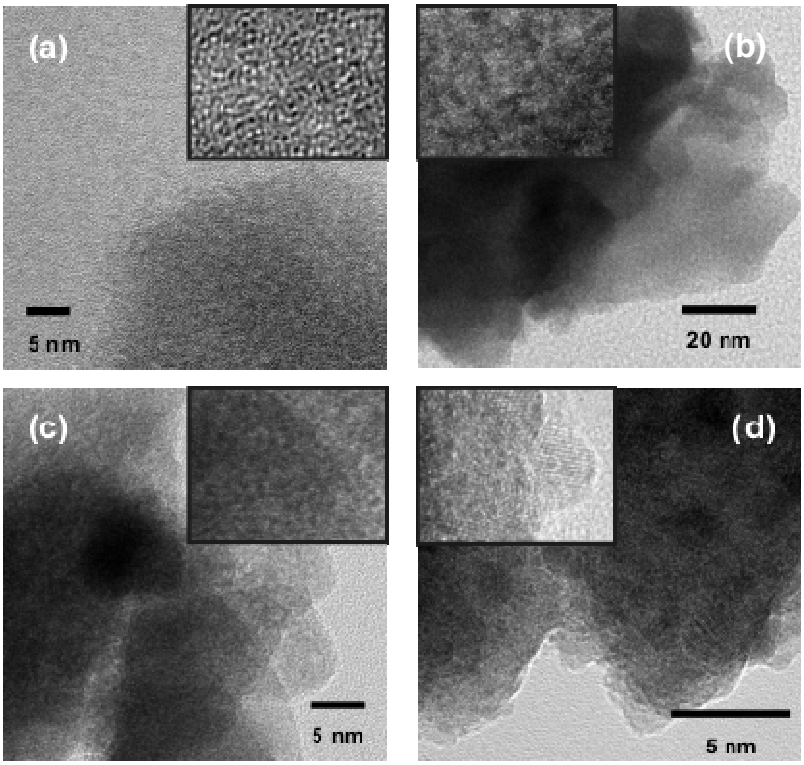

Figure 7.7: TEM pictures of PZT powders annealed at different temperatures. (a) Powder as dried at room temperature; (b-d) PZT powders annealed at 350, 450 and 550 °C, respectively, after drying at room temperature. The insets show enlarged areas of the overviews.

7.4. Conclusions

The experiments have shown that SAXS can be used as a tool to probe the structural evolution of PZT sols and thin film on a nanometer length scale. Hydrolyzed PZT sols

based on lead acetate, metal alkoxides, water and a mixture of acetic acid and 2-methoxyethanol as solvents seem to consist of small particles with a radius of gyration below 1 nm. A white precipitate with well-defined high intensity maxima in the scattering curve at $q > 3$ nm^{-1} formed in non-hydrolyzed PZT sol. Similar signatures with local maxima at $q > 3$ nm^{-1} were found in hydrolyzed sols with a water to PZT molar ratio below 10.

The reactivity of PZT stock solutions with water at room temperature was limited, even when a large excess of water was added. At 60 °C the reactivity was higher, although the radii of gyration of the sols remained below one nanometer after 60 min of reflux under water-rich conditions.

In-situ drying experiments on wet PZT thin films at room temperature and 60 °C indicated physical drying (solvent evaporation) accompanied by agglomeration of the 1.5-1.7 nm diameter sol particles. SAXS analysis of as-dried and thermally annealed thin films showed indications for grain growth with increasing annealing temperatures. The grain sizes calculated from the SAXS experiments were in close agreement with grain sizes estimated from TEM pictures of PZT films.

References

[1] Scott, J.F. and Paz De Araujo, C.A. *Science*, 246, 1400-1405, **1989**

[2] Scott, J.F. *Science*, 315, 954-959, **2007**

[3] Muralt, P. *J.Micromech. Microeng*. 10, 136-146, **2000**

[4] Kondo, M.; Sato, K.; Ishii, M.; Wakiya, N.; Shinozaki, K.; Kurihara, K. *Jpn. J. Appl. Phys*. 45, 7516-7519, **2006**

[5] Kim, H.R.; Jeong, S.; Jeon, C.B.; Kwon, O.S.; Hwang, C.S. *J. Mater. Res.*, Vol. 16, No.12, 3583-3591, **2001**

[6] Otani, Y.; Okamura, S.; Shiosaki, T. *J. Electroceram*. 13, 15-22, **2004**

[7] Lin, Y.C.; Chuang, H.A.; Shen, J.H. *Vacuum*, 83, 921-926, **2009**

[8] Bouregba, R.; Poullain, G.; Vilquin, B.; Murray, H. *Mater. Res. Bull.* 35, 1381-1390, **2000**

[9] Zhu, T.J.; Lu, L.; Lai, M.O. *Appl. Phys. A.* 81, 701-714, **2005**

[10] Dekkers, M.; Nguyen, M.D.; Steenwelle, R.; te Riele, P.M.; Blank, D.H.A.; Rijnders, G. *Appl. Phys. Lett.* 95, 0129021-0129023, **2009**

[11] Schwartz, R.W. *Chem. Mater.* 9, 2325-2340, **1997**

[12] Schwartz, R.W.; Boyle, T.J.; Lockwood, S.J.; Sinclair, M.B.; Dimos, D.; Buchheit, C. *Integr. Ferroelectrics* 7, 259-277, **1995**

[13] Yi, G.; Sayer, M. *Ceram. Bull*. Vol. 70, No. 7, 1173-1179, **1991**

[14] Klee, M.; Eusemann, R.; Waser, R.; Brand, W.; van Hal, H. *J. Appl. Phys*. 72(4), 1566-1576, **1992**

[15] Cui, T.; Markus, D.; Zurn, S.; Polla, D.L. *Microsyst. Technol.* 10, 137-141, **2004**
[16] Schwartz, R.W.; Voigt, J.A.; Tuttle, B.A.; Payne, D.A.; Reichert, T.L.; DaSalla, R.S. *J. Mater. Res.* 12, 444-456, **1997**
[17] Assink, R.A.; Schwartz, R.W. *Chem. Mater*. 5, 511-517, **1993**
[18] Zhang, M.; Salvado, I.M.M. Vilarinho, P.M.; Silvestre, A.J.D.; Silva, A.M.S. *J. Am. Ceram. Soc.* 90, 358-36, **2007**
[19] Caruso, R.; de Sanctis, O.; Frattini, A.; Gil, C.S.R. *Surface and Coating Techn.* 122, 44-50, **1999**
[20] Boyle, T.J.; Dimos, D.; Schwartz, R.W.; Alam, T.M.; Sinclair, M.B.; Buchheit, C.D. *J. Mater. Res.* Vol. 12, No. 4, 1022-1030, **1997**
[21] Zhang, Q.; Huang, Z.; Vickers, M.E.; Whatmore, R.W. *J. Eur. Ceram. Soc.* 19, 1417-1421, **1999**
[22] Zhang, Q.; Vickers, M.E.; Patel, A.; Whatmore, R.W. *J. Sol-Gel Sci. Technol.* 11, 141-152, **1998**
[23] Zhang, Q.; Whatmore, R.W.; Vickers, M.E. *J. Sol-Gel Sci. Technol*. 15, 13-22, **1999**
[24] Schwartz, R.W.; Schneller, T. S.; Waser, R. *C.R. Chimie* 7, 433-461, **2004**
[25] Schwartz, R.W.; Narayanan, M. Chemical Solution Deposition—Basic Principles, In *Solution Processing of Inorganic Materials*, ed. D.B. Mitzi, John Wiley & Sons, Inc., New Jersey. pp. 33-76, **2009**
[26] Malic, B.; Kosec, M.; Arcon, I.; Kodre, A. *J. Europ. Ceram. Soc.* 25, 2241-2246, **2005**
[27] Chae, H.K.; Payne, D.A.; Xu, Z.; Ma, L. *Chem. Mater.* 6, 875-877, **1994**
[28] Brethon, A.; Hubert-Pfalzgraf, L.G. *J. Sol-Gel Sci. Technol.* 39, 159-167, **2006**
[29] Brethon, A.; Hubert-Pfalzgraf, L.G., Daran, J.C. *Dalton Trans.* 250-257, **2006**
[30] Hubert-Pfalzgraf, L.G.; Daniele, S.; Papiernik, R.; Massiani, M.C.; Septe, B.; Vaissermann, J.; Daran, J.-C. *J. Mater. Chem.* 7, 753-762, **1997**
[31] Daniele, S.; Papiernik, R.; Hubert-Pflazgraf, L.G.; Jagner, S.; Hikansson, M. *Inorg. Chem.* 34, 628-632, **1995**
[32] Brinker, C.J.; Hurd, A.J.; Schunk, P.R.; Frye, G.C.; Ashley, C.S. *J. Non-Cryst. Solids* 147-148, 424-436, **1992**
[33] Wilkinson, A.P.; Xu, J.; Pattanaik, S.; Billinge, S.J.L. *Chem. Mater.* 10, 3611-3619, **1998**
[34] Khan, S.U.; Göbel, O.F.; Blank, D.H.A. ten Elshof, J.E. *Appl. Mater. Interfaces* 10, 2250-2255, **2009**
[35] Craievich, A.F. *Mater. Res.* 5, 1-11, **2002**
[36] Glatter, O.; Kratky, O. Small Angle X-ray Scattering, Academic Press, London, pp. 17-52, **1982**

[37] Bras, W.; Dolbnya, I.P.; Detollenaere, D.; van Tol, R.; Malfois, M.; Greaves, G.N.; Ryan, A.J.; Heeley, E. *J.Appl. Crystallogr.* 36, 791-794, **2003**

[38] Förster, S.; Apostol, L.; Bras, W. *J. Appl. Crystallogr.* accepted, **2010**

[39] Malic, B.; Kosec, M.; Arcon, I.; Kodre, A. *J. Sol-Gel Sci. Technol.* 19, 153-156, **2000**

[40] Craievich, A. "Small-Angle X-ray Scattering by Nanostructured Materials," In Handbook of Sol-Gel Science and Technology, Vol. 2, Characterization of Sol-Gel Materials and Products, Ed. S. Sakka, Springer, 2004, pp. 161 – 189, **2004**

[41] Torma, V.; Peterlik, H.; Bauer, U.; Rupp, W.; Husing, N.; Bernstorff, S.; Steinhart, M.; Goerigk, G.; Schubert, U. *Chem. Mater.* 17, 3146-3153, **2005**

[42] Sengupta, S.S.; Ma, L.; Adler, D.L.; Payne, D.A. *J. Mater. Res.* 10, 1345-1348, **1995**

[43] Malic, B.; Arcon, I.; Kodre, A.; Kosec, M. *J. Sol-Gel Sci. Technol.* 16, 135-141, **1999**

[44] van Beurten P.; Vrij A. *J. Chem. Phys.* 74, 2744-2748, **1981**

8

Patterning Lead Zirconate Titanate Nanostructures at sub-200 nm Resolution by Soft Confocal Imprint Lithography and Nano-Transfer Molding[§]

Abstract

Patterned sol-gel derived lead zirconate titanate (PZT) thin films with lateral resolutions down to 100 nm on silicon are reported. Both an imprint and a transfer molding method were employed. The formed patterns after annealing were characterized with scanning electron microscopy (SEM), atomic force microscopy (AFM) and x-ray diffraction (XRD). Despite the small dimensions and flexibility of the PDMS stamps used for patterning, the quality of replication was found to be good. The influence of the surface energies of substrate, PDMS mold and precursor solution on the quality of pattern replication is discussed. The colloidal structure of the PZT sol-gels from which the patterns were made was studied with small angle x-ray scattering (SAXS). The sols were found to be chemically homogeneous down to a length scale of ~2 nm and higher, which is sufficient for pattern replication on ~100 nm scale.

8.1. Introduction

The fabrication of nanometer-scale structures of functional oxides is an important issue in modern materials science and technology. Among these oxides, ferroelectric oxide thin films and functional patterns are of great importance because of their physically and technologically important properties, such as spontaneous polarization, high dielectric constant, and piezo- and pyroelectricity.[1-3] The ability to pattern functional oxides with nanometer-scale resolution is desirable for application in modern miniaturized systems, e.g., sensors, actuators, or information storage media.[1] While conventional photolithographic techniques are expensive and have certain limitations for patterning oxide materials,[4,5] the so-called soft-lithographic techniques, developed in the Whitesides group at Harvard University, may be used alternatively, because of their versatility, technical simplicity and low cost.[4] These techniques can be combined with

---

[§] This chapter is published in the ACS Applied Materials and Interfaces

the use of sol-gel based precursors to yield materials such as lead zirconate titanate (PZT).

Soft-lithography has been utilized by several research groups to micropattern a variety of oxide materials.[6-9] PZT has been patterned from sol-gel precursor solutions by Micromolding in Capillaries (MIMIC),[10,11] a soft-lithographic technique with which patterns can be formed on micrometer and sub-micrometer length scale. Martin *et al.* observed non-uniform shrinkage across patterned PZT films with 2-20 μm resolution, resulting in "double-peak" film topographies whereby the film thickness was greater at the lateral edges than in the middle.[11] The effect was explained in terms of accelerated drying rates in the corners of the replicated pattern. As the lateral feature sizes of structures to be patterned diminish, this effect is expected to become less pronounced. However, MIMIC is not efficient for submicron-sized channels, because friction from the channel walls prevents the penetration of precursor solution by capillary force in narrow channels. MIMIC is also easily disturbed by local contaminants with low surface energy. Fabrication techniques such as soft-lithographic micromolding and nanoimprint lithography are therefore more often considered for smaller feature sizes. It has been shown possible to pattern 350 nm PZT features by nanoimprint lithography using PDMS as a stamp.[12] Hampton *et al.* communicated the imprinting of various oxides at ~500 nm lateral resolution with a perfluoropolyether elastomer master.[13]

Hitherto, soft-lithographic patterning of PZT with resolutions below 200 nm has not been reported. We employed soft confocal imprint lithography (SCIL)[14] with flexible polydimethylsiloxane (PDMS) molds. The process is schematically shown in **Figure 8.1a.** Since an imprint is made in a pre-formed deformable film, some residue layer will usually stay between patterned features. An alternative to imprint lithography is transfer lithography, schematically depicted in **Figure 8.1b**. We termed this process nano-transfer molding (NTM). It is equivalent to microtransfer molding, but operates on the nanometer scale. The use of microtransfer molding has only been reported few times for the patterning of functional oxides on micrometer-scale.[15-17] The SCIL and NTM processes will be compared. It will be demonstrated that PDMS can be used to imprint and transfer PZT patterns with 100 nm lateral features without shape distortion of the flexible stamp, even when some external pressure is applied.

8.2. Experimental Section

8.2.1. PZT synthesis

Lead (II) acetate trihydrate (99%, Aldrich), zirconium (IV) n-propoxide (70% w/w in n-propanol, Alfa Aesar), and titanium (IV) iso-propoxide (99.99 %, Aldrich) were used as precursors. Glacial acetic acid (99.8%, Merck) and 2-methoxyethanol (>99.3%, Aldrich) were used as solvents. The PZT solution was prepared following sol-gel recipes described in detail elsewhere.[18,19] Essentially, two separate stock solutions were made.

One of them is a solution of lead acetate in glacial acetic acid, the other one is a mixture of zirconium and titanium iso-propoxides in 2-methoxyethanol in 52 : 48 molar ratio. After removal of all residual water from the lead acetate solution by refluxing at 105°C, the stock solutions were mixed in appropriate molar ratio. The concentration of PZT in the final solution was kept at 0.6 M. A molar excess of lead acetate of 15 mol% was added in order to compensate for the Pb loss during thermal annealing.

8.2.2. Nanopatterning experiments

Two techniques were employed in the present work to pattern PZT from a sol-gel precursor solution. They are shown in **Figure 8.1**. In the SCIL process[14] shown in **Figure 8.1a**, a drop of PZT sol was placed on a Si (100) substrate and homogenously distributed, e.g. by casting or spin-casting with 500-1000 rpm. Then a patterned polydimethylsiloxane (PDMS) mold was gently placed on the wet film and dried on a hot plate at 80°C for 15-30 min. All PDMS molds were made from Sylgard 184 (Dow Corning Inc.) and cured at 60°C for 24 h. The lateral resolution of the features in the PDMS stamps was 150-400 nm. The feature depth was 100 nm in all cases. The advantages of using a soft PDMS mold are that it provides good conformal contact, has a low reactivity with organic materials and can be removed easily from the replicated pattern without distortion of the pattern.[20]

The second technique, shown in **Figure 8.1b**, is nanotransfer molding (NTM). Here the PZT sol was poured onto a patterned PDMS mold, distributed homogenously, transferred to the substrate and dried under similar conditions as in SCIL. Excess material was in both cases removed either with a soft PDMS block, or with a hard material, e.g. a steel block.

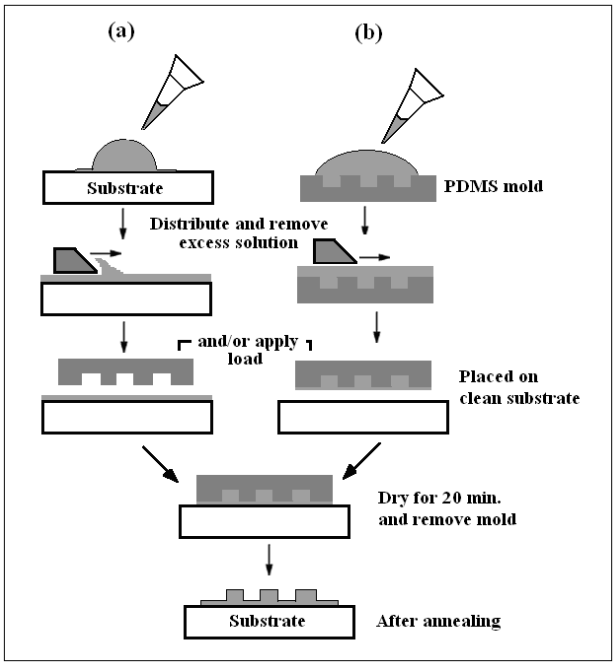

Figure 8.1: Schematic illustration of the modified patterning techniques: (a) soft confocal imprint lithography (SCIL); (b) nano-transfer molding (NTM).

8.2.3. Small Angle X-ray Scattering (SAXS) Analysis

Small-angle X-ray scattering were carried out using synchrotron radiation on the Dutch-Belgian DUBBLE beamline BM-26B of the ESRF in Grenoble,[21] using a beam energy of 12 keV. The beam was focused on a corner of the 2D CCD detector to maximize the range of accessible q values. By placing the 2D detector of DUBBLE at a distance of 1.5 m from the sample, the scattered intensity was measured for q (scattering vector) between 0.13 and 5.56 nm^{-1}. A beam stop was applied to shield the detector from the direct beam and to avoid saturation of the outgoing signal. The raw data were corrected for the pixel-dependent detector sensitivity and integrated for channels with the same q values. In a typical SAXS analysis the scattering intensity I is plotted against the scattering vector Q (nm^{-1}), which is related to the scattering angle θ and wavelength λ of the incident beam by $Q = \frac{2\pi}{\lambda}$ *sin (2θ).* All measured solutions were contained in a capillary glass tube (∅ 1.5 mm, glass no. 14, Hilgenberg, Malsfeld, Germany). The background signal, i.e., the scattering pattern of a capillary containing pure solvent or a mixture of solvents measured under the same conditions, was subtracted from the scattering pattern of the PZT sol.

8.2.4. XRD and AFM analysis

X-ray diffraction (XRD) analysis was carried out with a Philips X'Pert diffractometer using Cu Kα radiation. Atomic force microscopy (AFM) analysis was done with a Nanoscope IV (Veeco Instruments, Digital Instruments, USA) in tapping mode.

8.3. Results and Discussion

8.3.1. SAXS analysis

Knowledge of the colloidal structure of the precursor solution is therefore of importance. The primary building blocks should be at least an order of magnitude smaller than the channels of the mold in order to be able to reproduce its features with a high fidelity. The chemical homogeneity and microstructure of the final sintered product are also affected by the shape and size of the PZT sols.[19] PZT sols that are inhomogeneous on a length scale of ~6 nm have been reported, which is a considerable value if 100 nm nanostructures are targeted.[22] SAXS experiments were performed on both the lead and the titanium/zirconium containing stock solutions, and on the mixed PZT precursor solution. The log *I*-log *Q* Porod plots of the scattering curves of the stock solutions and a PZT precursor solution after background subtraction are shown in **Figure 8.2**. The scattering curve of the lead acetate stock solution showed no variation in intensity *I* with *Q* within experimental error. This indicates a homogeneous solution, as is indeed expected for lead acetate in acetic acid. On the other hand, the zirconium/titanium alkoxide in 2-methoxyethanol stock solution showed a clear variation in scattering intensity, indicating the presence of nanometer-sized structures in the solution. The size and shape of these structures can be interpreted in terms of their radius of gyration R_g and fractal dimension D_f, respectively.[23] The latter parameter relates the mass M and effective radius of gyration R_g of colloidal particles via $M \sim R_g^{Df}$.[23-25] The scattering curve of the zirconium/titanium alkoxide solution could be fitted to the Teixeira function.[24,26,27] From the best fit the fractal correlation length ξ and fractal dimension D_f could be determined. The effective particle size in solution R_g can then be calculated from $R_g^2 = \frac{1}{2} D_f (D_f + 1) \xi^2$. The values of ξ and D_f in the zirconium/titanium stock solution were approximately 0.3-0.4 nm, and 2.3-2.4, respectively. Thus, R_g is ca. 1.0 nm. The effective particle diameter in solution is ca. $2R_g$ ~ 2 nm. Reasonably similar values have been determined from SAXS on ethanol-based titania sols.[24] The scattering curve of the PZT mixed solution did not show any structure either. This is caused by the fact that the scattering and absorption by the element lead overwhelms the scattering signal of any other entities present in solution, such as the zirconia-titania nanoparticles.

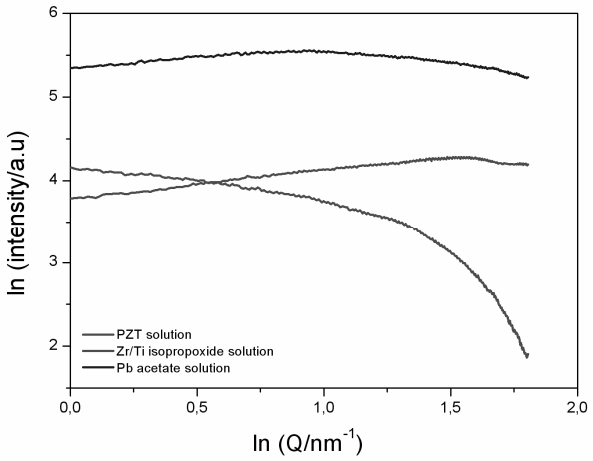

Figure 8.2: SAXS curves showing Porod plots of a solution of lead acetate in acetic acid (blue curve), a solution of zirconium and titanium isopropoxide in 2-methoxyetanol (red curve), and a stoichiometric PZT solution made by mixing the two separate solutions, and ageing (green curve).

If the lead ions would somehow have associated with these titania-zirconia sols, then a different scattering curve would have been observed for PZT solution. Hence, the observed curve strongly suggests that the structure of the PZT precursor solution used in this work is composed of a mixture of heavily branched 2 nm-sized mixed zirconia/titania sol particles with a fractal dimension 2.3-2.4, and unassociated dissolved lead ions, probably coordinated by acetate and/or 2-methoxyethanol ligands. The precursor solution is therefore chemically homogeneous down to a length scale of ~2 nm. This is much smaller than the features of the patterns to be formed, and ensures chemical homogeneity in the final material.

8.3.2. Patterning experiments

Marzolin *et al.* suggested that the liquid should spontaneously dewet the elastomer surface in imprinting processes such as SCIL, so that the protruding parts of the mold make conformal contact with the substrate, and thus avoid a residual layer.[28] This requires the surface tension of the precursor solution (γ_{sol}) to be larger than that of PDMS (γ_{PDMS}). The surface tensions of acetic acid and 2-methoxyethanol are 27.6 and 31.8 mJ/m^2 at 20°C, respectively, so the surface tension of a PZT sol γ_{sol} will be around 30 mJ/m^2. The surface energy of PDMS γ_{PDMS} is 21.6 mJ/m^2. Hence, the sol is indeed expected to dewet the elastomer surface spontaneously.

In transfer molding processes, the requirements on the surface energies of both the PDMS mold and the silicon substrate are more stringent. First of all, their surface energies should be such that PZT sols fill the features of the mold spontaneously, which implies that good wetting of the mold by PZT sol is needed. So γ_{sol} should be smaller than γ_{PDMS}. Furthermore, the sols should also adhere to the silicon substrate, and then be released from the PDMS mold after initial drying.[16] For proper de-molding of the PZT precursor from the mold and adherence to the silicon substrate (with surface tension γ_{SiOx}), the binding energy between PDMS and PZT should be smaller than the energy between substrate and PZT. This means that $\gamma_{PDMS}A_{PDMS} < \gamma_{SiOx}A_{SiOx}$, where A_{SiOx} and A_{PDMS} are the interfacial surface areas of substrate and PDMS inside the mold, respectively. For rectangular channels with a height: width ratio of b, these surface areas are related via $A_{PDMS} = (2b+1)A_{SiOx}$. Hence, the full requirement for the patterning of line structures with an aspect ratio of unity by NTM can be written as:

$$\gamma_{sol} < \gamma_{PDMS} < 1/(2b+1)\gamma_{SiOx} \qquad (1)$$

The requirement implies that there is a theoretical upper limit to the aspect ratio b of the structure that can be patterned by NTM. Namely, $b < ½ (\gamma_{SiOx} / \gamma_{sol} - 1)$. In the present work, the value of b varied between 0.25 and 0.7, which is well below the threshold. Since $\gamma_{sol} > \gamma_{PDMS}$, PDMS is not *a priori* suitable for NTM of PZT sols. However, when PDMS and silicon are treated in oxygen plasma their surfaces become oxidized. This increases their surface energies, and thereby the polarity and hydrophilicity of these interfaces.[29,30] In the present work plasma treatment (Harrick Plasma, 200W) was carried out at a pressure of 80 Pa using molecular oxygen as source. The surface energy of oxidized silicon is not known exactly, but is expected to be higher than 103 mJ/m^2.[31] Hence, if the above-mentioned requirement Eq. (1) for transfer molding is satisfied, the surface energy of the PDMS mold after plasma treatment should be higher than approximately 30 mJ/m^2 (γ_{sol}), and smaller than approximately 45-70 mJ/m^2 [~ $1/(2b+1)\gamma_{SiOx}$]. It is well known that the surface properties of PDMS after oxygen plasma treatment are not stable. PDMS slowly regains its hydrophobic nature over time. This is due to diffusion of small oligomeric PDMS chains to the surface, and/or the adsorption of organic components from the gas phase. Both phenomena lead to an effective lowering of the surface energy.[32] We studied the changes in the contact angle of water on PDMS in air over time after 2 min treatment in oxygen plasma. The contact angle changed considerably, from very hydrophilic just after the treatment, to hydrophobic after ~24 h, as shown in **Figure 8.3**. The contact angle of untreated PDMS is shown for the sake of comparison. Indeed, the NTM experiments demonstrated that PDMS molds with very small contact angles for water (<10^o) transferred much less of the patterning solution to the substrate than PDMS that

had been plasma-treated for shorter periods of time. Under these conditions the precursor adhered to the mold rather than to the substrate. We observed that plasma-treated PDMS with a water contact angle of ca. 30-40° gave good transfer of the PZT precursor sol to the substrate. Such a contact angle was accomplished by treating the PDMS mold in oxygen plasma for 10-20 sec prior to use.

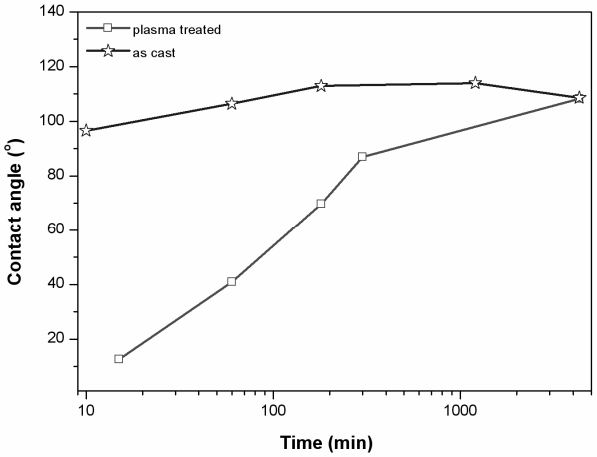

Figure 8.3: Change in water contact angle on PDMS without (blue curve) and after (red curve) 2 min of oxygen plasma treatment. The PDMS samples were stored in a sealed Petri dish in between measurements.

8.3.3. PZT nanopatterns

Figures 8.4 and 8.5 show scanning electron microscope (SEM) images of ceramic PZT patterns on Si substrates fabricated by SCIL and NTM, respectively. All patterns were annealed for 10 min at 650°C after initial drying at 80°C. It was observed that application of pressure to the mold of ~0.6 bar led to a significant improvement of the quality of the patterns, and reduced the residual layer thickness. Although the flexibility of PDMS complicates the replication of features <200 nm,[33] the low aspect ratios in this work, and the low density of recessed features probably prevented stamp deformation to happen.

The elevated light grey features in **Figure 8.4a** are a SCIL pattern with a line width of ca. 380 nm. Replication of the lateral shape of the features of the mold was very good. Various pit patterns with a pit diameter in the range of 65 to 300 nm were also fabricated with SCIL. **Figure 8.4b** shows an overview of a pattern with a pit diameter of ca. 150 nm. **Figure 8.4c** shows a high resolution SEM image of a pit pattern with a hole diameter of ca. 200 nm. The average PZT grain size was estimated from Figure 8.4c, and appears to be in the range between 6 and 15 nm. As will be shown below, this

corresponds well with estimates from XRD analysis. **Figure 8.5** shows several PZT patterns obtained with NTM. The line width in **Figure 8.5b** is ca. 100 nm and the length of the lines is 1 mm. In few cases the transfer process was not optimal, and adhesion of PZT features to the substrate was problematic, especially when nanodots were made. This is evident from a few missing dots in the array shown in **Figure 8.5c**. However, the adherence of line structures was good. It was also found that the residual layer between the patterned lines is much thicker in SCIL than in NTM. This is due to the fact that the mold is directly imprinted into a continuous wet film in SCIL, while in NTM the sol is first transferred to the mold, after which all excess sol is removed from the protruding features. Obviously, less material will be present under the protruding features of the mold in NTM.

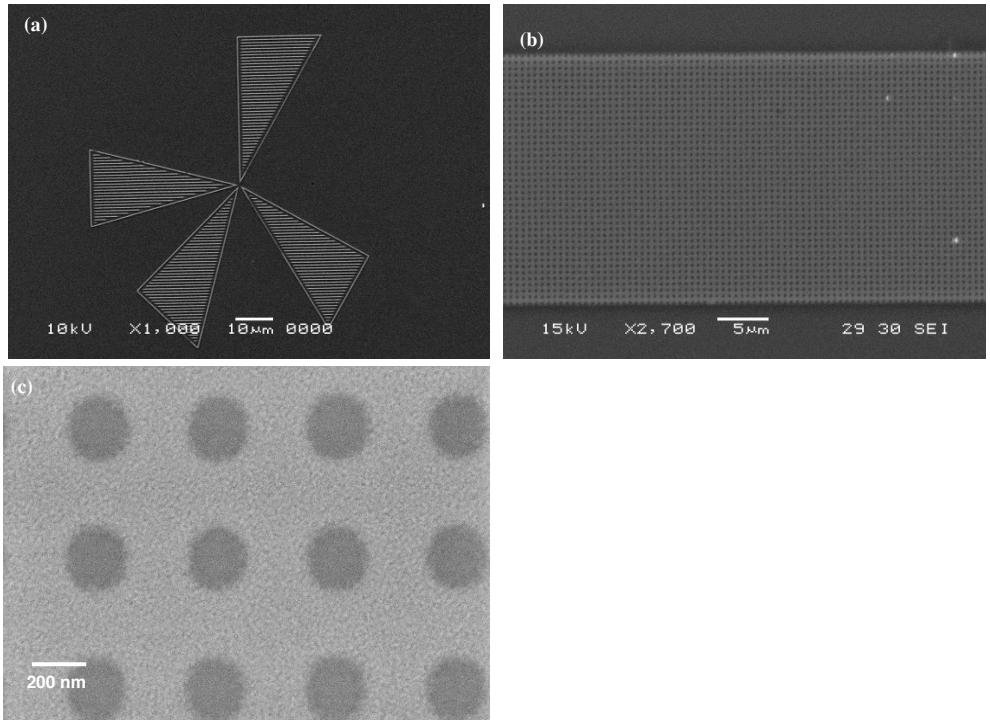

Figure 8.4: Scanning electron microscope (SEM) images of PZT patterns by SCIL on Si (100) substrates after annealing at 650°C in air. (a) Pattern with a line width of 380 nm; (b,c) pit-patterned films, with a pit diameter of 150 nm and 200 nm, respectively.

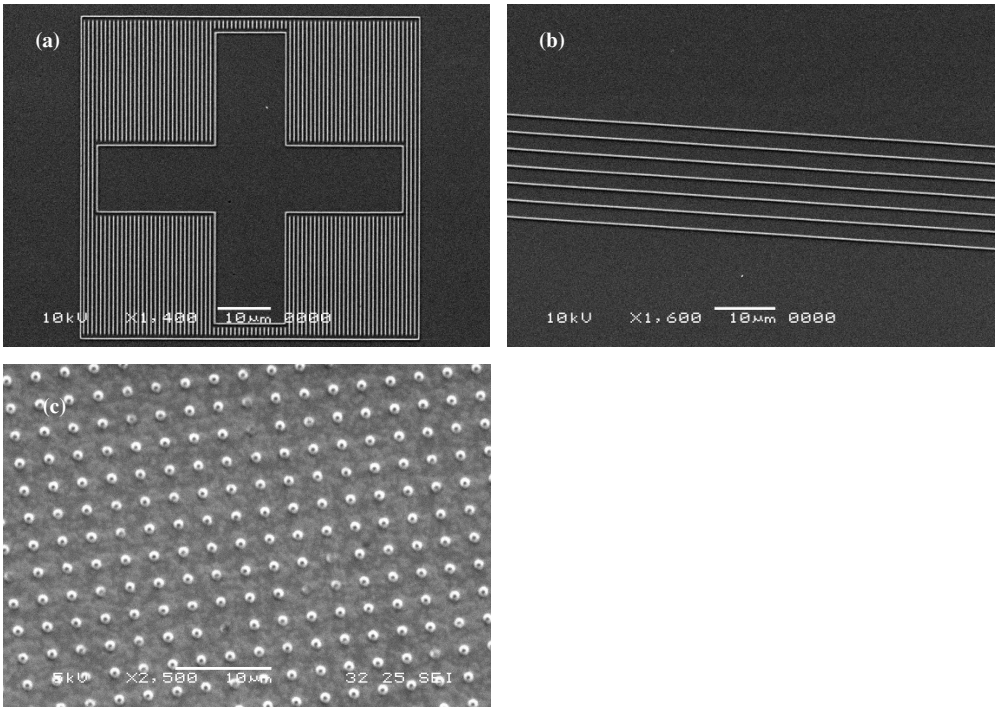

Figure 8.5: Scanning electron microscope (SEM) images of PZT patterns by NTM on Si (100) substrates after annealing at 650°C in air. (a) Pattern with a line width of 380 nm; (b) line pattern with a line width of 100 nm; (c) array of nanodots with a feature size of 800 nm.

AFM was used to determine the height of the patterned features shown in Figures 8.4 and 8.5. **Figure 8.6** shows AFM height images of the line patterns shown in Figure 8.4a. The results indicate that the maximum height is 25 nm. Interestingly, the line patterns do not have the double-peak profile observed in micron-scale MIMIC patterns.[11] The difference is most likely related to the differences in the lateral dimensions of the patterns. In MIMIC, channel filling and sol drying occur simultaneously, and in micron-sized channels the evaporation of solvent is considerably faster at the edges and in the corners of the channel. On the other hand, in imprinting and transfer lithography techniques the filling and drying are separated in time, while the effect of the much smaller feature size is that the drying process is much faster, and occurs more homogenously throughout the sample.

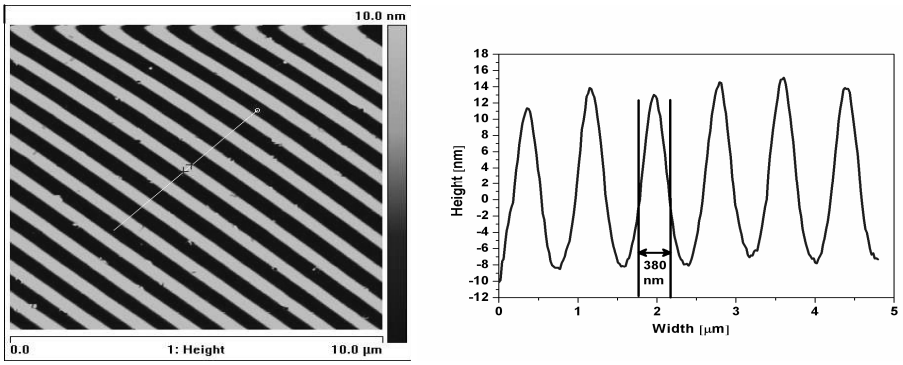

Figure 8.6: AFM height and section analysis of PZT pattern obtained with SCIL technique. Width is 380 nm; height is approximately 25 nm.

It can be inferred from the AFM analysis that the shrinkage of features in vertical direction is comparatively larger than in horizontal direction. The height and width of the lines were reduced from 100 nm x 400 nm before drying to 25 nm x 380 nm after drying and heat-treatment. This corresponds to a volumetric shrinkage of ~ 24%. This value is close to the values reported by Vartuli *et al.*[10] for micron-sized PZT and Beh *et al.*[34] for micron-sized ZrO_2 and SnO_2 line patterns. It was observed that 2/3 of the total volumetric shrinkage occurred in the primary stage of drying at 80 °C, the other 1/3 occurs at the thermal annealing stage.

8.3.4. Phase analysis and microstructure

Figure 8.7 shows θ-2θ spectra of a patterned PZT film after thermal annealing at 650°C. All peaks correspond to the perovskite PZT phase and Si (100) substrate. The width of the XRD peaks was used to estimate the grain size d of a given powder, pattern or film, by employing the Scherrer equation $d = 0.9\lambda / (W \cos \theta)$, where λ is the wavelength, W is the full-width-at-half-maximum (FWHM) of the peak, and θ is the position of the respective XRD peak. The average grain size in patterns was estimated from the PZT (111) peak and was found to be 8-10 nm. This is in good quantitative agreement with the grain sized observed by high resolution SEM, where a primary grain size of 6-15 nm was determined. Hence, the average PZT grain sizes are at least one order of magnitude smaller than the lateral dimensions of the pattern.

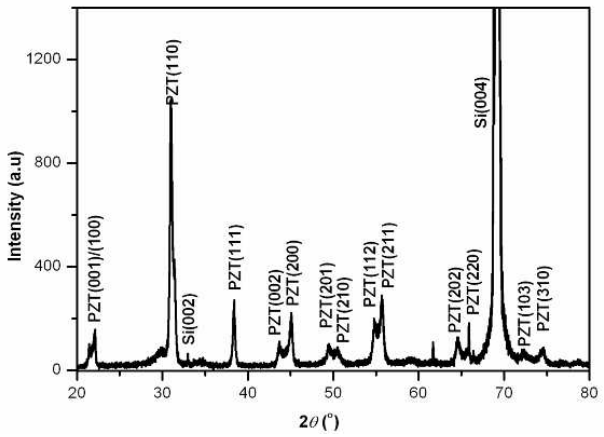

Figure 8.7: X-ray diffraction pattern of patterned PZT film on Si(100) substrate.

8.4. Conclusions

We demonstrated two soft-lithographic techniques with which PZT nanopatterns with a resolution down to 100 nm were made using flexible PDMS stamps. Both SCIL and NTM are promising for future nanofabrication of advanced functional oxides and composite materials, and the quality of formed patterns was similar. The sol-gel precursor solution consisted of entities of ~2 nm or less, which is sufficiently small to be suitable for pattern replication of features of ~25 nm or more. The advantage of SCIL is that the requirements regarding the surface energies of mold, substrate and precursor solution are less strict than with NTM, and that adhesion between substrate and PZT was good. The advantage of NTM is that much less residue stays behind between patterned features. The severe shrinkage of sol-gel derived materials still remains a challenge. These patterns could be interesting for many applications e.g. in non-volatile memory devices, sensors, piezoelectrical materials and nano-electromechanical systems (NEMS).

References

[1] Scott, J. F. *Science 315*, 954-959, **2007**

[2] Scott, J. F.; Dearaujo, C. A. P. *Science 246*, 1400-1405, **1989**

[3] Moulson, A. J.; Herbert, J. M. *Electroceramics: Materials, Properties, and Applications*; 2nd revised Ed. ed.; Wiley: Chichester, **2003**

[4] Xia, Y. N.; Whitesides, G. M. *Annu. Rev. Mater. Sci. 28*, 153-184, **1998**

[5] Seraji, S.; Wu, Y.; Jewell-Larson, N. E.; Forbess, M. J.; Limmer, S. J.; Chou, T. P.; Cao, G. Z. *Adv. Mater. 12*, 1421-1424, **2000**

[6] Gobel, O. F.; Nedelcu, M.; Steiner, U. *Adv. Funct. Mater. 17*, 1131-1136, **2007**

[7] Yang, P. D.; Rizvi, A. H.; Messer, B.; Chmelka, B. F.; Whitesides, G. M.; Stucky, G. D. *Adv. Mater. 13*, 427-431, **2001**

[8] Heule, M.; Gauckler, L. J. *Adv. Mater. 13*, 1790-1793,**2001**
[9] Martin, C. R.; Aksay, I. A. *J. Electroceram. 12*, 53-68, **2004**
[10] Vartuli, J. S.; Ozenbas, M.; Chun, C. M.; Trau, M.; Aksay, I. A. *J. Mater. Res. 18*, 1259-1265, **2003**
[11] Martin, C. R.; Aksay, I. A. *J. Phys. Chem. B 107*, 4261-4268, **2003**
[12] Harnagea, C.; Alexe, M.; Schilling, J.; Choi, J.; Wehrspohn, R. B.; Hesse, D.; Gosele, U. *Appl. Phys. Lett. 83*, 1827-1829, **2003**
[13] Hampton, M. J.; Williams, S. S.; Zhou, Z.; Nunes, J.; Ko, D. H.; Templeton, J. L.; Samulski, E. T.; DeSimone, J. M. *Adv. Mater. 20*, 2667-2673, **2008**
[14] Verschuuren, M.; Van Sprang, H. In *Materials Research Society Symposium Proceedings Vol. 1002E*; Gigli, G., Ed.; Materials Research Society: Vol. 1002, p N03-05, **2007**
[15] Kim, J. H.; Lange, F. F.; Cheon, C. I. *J. Mater. Res. 14*, 1194-1196, **1999**
[16] Moran, P. M.; Lange, F. F. *Appl. Phys. Lett. 74*, 1332-1334, **1999**
[17] Yang, P. D.; Wirnsberger, G.; Huang, H. C.; Cordero, S. R.; McGehee, M. D.; Scott, B.; Deng, T.; Whitesides, G. M.; Chmelka, B. F.; Buratto, S. K.; Stucky, G. D. *Science 287*, 465-467, **2000**
[18] Schwartz, R. W.; Boyle, T. J.; Lockwood, S. J.; Sinclair, M. B.; Dimos, D.; Buchheit, C. D. *Integrated Ferroelectrics 7*, 259-277, **1995**
[19] Zhang, Q.; Huang, Z.; Whatmore, R. W. *J. Sol-Gel Sci. Technol. 23*, 135-144, **2002**
[20] Kim, W. S.; Kim, K. S.; Kim, Y. C.; Bae, B. S. *Thin Solid Films 476*, 181-184, **2005**
[21] Bras, W.; Dolbnya, I. P.; Detollenaere, D.; van Tol, R.; Malfois, M.; Greaves, G. N.; Ryan, A. J.; Heeley, E. *J. Appl. Crystallogr. 36*, 791-794, **2003**
[22] Zhang, Q.; Whatmore, R.; Vickers, M. E. *J. Sol-Gel Sci. Technol. 15*, 13-22, **1999**
[23] Boffa, V.; Castricum, H. L.; Garcia, R.; Schmuhl, R.; Petukhov, A. V.; Blank, D. H. A.; ten Elshof, J. E. *Chem. Mat. 21*, 1822-1828, **2009**
[24] Sekulic, J.; ten Elshof, J. E.; Blank, D. H. A. *Adv. Mater. 16*, 1546-1550, **2009**
[25] Mandelbrot, M. M. *The fractal geometry of nature*; W.H. Freeman and co.: New York, **1982**
[26] Teixeira, J. In *On growth and form*; Stanley;, H. E., Ostrowsky, N., Eds.; Martinus Nijhof: Dordrecht, p 145-162, **1986**
[27] Teixeira, J. *J. Appl. Crystallogr. 21*, 781-785, **1988**
[28] Marzolin, C.; Smith, S. P.; Prentiss, M.; Whitesides, G. M. *Adv. Mater. 10*, 571-574, **1998**
[29] Hillborg, H.; Ankner, J. F.; Gedde, U. W.; Smith, G. D.; Yasuda, H. K.; Wikstrom, K. *Polymer 41*, 6851-6863, **2000**
[30] Ginn, B. T.; Steinbock, O. *Langmuir 19*, 8117-8118, **2003**
[31] David, B. A.; Seong, H. K. *The Journal of Chemical Physics 124*, 174712, **2006**
[32] Barbier, V.; Tatoulian, M.; Li, H.; Arefi-Khonsari, F.; Ajdari, A.; Tabeling, P. *Langmuir 22*, 5230-5232, **2006**
[33] Huang, Y. G. Y.; Zhou, W. X.; Hsia, K. J.; Menard, E.; Park, J. U.; Rogers, J. A.; Alleyne, A. G. *Langmuir 21*, 8058-8068, **2005**
[34] Beh, W. S.; Xia, Y. N.; Qin, D. *J. Mater. Res. 14*, 3995-4003, **1999**

9

Conclusions and Outlook

Soft-lithography has emerged as an important technology for exploratory research in the last decade. It is a diverse technology having a variety of techniques, and is applicable to a variety of materials such as polymers, sol-gel solutions, dispersions, suspensions, and glasses, to name a few. This is the reason it has attracted researchers from different areas such as physics, chemistry, materials sciences, and biotechnology. Although photolithography is a dominant technology for the microfabrication of materials, it has matured over the last decades. Soft-lithography is a convenient, inexpensive and easily adaptable technology from both academic and commercial view points. It is applicable to many more materials than photolithography.
In this work molding-based soft-lithographic techniques and their applicability to sol-gel based oxides and composite materials were studied in a methodological way. The approach was to establish the techniques for these materials at different shapes and sizes, and to get control over their formation. It was shown that these techniques can be applied universally to other materials with little or no variation in the process. These techniques could be an alternative choice (if not substitute) for the fabrication of advanced functional materials at low capital cost in a technologically simple manner.

This research work was carried out from both technological and scientific view points. In the technological part, the applicability of molding based soft-lithographic techniques to sol-gel based oxides and composite materials was investigated both at micrometer and nanometer scales. A major challenge associated with such materials was found to be the volumetric shrinkage upon the evaporation of their respective solvents. Shrinkage leads to variations in size and shape of patterned features. It was observed that the shape obtained from the same technique varied from one material to another. This could be one of the limitations in areas where exact replication of the master mold is targeted. Similarly, the use of two different techniques for the same material may not guarantee the same shape profile, porosity & density, and adhesion to the substrate. It was found that the way the solvent evaporates from the confined precursor has certain effects on the cross-sectional shape of the final patterns. Furthermore, the modification of surface properties (surface energies) of the substrate and molding material might change from one material to another and similarly from one technique to another. Thus, it could be concluded that process variables involved in

these techniques such as surface energy should be adjusted independently for new materials. The problem of residue layer formation and its prevention was another technological aspect studied. A method was proposed to avoid its occurrence when not desirable. However, there are certain applications where it can be an advantage to have a residue layer.

The scientific part of this research was related to the study of particle sizes and shapes of PZT sol-gel solutions. When patterning oxides at lateral length scales below 100-200 nm, it becomes important to have knowledge of the size of the structural entities in solution. Small angle x-ray scattering (SAXS) was used to probe the structure of PZT in all stages of preparation, from liquid sols to final solid state form. The role of processing methods, water addition, aging, and heating of the solution during drying were studied. The results indicated that the solutions consisted of structural entities of ~2-5 nm size, suggesting their appropriateness for patterning at length scales of 100 nm. These solutions were used for patterning with two modified soft-lithographic techniques, namely soft confocal imprint lithography (SCIL) and nano transfer molding (NTM). We believe that these techniques can be promising for future fabrication of advanced functional materials in applications such as sensors, memory devices, and nano-electromechanical systems (NEMS).

The inability of soft-lithography for registry of formed patterns, *i.e.*, the impossibility to position a structure on a predefined location, could be one of the main hurdles to the application of soft-lithographic patterning in industry. It makes fabrication of more complex multiple layer patterns rather complicated. Some efforts have been made to combine the versatility of soft-lithography with the registration tools developed for photolithography. Other researchers have proposed strategies to use photolithography itself instead to define the pattern. Such strategies; discussed in chapter 2 of this thesis, present a viable approach to industrial parallel patterning of ceramics and hybrids on length scales that are only limited by the resolution of the photolithographic process. As a final concluding remark: though soft-lithography is still in its early stages of development, it has a potential to become an important technology when simplicity, cost effectiveness, and diversity are targeted.

Acknowledgements

Appreciation is expressed to all those who have made contribution to this work. First of all, I would like to acknowledge my promoter Professor Dave Blank. Dave! I am very lucky to work at your group, the study tours and the useful discussions, and the PhD dinners in your kitchen, I will always remember them. I would like to express my deepest gratitude to Dr. André ten Elshof for his constant availability, fruitful discussions and suggestions in connection with different aspects of this work. André thank you for shaping up my career. It is my great pleasure to acknowledge Ole Göbel for his never ending help from start of the project until writing of this report (Kiel-Enschede). I am very fortunate to have my office mates: Michiel, Antony, Nicolas, Vittorio and Eddy for the great time and all sorts of discussions we have all this time. I will miss it a great deal! A thank you note to Torsten (Münster), Sandra, Rogier, and Frank for their contribution to the work reported here. I also wish to thank Wim, Hessel, Tomasz and Sjoerd for their assistance in SAXS experiments. I am also thankful to Mark Smithers for the electron microscopy and Boris Vratzov for providing the masters. My genuine thanks to Marion for her kind assistance during all this period in administration work. I am indebted to Henk for his constant technical assistance from the very first till the last day. Frank (ICE)! Thank you for your help with all instruments at the MESA$^+$ labs.

I would like to thank all the colleagues (Previous and Present) from the IMS group for the nice time we have during these fours years, the study tours, the brain storming, journal clubs, all the sports activities, the dinners all is a great part of my memories.

I wish to thank my external graduation committee members Prof. G. van der Steenhove, Prof. R. Lammertink, Prof. H. Gardeniers, Dr. H.T.J.M. Bert Hintzen, and Prof. B.J. Kooi for their efforts in reviewing this thesis and their valuable comments and suggestions.

I would like to thank all my friends from Pakistan here in UT and from ITC for making my stay here in Enschede very enjoyable with all the cricket and parties. Finally, I would like to thank my *mother* and all my family for their never ending love and affection.